AMRL-TR-79-110

WIND TUNNEL MEASUREMENTS OF TOTAL FORCE AND EXTREMITY FLAIL POTENTIAL FORCES ON A CREW MEMBER IN CLOSE PROXIMITY TO A COCKPIT

HAROLD L. NEWHOUSE
PETER R. PAYNE
JAMES P. BROWN

PAYNE, INC.
1933 LINCOLN DRIVE
ANNAPOLIS, MARYLAND 21401

DECEMBER 1980

JUL 6 1981

A

Best Available Copy

81 7 02 122

NOTICES

When US Government drawings, specifications, or other data are used for any purpose other than a definitely related Government procurement operation, the Government thereby incurs no responsibility nor any obligation whatsoever, and the fact that the Government may have formulated, furnished, or in any way supplied the said drawings, specifications, or other data, is not to be regarded by implication or otherwise, as in any manner licensing the holder or any other person or corporation, or conveying any rights or permission to manufacture, use, or sell any patented invention that may in any way be related thereto.

Please do not request copies of this report from Air Force Aerospace Medical Research Laboratory. Additional copies may be purchased from:

> National Technical Information Service
> 5285 Port Royal Road
> Springfield, Virginia 22161

Federal Government agencies and their contractors registered with Defense Documentation Center should direct requests for copies of this report to:
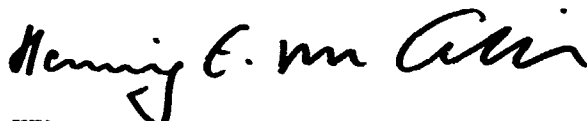
> Defense Documentation Center
> Cameron Station
> Alexandria, Virginia 22314

TECHNICAL REVIEW AND APPROVAL

This report has been reviewed by the Office of Public Affairs (PA) and is releasable to the National Technical Information Service (NTIS). At NTIS, it will be available to the general public, including foreign nations.

This technical report has been reviewed and is approved for publication.

FOR THE COMMANDER

HENNING E. VON GIERKE
Director
Biodynamics and Bioengineering Division
Air Force Aerospace Medical Research Laboratory

REPORT DOCUMENTATION PAGE	READ INSTRUCTIONS BEFORE COMPLETING FORM

1. REPORT NUMBER AMRL-TR-79-110	2. GOVT ACCESSION NO. AD-A100 917	3. RECIPIENT'S CATALOG NUMBER

4. TITLE (and Subtitle) WIND TUNNEL MEASUREMENTS OF TOTAL FORCE AND EXTREMITY FLAIL POTENTIAL FORCES ON A CREW MEMBER IN CLOSE PROXIMITY TO A COCKPIT.	5. TYPE OF REPORT & PERIOD COVERED FINAL June 77 — Feb 80
	6. PERFORMING ORG. REPORT NUMBER

7. AUTHOR(s) Harold L. Newhouse Peter R. Payne James P. Brown	8. CONTRACT OR GRANT NUMBER(s) F33615-77-C-0523

9. PERFORMING ORGANIZATION NAME AND ADDRESS Payne, Inc. 1933 Lincoln Drive Annapolis, Maryland 21401	10. PROGRAM ELEMENT, PROJECT, TASK AREA & WORK UNIT NUMBERS 62202F 7231 13 03

11. CONTROLLING OFFICE NAME AND ADDRESS Air Force Aerospace Medical Research Laboratory Aerospace Medical Division, Air Force Systems Command, Wright-Patterson AFB, Ohio 45433	12. REPORT DATE December 1980
	13. NUMBER OF PAGES 89

14. MONITORING AGENCY NAME & ADDRESS(if different from Controlling Office)	15. SECURITY CLASS. (of this report) Unclassified
	15a. DECLASSIFICATION DOWNGRADING SCHEDULE

16. DISTRIBUTION STATEMENT (of this Report)

Approved for public release; distribution unlimited.

17. DISTRIBUTION STATEMENT (of the abstract entered in Block 20, if different from Report)

18. SUPPLEMENTARY NOTES

19. KEY WORDS (Continue on reverse side if necessary and identify by block number)

Aerodynamic Force Measurements
Human Body Aerodynamics
Ejection Aerodynamics

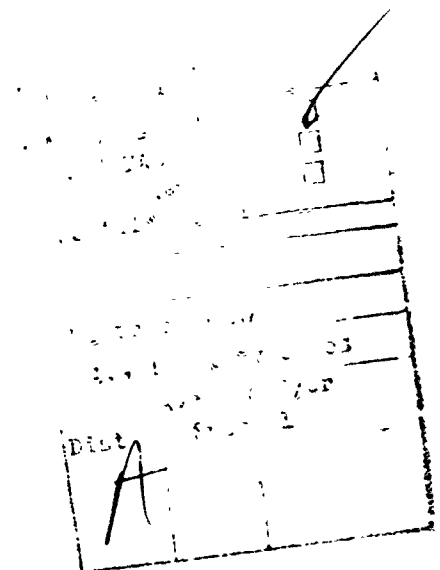20. ABSTRACT (Continue on reverse side if necessary and identify by block number)

In order to determine the aerodynamic forces acting upon a crewmember/escape seat combination at transonic speeds, and the flail potential forces acting on the crewmember's extremities, an existing half scale man/seat combination was integrated with a model of the forward portion of the F-16. The combination was tested in the Arnold Engineering Development Center Propulsion Wind Tunnel (PWT) Facility Transonic Wind Tunnel (16T) during the period September 9 to September 15, 1978, over the Mach number range
(continued on reverse side)

DD FORM 1473 1 JAN 73   EDITION OF 1 NOV 65 IS OBSOLETE

Block 20 continued

0.4 to 1.2. The basic data obtained in this way are reported in Reichenau (Reichenau, 1978). The present report describes the experimental set-up in detail and presents some typical force and force area (force/q plots.

From earlier work it was determined that the flow over the model was "supercritical", implying a turbulent boundary layer at separation, and a reasonably realistic simulation of full-scale conditions.

Very marked interference effects were observed on the man/seat combination, due to fuselage proximity. The most dramatic were large increases in upper arm and upper leg flail potential forces. In almost all cases, the most severe interference occurred when a "flow diverter" was mounted in front of the cockpit.

Comparisons with other sources of data revealed generally good agreement, except that the drag of the model was somewhat low; presumably due to the fact that the model was smoother than its full scale equivalent.

SUMMARY

In order to determine the aerodynamic forces acting upon a crewmember/
escape seat combination at transonic speeds, and the flail potential forces
acting on the crewmember's extremities, an existing half scale man/seat
combination was integrated with a model of the forward portion of the F-16.
The combination was tested in the Arnold Engineering Development Center
Propulsion Wind Tunnel (PWT) Facility Transonic Wind Tunnel (16T) during
the period September 9 to September 15, 1978, over the Mach number range
0.4 to 1.2 The basic data obtained in this way are reported in Reichenau
(Reichenau, 1978). The present report describes the experimental set-up in
detail and presents some typical force and force area (force/q^2) plots.

From earlier work it was determined that the flow over the model was
"supercritical," implying a turbulent boundary layer at separation, and a
reasonably realistic simulation of full-scale conditions.

Very marked interference effects were observed on the man/seat combina-
tion, due to fuselage proximity. The most dramatic were large increases in
upper arm and upper leg flail potential forces In almost all cases, the
most severe interference occurred when a "flow diverter" was mounted in front
of the cockpit.

Comparisons with other sources of data revealed generally good agree-
ment, except that the drag of the model was somewhat low; presumably due to
the fact that the model was smoother than its full scale equivalent.

-1-

PREFACE

The work described in this report was performed under United States Air Force Contract F33615-77-C-0523 "High Dynamic Pressure Windblast Experimentation". The Principal Investigator was Peter R. Payne.

The Air Force Technical Monitor was Lawrence Specker of the Biomechanical Protection Branch, Biodynamics and Bioengineering Division.

TABLE OF CONTENTS

LIST OF TABLES

LIST OF ILLUSTRATIONS

Page

Figure

MODEL DESCRIPTION

Crewman/Ejection Seat Configuration

A 1/2 scale crewman model representing a 50th percentile body size seated in an ACES II seat was required for testing of dynamic pressures up to 600 pounds per square foot and velocities ranging up to Mach 1.5. The model was designed to meet the structural requirements of the Arnold Engineering Development Center (AEDC) PWT facility and its Quality Control Procedures and was approved by AEDC engineering personnel prior to commencement of testing.

The crewman/seat model was designed and constructed (Figures 1 and 2) under a previous contract.* Its dimensions were matched to the projected anthropometry of 1985 Air Force Rated Flying Personnel as supplied by the Department of the Air Force. The model crewman was instrumented with strain gauges on his "skeletal" structure to enable limb flail potential forces to be measured. A three component strain gauged beam also enabled helmet lift, drag and side forces to be measured.

The crewman design was such that a number of body configurations could be investigated. These included the normal seated condition, one asymmetric arm "flail" condition, one asymmetric leg condition, and one condition with an arm and a leg in "flailing" positions. The asymmetric arm and leg were designed to be bolted to the body structure in place of the instrumented limbs used for the normal seated position. These asymmetric members were not instrumented.

Force Measuring Instrumentation

Limb forces were measured by instrumented beams. These beams varied in dimension but were all of similar construction. (See Figure 3 for the beams as installed.)

As shown in Figure 4 each beam consists of end mounting bosses with the connecting center portion machined to provide a more flexible section. Gauges were mounted to the center section to measure the strain present. The location of these strain gauges was determined and recorded, (see Figures 5 and 6) during construction.

The limb force data presented by Reichenau (1978) were obtained using equations that assumed a concentrated load on each segment, creating bending moments M_1 and M_2 at the strain gauge locations. Knowing values for the bending moments M_1 and M_2 and the distance between them, the value of the concentrated load and its point of application (i.e. center of pressure) were then calculated. This method was good for a first approximation of limb loading, however, it should be noted that this also requires the assumption of a linear bending moment distribution. Furthermore, there is no restriction that the force must act on the limb. It can be shown that when M_1 and M_2 are approximately the same magnitude, the point of application of the concentration load is not located on the limb. It should also be pointed out that the upper limb data

---

*Contract Number F33615-76-C-0530

(i.e. upper arm and upper leg) presented by Reichenau (1978) contained force and moment contributions from the lower limb (i.e. lower arm and lower leg).

The limb force data presented in this report was obtained using equations that assumed a linear load distribution acting on the load bearing limb. The equations are:

$$f_o = \frac{2(M_2 X_2^3 - M_1 X_1^3)}{X_2^2 X_1^2 (X_1 - X_2)}$$

$$f_1 = \frac{M_2 - f_o(\frac{X_2^2}{2} - \frac{X_2^3}{6})}{\frac{X_2^3}{6X}}$$

$$F_t = (f_o + f_1) \frac{\bar{X}}{2} \qquad \text{(resultant force acting on the limb)}$$

$$M_j = f_o (\frac{X_j \bar{X}}{2} - \frac{\bar{X}^2}{6}) + f_1 (\frac{X_j \bar{X}}{2} - \frac{\bar{X}^2}{3}) \qquad \begin{array}{l}\text{(moment contribution applied by} \\ \text{the lower limb to the upper} \\ \text{limb at the joint)}\end{array}$$
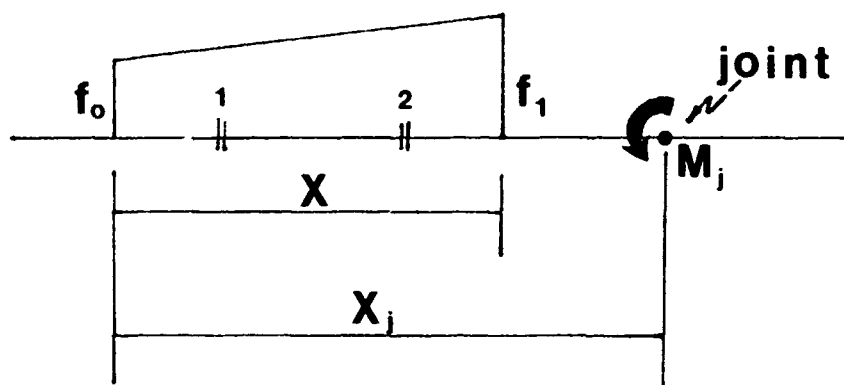
Where X_1 and X_2 are the strain gauge locations and X is the distance over which the distributed load acts. All of the distances were measured from a reference point on each limb. M_1 and M_2 are the bending moments at the strain gauge locations. The forces per unit length, f_o and F_1 are the initial and final values of the distributed loading. The distributed load analysis, unlike the point load analysis, requires that the resultant force (F_t) act on the member. The moment, M_j is the moment contribution of the lower limb distributed load, acting at the joint (i.e. elbow and knee) and the X_j is the location of the joint measured from the reference point on the lower limb.

For the force calculations in the upper limb, the force (F_t) and moment contributions (M_j) of the lower limb were subtracted out, unlike the upper limb force calculated in the previous point load analysis.

All limbs had these instrumented beams made of aluminum alloy. The head sting differed in that it measured bending moments at one location only and also incorporated a gauged ring for measuring lift loads (see Figure 7). It was assumed that the drag and side force could be considered essentially applied at the center of the head. Also the head sting was manufactured from heat treated steel bars to provide an additional safety margin against failure.

Static Pressure Measurement (Crewman/seat Model)

Static pressure taps were provided at five locations on the crewman model (Figure 8). In addition, a static pressure tap was mounted in the center of the seat back.

These static pressure taps were connected to a scanner type valve located in the lower portion of the seat which in turn was connected to the tunnel instrumentation system.

Construction Details (Crewman/seat Model)

The crewman portion of the model was sculptured from mahogany to conform as closely as possible to the projected anthropometry of the 1985 Air Force Rated Flying Personnel. The limbs were made in two halves and the center machined out to fit around the instrumented beams. One half of each limb was attached by bolting it to the opposite half. A layer of glass reinforced plastic (polyester resin) was applied to the outer surface, dressed smooth and painted.

The head and torso sections were both made of glass reinforced polyester resin laminates. They were laid into molds fabricated from carved wooden master models. As the laminate was being built up, metal inserts were installed where attachment and hard mounting surfaces were desired. Access to mounting bolts was provided by small removable panels or cover sections.

The seat structure was designed to aerodynamically simulate an ACES II ejection seat. It was fabricated of aluminum alloy except for the headrest which was a glass reinforced polyester resin laminate over a wooden form. (See Figures 9 and 10).

The distance between the main side members of the seat structure was selected to fit the wind tunnel balance sleeve. This balance was supported by the tunnel sting from the ceiling of the 16 ft. x 16 ft. trasonic wind tunnel at AEDC. These side members also had mounting provisions for attaching the upper arm and leg instrumented beams, thus providing direct load paths for these members. The head sting was attached to a cross member between the two side members. The crewman model torso shell was also mounted to these side members. The remainder of the seat was for aerodynamic shaping and carried no major loads.

Half-Scale F-16 Forebody Model

The crewman/seat model described above was designed and manufactured by Payne, Inc., under a previous contract to determine the loads on a crewman when ejected from a high-speed aircraft. To determine the change in this loading when the crewman is in the proximity of the aircraft, a half-scale model of the nose and cockpit section of the U. S. Air Force F-16 fighter aircraft was constructed. To minimize cost, it was necessary to mount this forebody model

on an existing sting. It was necessary that the crewman/seat model be able to be displayed relative to the forebody model in a manner that would simulate an ejection from an operational aircraft.

Since the crewman/seat model and balance were designed to attach to a sting, it was decided to leave this arrangement unaltered, and allow all loads to be measured exactly as in previous tests. This then required a forebody model that could be supported directly from the same sting and could move relative to the crewman/seat model on a path parallel to that of the ejection seat rails (an inclination angle of approximately $55^\circ 30$ from a water line). By mounting the forebody on the crewman/seat model sting the two could be inclined in pitch, and moved in yaw with the control mechanisms already available. The Forebody/Crewman/seat model assembly is shown in Figure 11.

Forebody Basic Structure

The major load carrying structure of the forebody--a central keel--was constructed of metal elements (Fig.re 12). Two steel tracks were attached to the center aluminum structure of the model. The tracks were inclined at an angle of $55^\circ 30$ from the water line. This center structure was integrated into a wooden structure consisting of wooden frames and bulkheads (Figure 13). These were planked with wooden splines, filled with polyester filler and sanded smooth. A glass reinforced polyester resin laminate was applied over the wood, sanded smooth (Figure 14), given a final coat of polyester gel coat and then painted (Figure 15).

Forebody/sting Attaching Structure

The existing wind tunnel sting was constructed of hardened high strength steel. Steel members were designed to clamp around this existing sting, and provide support for a system of track rollers which would guide the track fixed to the forebody structure (Figure 16). This then allowed the forebody structure to move with respect to the crewman/seat model along a line parallel to that of the seat track rollers.

To position the forebody with respect to the crewman/seat model a hydraulic cylinder with a stroke of 24 inches was attached at its fixed end to the pitch arms of the sting (Figure 17). The piston rod end was attached to the forebody structure just aft of the cockpit canopy area.

The relative position of the forebody and the crewman/seat model was measured by a ten turn potentiometer driven by a rack and pinion mechanism. The rack was fastened to the forebody and drove the pinion attached to the sting mounted track roller support structure (Figure 18).

Instrumentation on Forebody Model

Five dynamic pressure transducers were mounted in the cockpit region of the forebody model. Figure 19 shows the general location of the transducers. One transducer was also connected to a tap in the center of the crewman/seat model seat back in place of the static pressure tap.

These were Model EPG-400-25 hermetic pressure transducers manufactured by Entron Devices, Inc., and had a nominal resonant frequency of 25KHz.

Cockpit Accessories

A one-half scale model of the heads up display and gun sight was built and mounted in the appropriate area of the top portion of the instrument panel (Figure 20).

Along the right hand side of the cockpit a simulated side arm controller was also installed.

Alternate Model Configurations

Since it was desired to evaluate the crewman air loads with the canopy removed, with a windshield and with a flow diverter in place, a simulated windshield was fabricated to the forward canopy lines. This model addition could be attached over the front of the instrument panel to simulate a fixed windshield (Figure 21).

A flow diverter concept was also fabricated of metal and positioned to simulate a device that might be used to protect the pilot from windblast should the canopy be unexpectedly lost in flight. This is shown in Figure 22.

EXPERIMENTAL MEASUREMENTS

The model was tested at AEDC in the Propulsion Wind Tunnel (16T) (Figure 23) in accordance with the test matrices given in Table 4. The resulting data was presented in Reichenau (Reichenau, 1978). A detailed comparison of these data with those of the original crew member and seat alone (Figure 24) (Ervin, 1978; Anthony, 1978) is currently being prepared under Contract No. AF-F33615-79-C0927).

DISCUSSION

Gross Forces and Moments

The first question which arises concerns the overall validity of data which was obtained at rather low Reynolds numbers (Re). It was originally intended to test at a dynamic pressure of q_o= 600 lb/ft^2 which would have resulted in Re = 3 x 10^6 (per foot). Thus, a two inch diameter leg element would have had Re = 0.5 x 10^6, which is clearly supercritical. The highest values of q_o actually employed varied from 145 lb/ft^2 at M = 0.4 to 326 lb/ft^2 at M = 1.2. The Reynolds numbers actually employed 1 x 10^6 and 1.6 x 10^6 (per foot) so that the test Re was between one half and one third of the target values, giving 1.7 x 10^5–2.7 x 10^5 for the same two inch diameter limb. This is close to the range of transition from laminar to turbulent boundary layer flows for smooth circular cylinders. Thus there was a possibility that these data could not be applied to the full scale problem.

We first looked at some data from a previous contract (Ervin, 1978; Anthony, 1978) in which the same crewmember/seat combination was tested alone, over a dynamic pressure range of 40-150 lb/ft^2; as shown in Figures 26 to 29, the relationship between q_o and Re for those tests being given in Figure 25. In each case, the data for q_o= 100 and 150 lb/ft^2 was more or less in agreement, whereas both values and trends for q_o = 40 lb/ft^2 were quite different. It was concluded that this difference probably represented the difference between subcritical and supercritical flow, and that the q_o = 100 ft/lb^2 data were therefore useful. The lowest value in the present program (q_o = 145 lb/ft^2) was comfortably above this figure, and the Reynolds number difference was even greater.

The next step in validating the data was to compare it with the results of other experiments, both model and full scale, itemized in Table 1, and plotted in Figures 30 to 35.

In Figure 30, we see that the lift force on the man and seat alone (Ervin, 1978) compares well with that measured on the full scale Aces II seat at a lower Mach number; which alone is sufficient to explain the differences. The lift in proximity to fuselage—even at the 24 inch separation--is significantly higher, indicating a strong interference effect. This is reasonable, being equivalent to a pitch angle increase of roughly 15°.

Figure 31 shows the model drag to be between 60% and 75% of the full scale value. This might be explained by the difference between the smooth highly polished man model and the clothed, deformable live human subjects used in the full scale tests. (Earlier work [Payne, 1975] has shown flapping clothing to give a 25% drag increase.) Thus, the drag differences can be regarded as

-12-

explained. The further reduction due to fuselage proximity is readily under-
standable as an interference effect (about 10° increase in effective pitch
angle) of the same type as that which caused the life increase.

The side force due to yaw comparison in Figure 32 is also good, and
increases our confidence in the data. The small increase due to fuselage
proximity is again an anticipated interference effect because the seat/man
is in the sidewash of the yawed fuselage, and thus has an effectively
increased yaw angle.

The markedly reduced pitching moments shown in Figure 33 are probably
due to a combination of factors. The reduced drag noted earlier almost cer-
tainly gives a change in the drag center, and pitching moment is very sensi-
tive to small variations in the nominal CG point about which moments are
measured—as one might suspect from the wide variations shown for the other
test seats.

Both yawing and rolling moments (Figure 34 and 35) conform to the full
scale values quite well at low yaw angles, but fall off uncharacteristically
at 30° yaw. Presumably the same flow field change is responsible for both
effects, but its precise nature cannot be positively identified at this time.
Some form of flow separation is clearly occurring at a lower angle than in
the full scale tests, and presumably this is due to the lower Reynolds num-
ber. In low speed wing experience, it is typically found that, even though
the flow is supercritical at low angles, stall occurs at a lower lift
coefficient (C_L) (and therefore angle of attack) for the lower Reynolds
numbers.* In other words, $C_{L \ MAX}$ falls off with diminishing Reynolds numbers.

The foregoing analysis would seem to indicate that the data obtained in
the present program are, in fact, supercritical and applicable to the full
scale problem.

Table 1. Ejection Seat Data in Figures 30-35.

Code	Seat Type	Mach No.		Seat Back Angle During Tests When Angle of Attack = 0°
A[1]	Model Seat	0.4	Visconti, Nuber 1951	0°
A	Model Seat	0.8	Visconti, Nuber 1951	0°
C	Model Seat	0.6	Reichenau, 1969	0°
D	F-101 Seat	0.2	Glaigher, 1972	6°
B	F-101 Seat	≈ 0.16	Payne et al, 1975	13°
E	ACES-II Seat	≈ 0.16	Payne et al, 1975	13°

*See, for example, Page 30 of Reference 11, and Chapter 4 of Reference 12.

The Effect of Limb Flail on Gross Moments and Forces

The flailing arm and leg position are illustrated in Figure 36. Table 2 shows their effects on the pitching and yaw moments at zero pitch and yaw.

While the effects of pitching moment are not large – roughly a 10% change – the effect of the relatively small limb displacements on yawing moment is surprisingly large. For a yaw moment of inertia of 10 slugs ft , and M = 0.4, the combination of flailed leg and arm gives a yawing moment of 89.2 lb ft, and a yawing acceleration of $511^{\circ}/sec^2$.* Thus, at the end of a tenth of a second, a yaw excursion of 2.6° would have been achieved, with an angular velocity of $51^{\circ}/sec$. This is quite a major perturbation compared with the symmetrical conditions normally used in tests.

Table 2. Effect of flailing limbs on gross yawing and pitching moments (full scale values) for M = 0.4.

	Pitching Moment Volume (ft^2)	Yawing Moment Volume (ft^2)
Symmetrical conditions	-0.608	+0.048
Flailing arm only	-0.528	-0.168
Flailing leg only	-0.512	+0.184
Flailing arm and leg	-0.480	-0.376

The Effect of Separation Distance on Limb Flail Force

Figures 37 to 39 show typical outward acting forces on the limbs as a function of separation distance. While most of the trends are as might be expected, there is an enormous and surprising magnification of the upper arm "out" force in close proximity to the cockpit. The separation distance where this maximum occurs is very dependent on the cockpit configuration, as Table 3 shows. Again, it should be pointed out that the forces presented here were calculated by assuming a linear load distribution acting on the upper and lower portions of the arm. Furthermore, the force and moment contributions applied by the lower arm to the upper arm were subtracted out.

*If I = moment of inertia in yaw, = yaw angle, and M is the applied moment.
$$I \ddot{\psi} = M \text{ so } \dot{\psi} = (M/_I)t, \psi = (M/_I)t^2/_2.$$

14

Table 3. Maximum upper arm "out" force areas in comparison with free-stream values.

	Basic Cockpit	Flow Diverter	Windshield
Maximum (full scale) out force area (ft^2)	3.04	3.14	2.6
Critical (full scale) separation height (ins)	18.0	37.0	23.0
Free stream force area (ft^2)	1.41	1.41	1.41

The largest magnification occurs with the flow diverter, and is equal to an 122% increase. At M = 0.6 this critical outward force corresponds* to 1677 lb acting outwardly on the upper arm, instead of the free-stream value of 753 lb. We thus see that a relatively trivial variation in cockpit geometry can have a major effect on flail potential forces; and certainly not an effect which was anticipated.

The other limb segments do not experience anything like this variation, although there is a 20% increase in upper leg out force when no flow divertering devices are fitted.

The in-plane forces of limb lift and drag are plotted in Figures 40-42. There is some magnification of upper arm drag, particularly with the flow diverter (35%) and of the upper leg lift. The maximum value of the latter is 1.12 ft^2 (full scale) again with the flow diverter, and at the same separation as the maximum out-force on the upper arm occurs. This force area corresponds (at M = 0.6, sea level) to a lift force of 598 lb, compared with almost zero in the undisturbed free-stream.

Helmet Forces

Typical (zero yaw) helmet lift areas are plotted in Figure 43 in comparison with full scale low speed (M <0.2) data (Payne et al, 1975, and Cowgill, et al 1978). For M = 0.4 and 0.6 the data are in good agreement with Payne, and about twice as large as the Cowgill data. Transonically, the force area is significantly larger so that whereas we had previously estimated a helmet lift force of 600 lb at M = 1.0, sea level, this must now be revised to as much as 900 lb.

*Force is equal to the product of the force area and the free-stream dynamic pressure.

Typical helmet drag areas are given in Figure 44. Here the data (Payne, 1975 and Cowgill, 1978) are more or less in agreement; the half scale model data is very much lower. Presumably this is because the head, face mask and helmet are much smoother than the full scale articles, and do not contain gaps and joints.

Once again the transonic values are much higher, and we may expect a sea level drag force in excess of 700 lb at M = 1.0.

Figures 45-56 show the effect of seat separation distance on helmet lift and drag for the three different cockpit configurations. In nearly all cases, there is an intermediate separation distance where the forces are somewhat greater than at the furthest separation. The windshield reduces the peak forces somewhat; the flow diverter increases them slightly.

With either device there is still significant lift on the helmet when the crewmember is fully inside the cockpit (zero separation). The relevant force areas are plotted in Figure 57, and show a fairly simple trend to increasing lift with Mach number for the basic cockpit configuration. Addition of the windshield results in increased lift at M = 0.4 but thereafter a diminution. This behavior suggests that a shock starts to form over the windshield just above M = 0.4, deflecting the flow aft and slightly down into the cockpit, the deflection increasing with increasing M. (This hypothesis is supported by the drag area variation plotted in Figure 59)

The flow diverter causes a very strange "bucket" in the helmet lift area at M = 0.8, which however, is not reflected in the Figure 59 drag data. Since this might be thought to be due to a simple "bad data" point, we have added the data for $\pm 5°$ pitch to Figure 57 to show the phenomenon is consistent. Presumably it is again due to shock wave formation above the diverter, occuring at a higher Mach number because the flow diverter is considerably smaller than the windshield.

The corresponding (zero pitch) helmet lift forces are shown in Figure 58. Even at M = 0.4, the lift is 40 lb; sufficiently great to be a considerable embarrassment, especially if buffeting is also occurring. The transonic values of several hundred pounds would of course be intolerable if the helmet strap were strong enough to react it. In practice, helmet loss would occur at all the speeds tested.

The drag force areas are given in Figure 59 and the corresponding forces in Figure 60. While the figures for the open cockpit are unremarkable, there is a change from negative drag with the windshield at low speeds to positive drag above M = 0.78; a change compatible with the progressively deflected flow hypothesis mentioned above.

With the diverter, the drag is always negative; the reversed flow being strong enough to give a negative drag of 40-80 lbs at transonic speeds. It is unlikely that this could occur without severe buffeting.
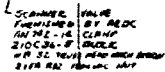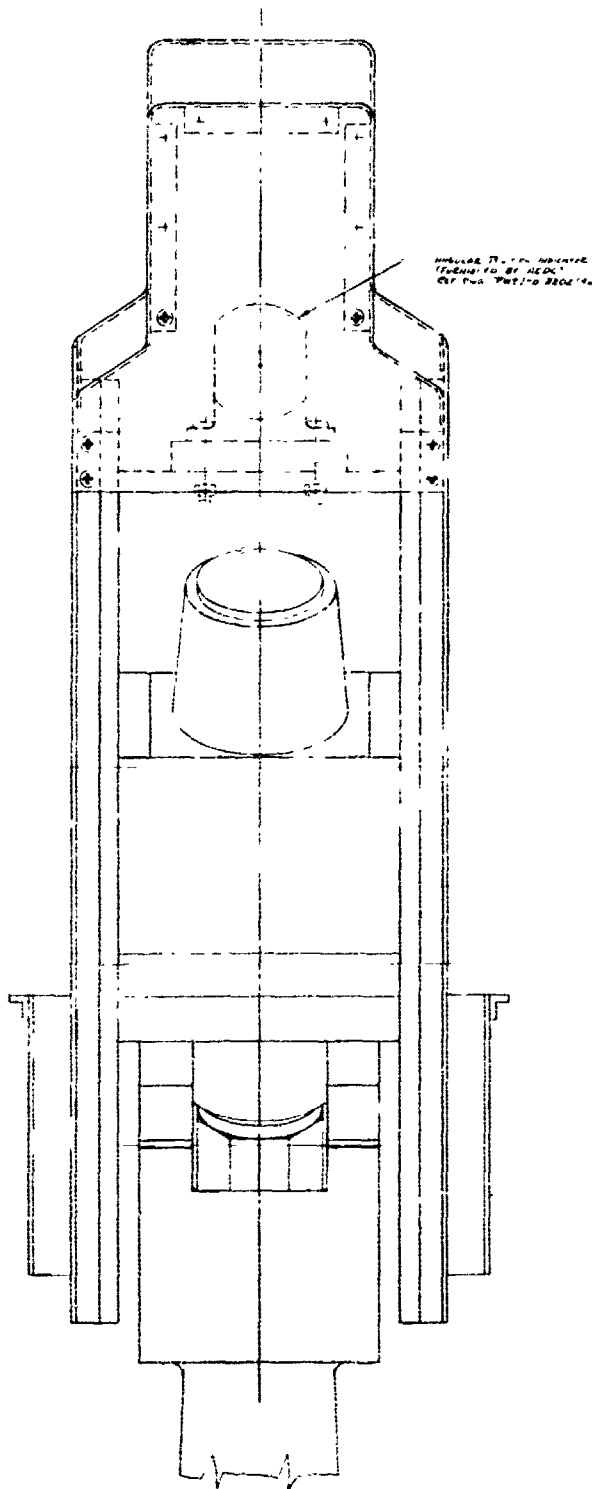
-16-

Figure 1a. Crewman model and seat assembly, half-scale, 50th percentile.

Figure 1b. Crewman model and seat assembly, half-scale, 50th percentile.

Figure 1c. Crewman model and seat
assembly, half-scale, 50th percentile.
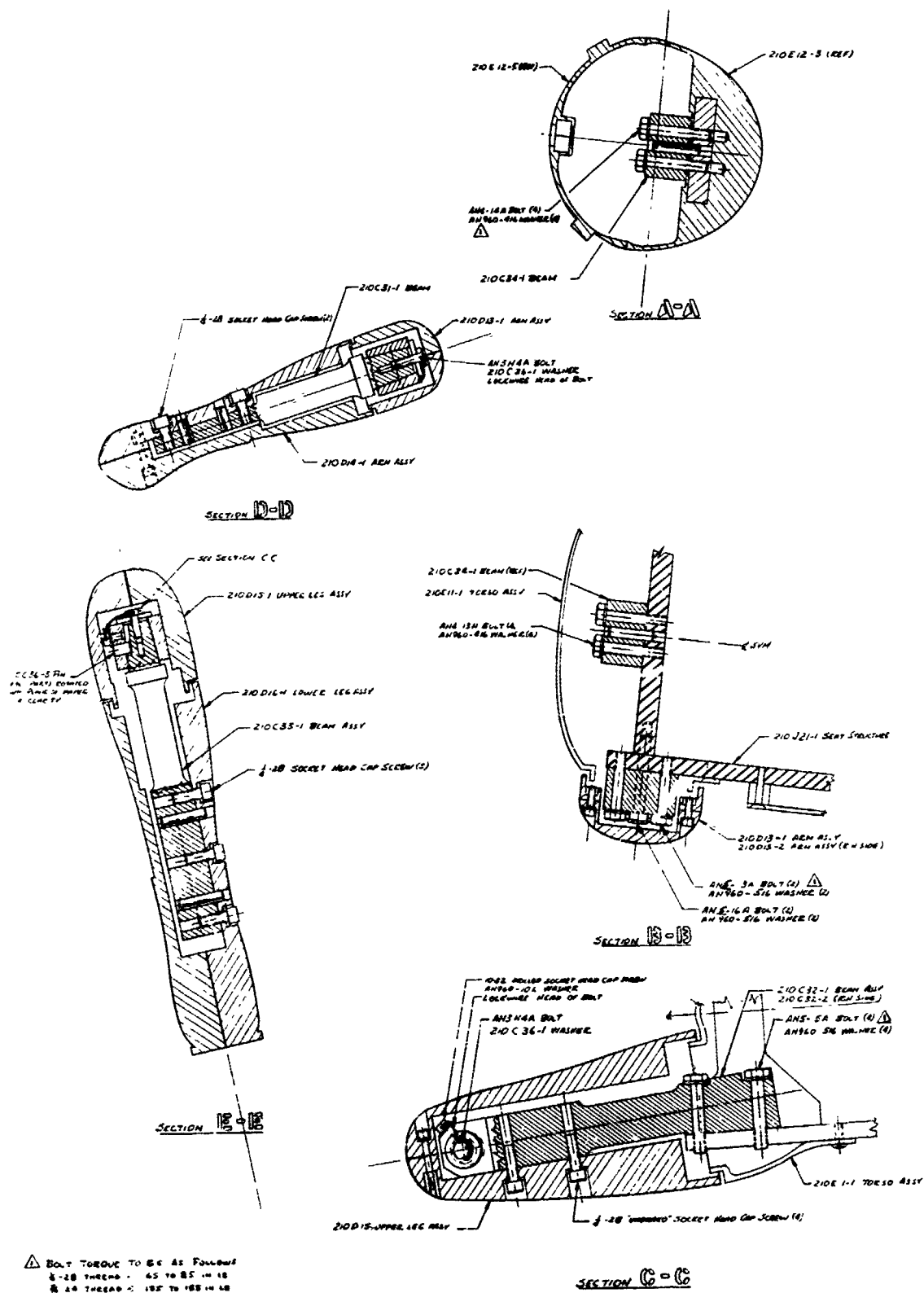
Figure 1d. Crewman model and seat assembly, half-scale, 50th percentile.
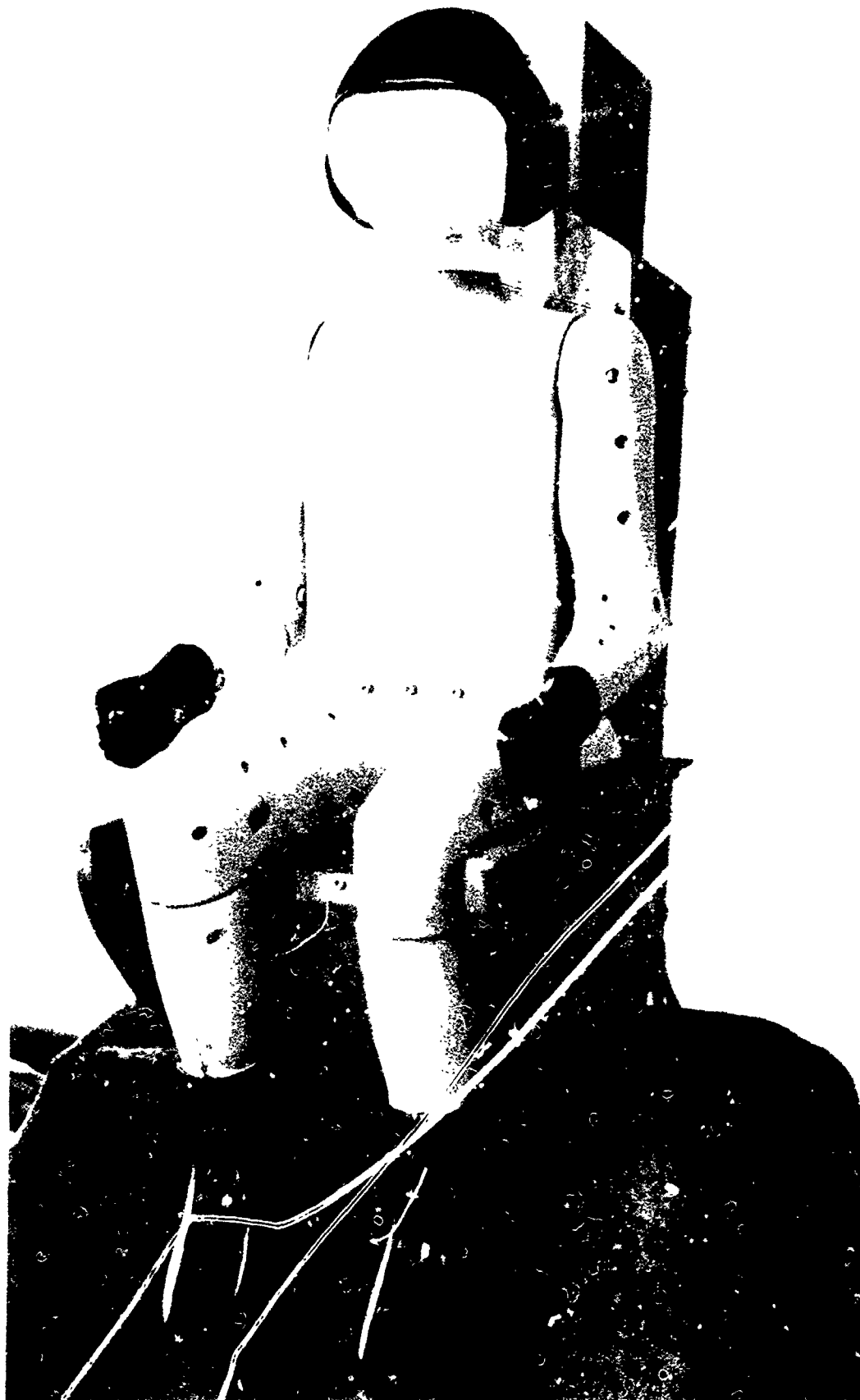
Figure 2. Half-scale crew member and ACES II seat.

-16-
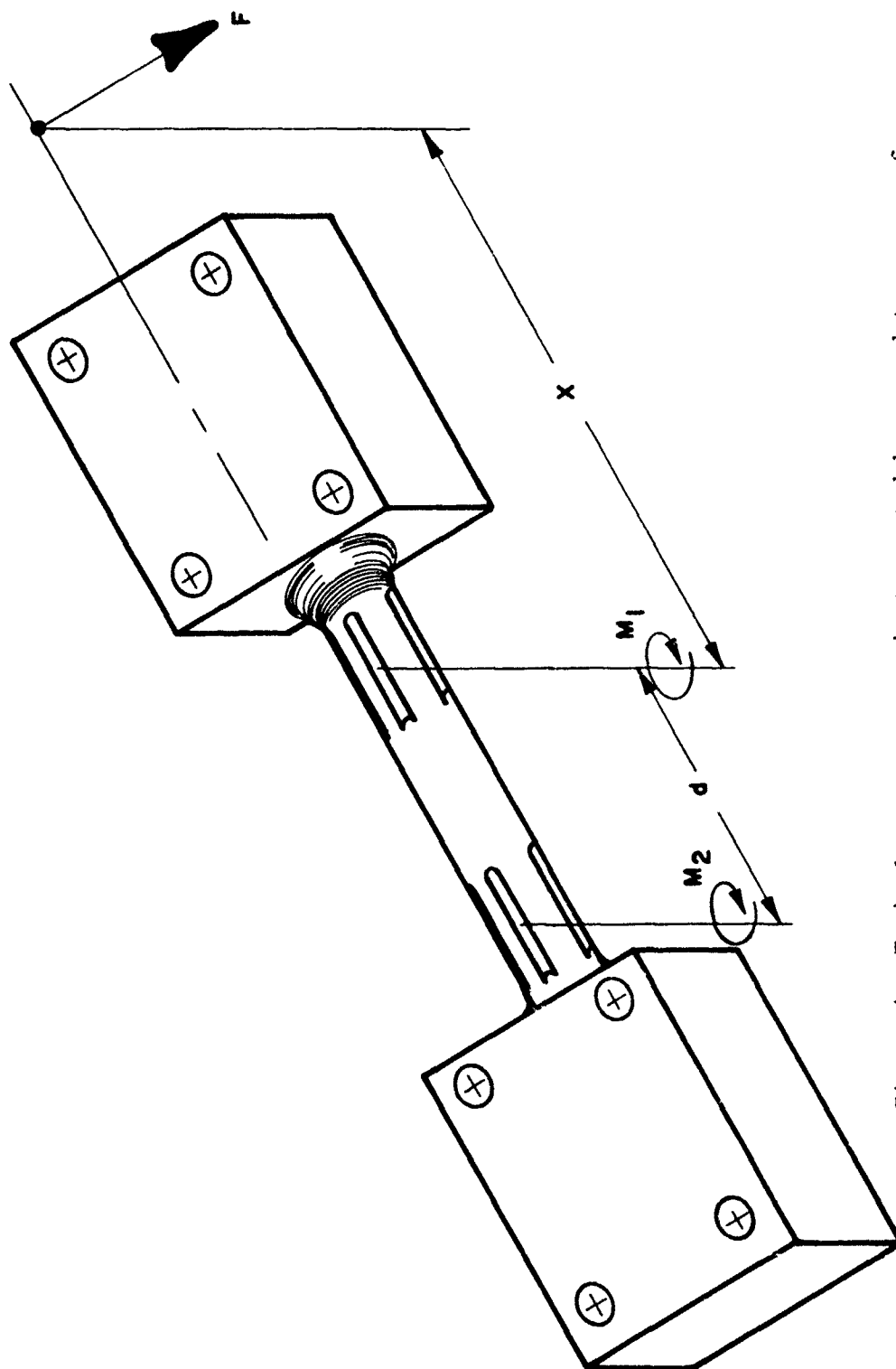
Figure 4. Typical two component instrumented beam used to measure forces and moments normal to the beam axis.
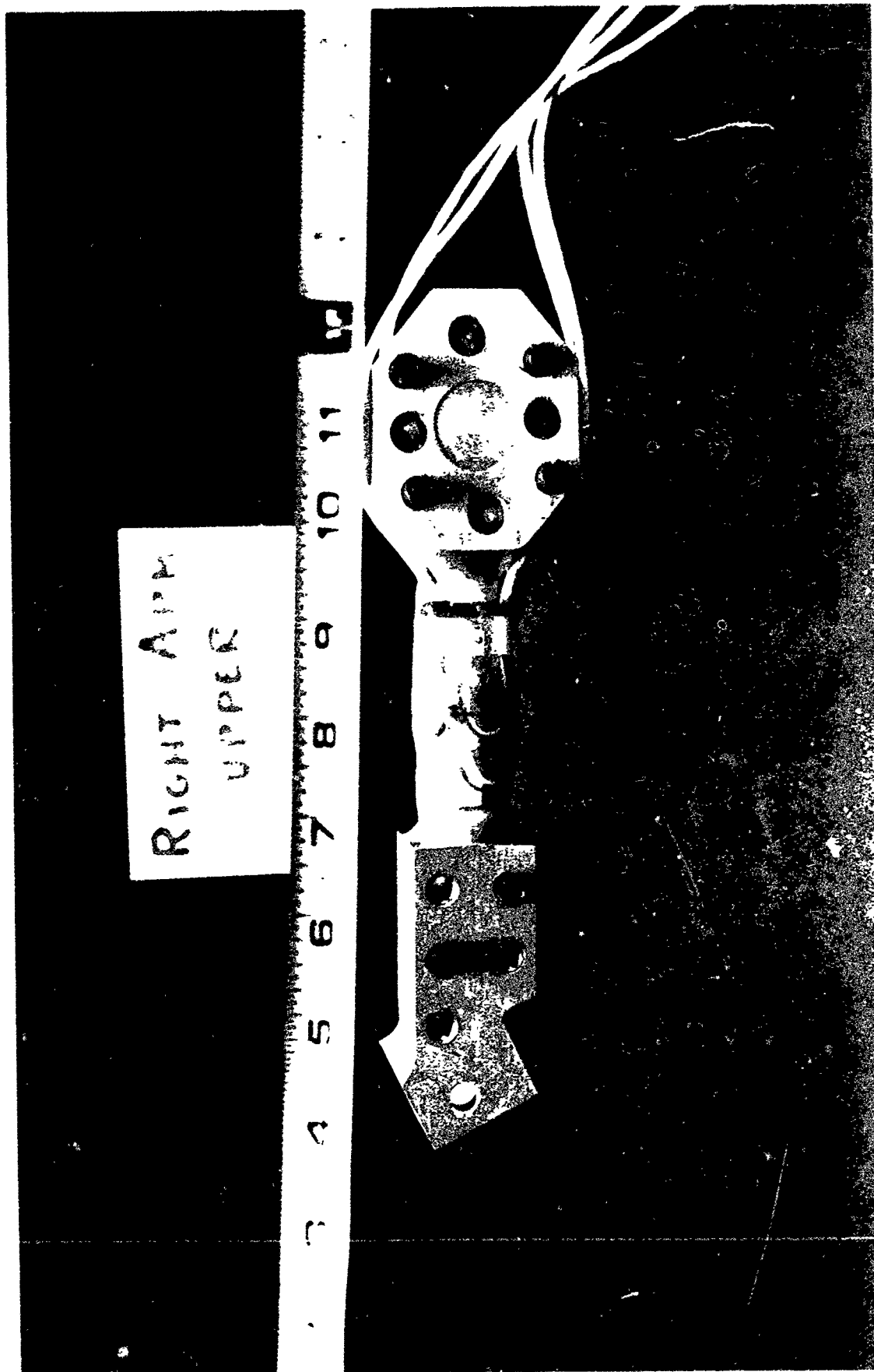
Figure 5. Typical strain gauge installation on an truncated beam.

Figure 6. Strain gauge and C-G Locating Dimensions
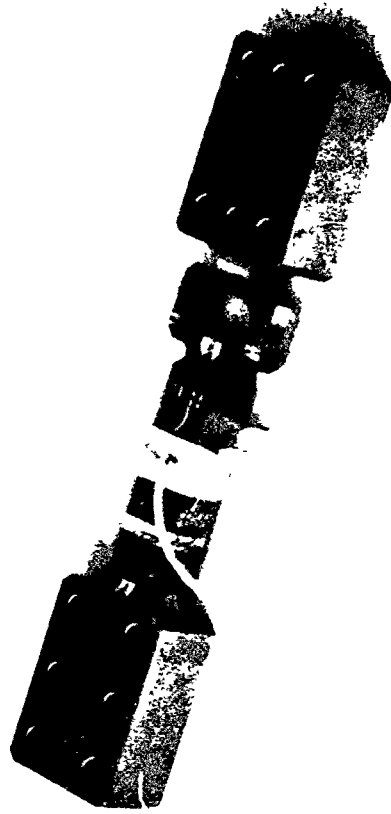
Figure 7. Three component head sting.

-23-

LEGEND

PSH   =   Pressure Static Head
PSSBR   =   Pressure Static Seat
            Back Reference
PSC   =   Pressure Static Chest
PSA   =   Pressure Static Abdomen
PSLL   =   Pressure Static Leg Left
PSLR   =   Pressure Static Leg Right
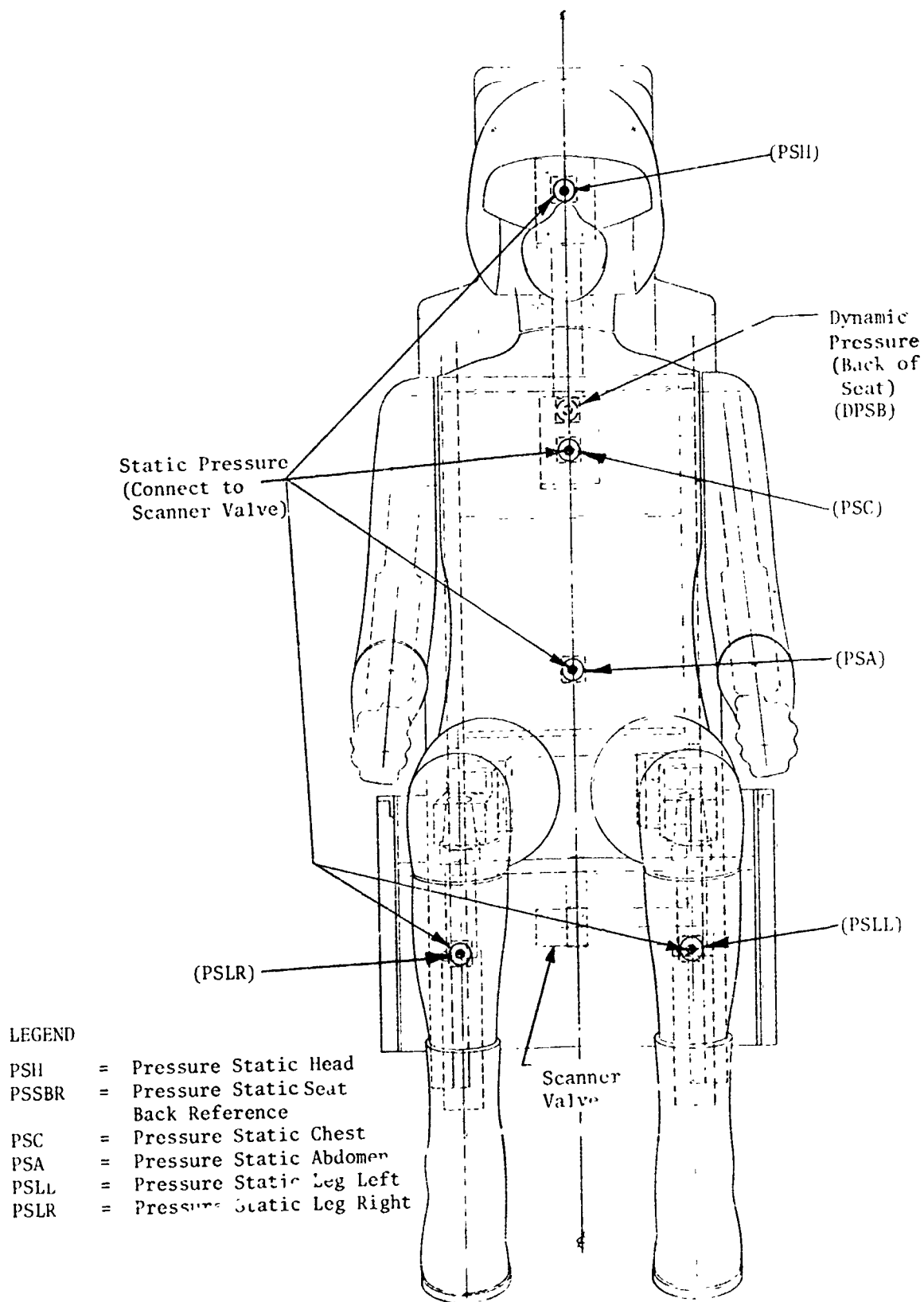
Figure 8.   Sketch showing location of pressure taps
            and scanner valve.

Figure ... full scale ... M... Function ...

Figure 33. Half-scale model box plow section, side view.

Figure 11. Fore body and r an/
seat assembly, half-scale
(1-16, 50%, XCI 3 I).

-27-

Figure 12. Minimum center structure of the half-scale
1/16 forebody model

Figure 15. Forklid Gas Manifolds prior to Integration

Figure 14   Glass reinforced polyester laminate over forebody substructure and planking.
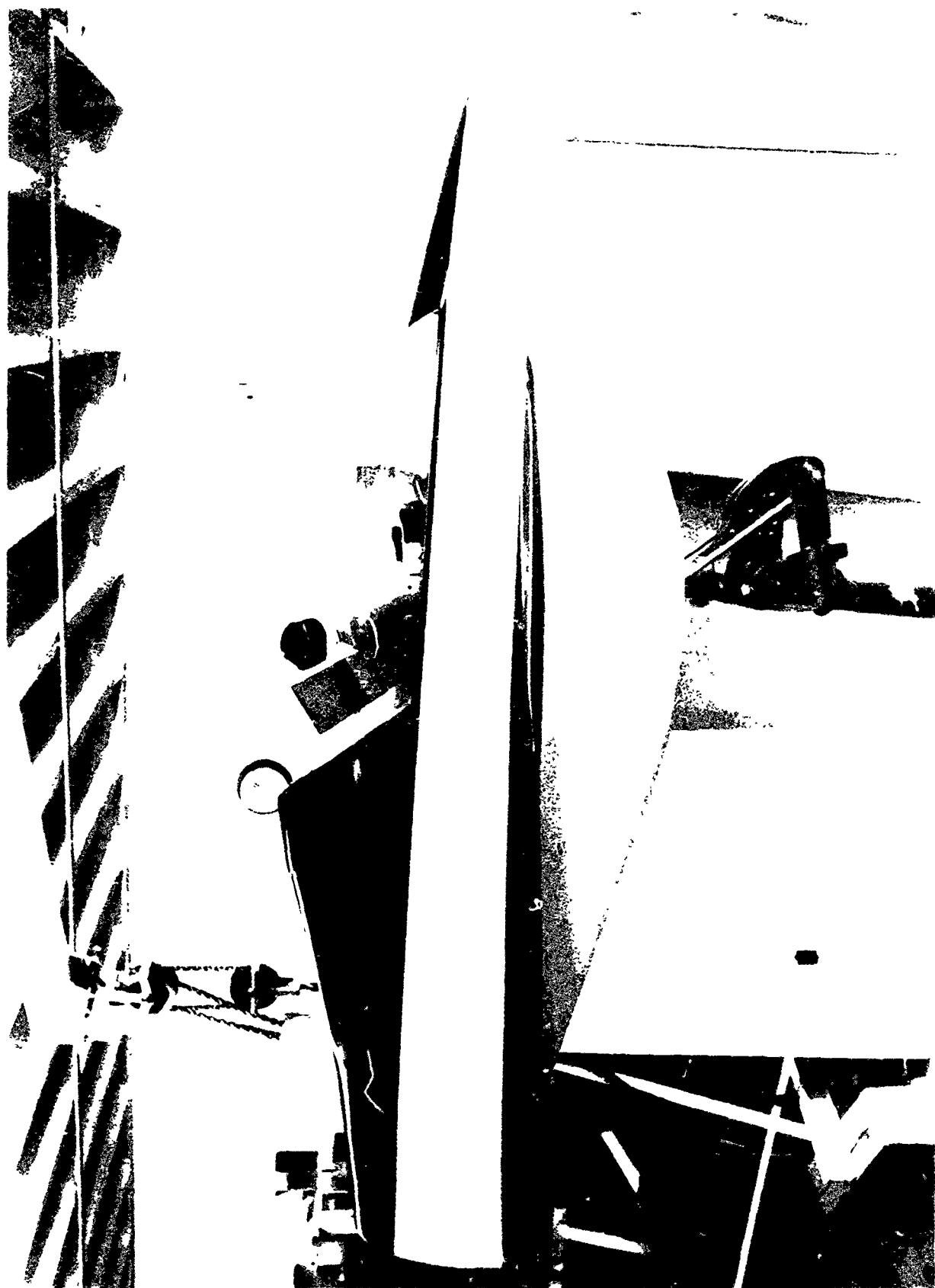
Figure 15. Left forebody/crewman/seat model completed.
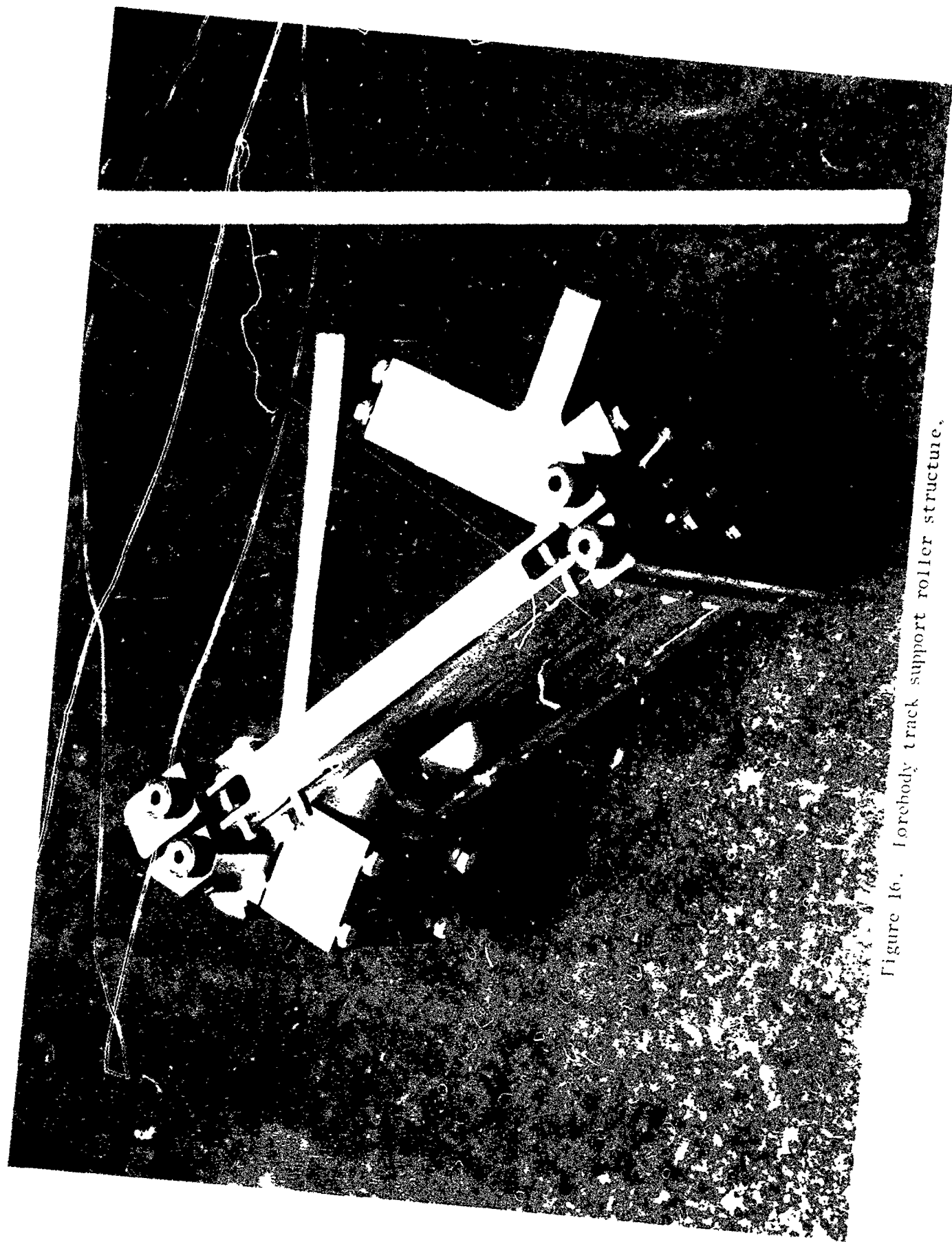
Figure 16. Forebody track support roller structure.
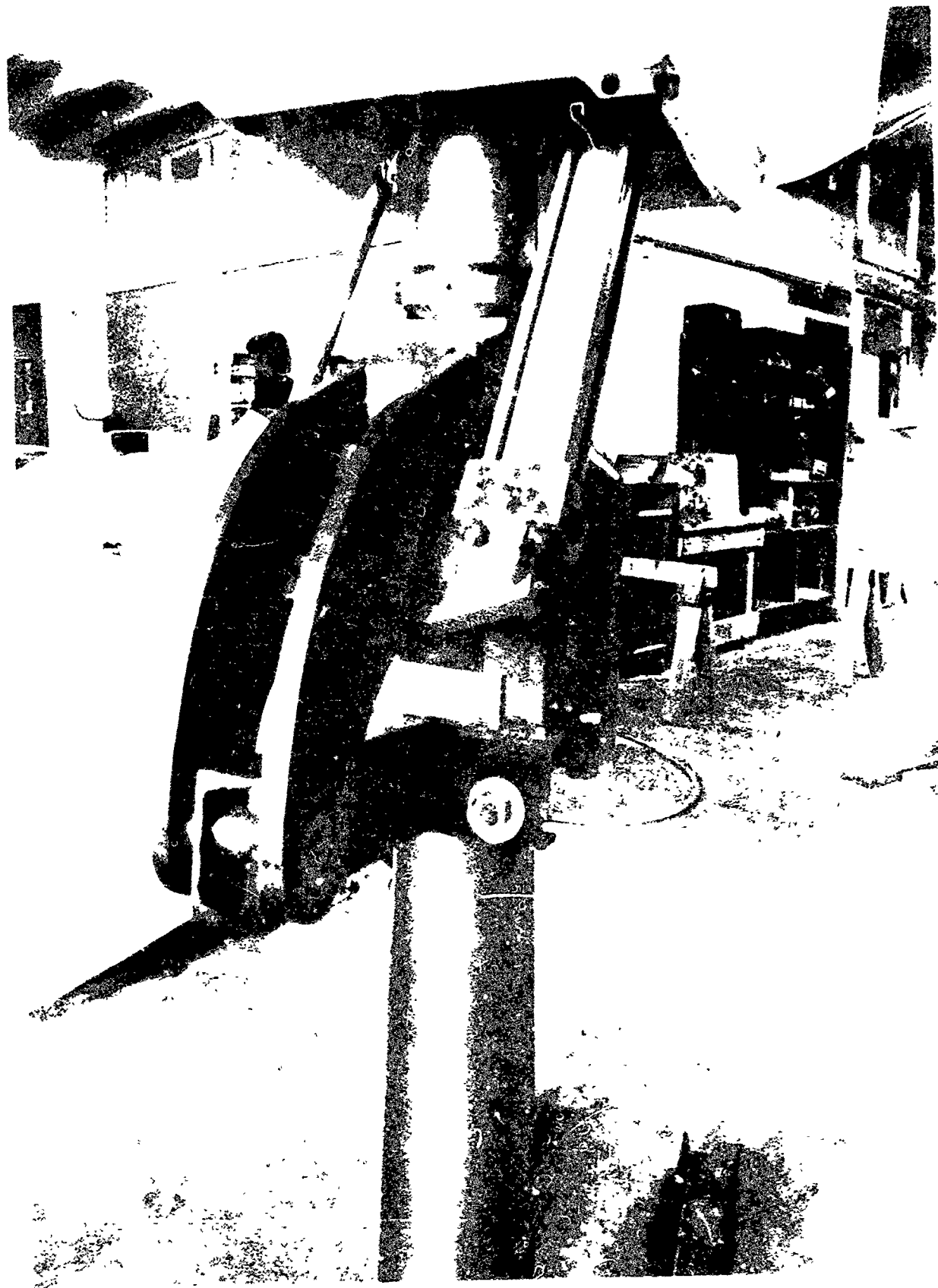
Figure 17. Attachment of cylinder to pitch arms
of wind tunnel scale.

Figure 18. Forebody position indicator potentiometer drive.

Legend

DPP   - Dynamic Pressure Panel
DPSR - Dynamic Pressure Seat Right
DPSL - Dynamic Pressure Seat Left
DPSB - Dynamic Pressure Seat Back
DPCR - Dynamic Pressure Canopy Right
DPCL - Dynamic Pressure Canopy Left

Figure 19. Forebody Pressure Transducer location

-55-
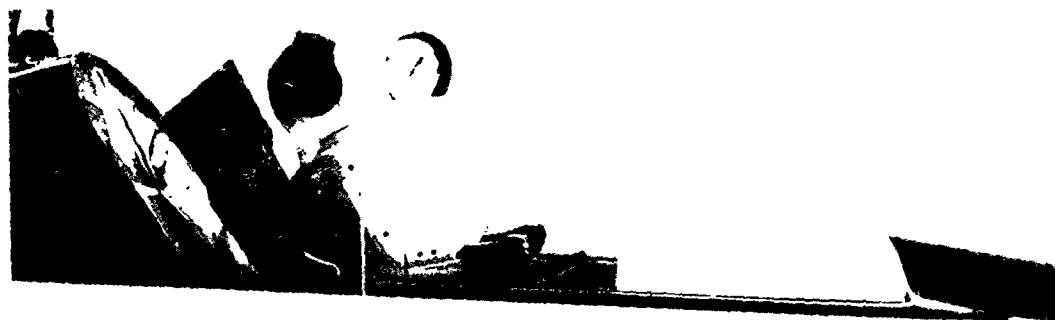
Figure 20. Forebody cockpit area showing heads up display and gunsight models.
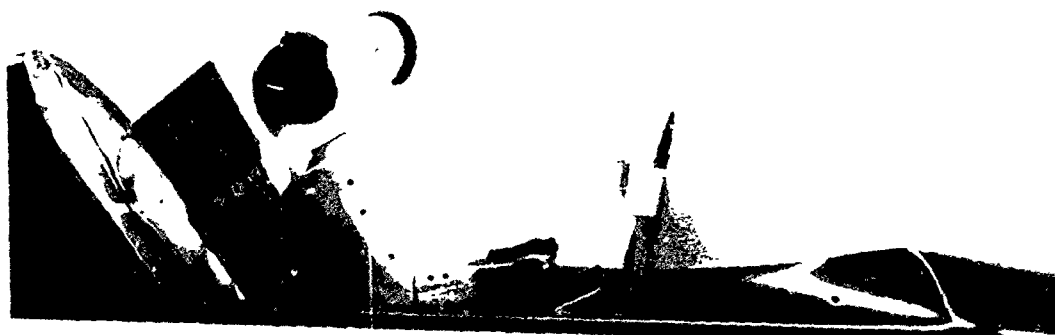
Figure 21. Forebody cockpit with windshield installed.
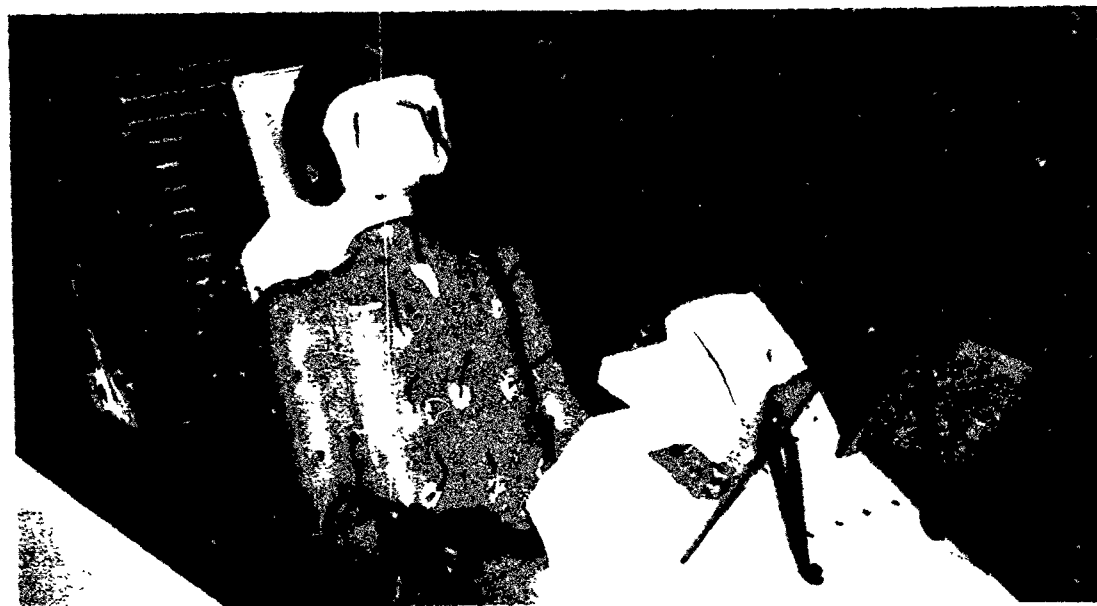
Figure 22. Forebody cockpit with flow diverter installed.

TABLE 4. Test Matrix Summary

PART NO., PN	MACH NO., M	DYNAMIC PRESSURE Q (PSF)	FOREBODY ANGLE OF ATTACK, AFFI6 (DEG.)	MODEL ANGLE OF SIDESLIP, BETAM (DEG.)	MAN/SEAT FOREBODY SEPARATION EJPOS (IN.)	MODEL CONFIGURATION	REMARKS
36	0.60	207	Variable (-5,0,5,10)	0	0.1	Basic Model	Large zero shifts on limb strain gauges during parts 36 and 37. Analog Tape Data
37	0.60	207	Variable (-5,0,5,10)	0	12.0		
42	0.40	145	Variable (-5,0,5,10) (0.5 missing)	0	0.1		Zero shifts on FHZ, FHZR, and FHYL during parts 42 through 51. Analog Tape Data
43	0.40	145	Variable (-5,0,5,10)	5	0.1		
44	0.40	145	Variable (-5,0,5,10)	5	6.0		
45	0.40	145	Variable (-5,0,5,10)	0	6.0		
46	0.40	145	Variable (-5,0,5,10)	0	12.0		
47	0.40	145	Variable (-5,0,5,10)	5	12.0		
48	0.40	145	Variable (-5,0,5,10)	5	18.0		
49	0.40	145	Variable (-5,0,5,10)	0	18.0		
50	0.40	145	(-5 missing)	0	23.6		
51	0.40	145	Variable (-5,0,5,10)	5	23.6		
55	0.60	207	Variable (-5,0,5,10)	0	0.1		Zero shifts on FHZ, FHZL and FHYL during parts 55 through 96. Analog Tape Data
56	0.60	207	Variable (-5,0,5,10)	5	0.1		
57	1.60	207	Variable (0,5,10)	5	6.0		
58	0.60	207	Variable (5,0,-5)	0	6.0		
59	0.66	207	Variable (-5,0,5,10)	0	12.0		
60	0.60	207	Variable (-5,0,5,10)	5	12.0		
61	0.60	207	Variable (-5,0,5,10)	5	18.0		
62	0.60	207	Variable (-5,0,5,10)	0	18.0		
63	0.60	207	Variable (-5,0,5,10)	0	23.2		
64	0.60	207	Variable (10 missing)	5	23.2		
65	0.80	258	Variable (-5,0,5,10)	0	0.2		
66	0.80	258	Variable (-5,0,5,10)	5	0.2		
67	0.80	258	Variable (-5,0,5,10)	5	6.0		
68	0.80	258	Variable (-5,0,5,10)	0	12.0		
69	0.80	258	Variable (-5,0,5,10)	0	12.0		
70	0.80	258	Variable (-5,0,5,10)	5	12.0		
71	0.80	258	Variable (0,5,10)	5	18.0		
72	0.80	258	Variable (0,5,10)	0	18.0		

TABLE 4 (a).

PART NO., PN	MACH NO., M	DYNAMIC PRESSURE Q (PSF)	FOREBODY ANGLE OF ATTACK, AFF16 (DEG.)	MODEL ANGLE OF SIDESLIP, BETAM (DEG.)	MAN/SEAT FOREBODY SEPARATION EJPOS (IN.)	MODEL CONFIGURATION	REMARKS
73	0.80	258	Variable (-5,0,5,10)	0	23.4	Basic Model	Analog Tape Data
74	0.80	258	Variable (0,5,10)	5	23.4		
75	1.00	298	Variable (-5,0,5,10)	0	0.1		
76	1.00	298	Variable (-5,0,5,10)	5	0.1		
77	1.00	298	Variable (-5,0,5,10)	5	6.0		
78	1.00	298	Variable (-5,0,5,10)	0	6.0		
79	1.00	298	Variable (-5,0,5,10)	0	12.0		
80	1.00	298	Variable (5,10)	5	12.0		
81	1.00	186	Variable (-5,0,5,10)	5	12.0		
82	1.00	186	Variable (-5,0,5,10)	5	18.0		
83	1.00	186	Variable (-5,0,5,10)	0	18.0		
84	1.00	186	Variable (-5,0,5,10)	0	23.5		
85	1.00	186	Variable (-5,0,5,10)	5	23.5		
86	1.20	526	Variable (-5,0,5,10)	0	0.0		
87	1.20	526	Variable (-5,0,5,10)	5	0.0		
88	1.20	526	Variable (-5,0,5,10)	5	6.1		
89	1.20	526	Variable (-5,0,5,10)	0	6.1		
90	1.20	526	Variable (-5,0,5,10)	0	12.0		
91	1.20	204	Variable (-5,0,5,10)	0	12.0		
92	1.20	204	Variable (-5,0,5,10)	5	12.0		
93	1.20	204	Variable (-5,0,5,10)	5	18.0		
94	1.20	204	Variable (0,5,10)	0	18.0		
95	1.20	204	Variable (-5,0,5,10)	5	25.2		
96	1.20	204	Variable (-5,0,5,10)	5	25.2		
100	0.10	115	Variable (-5,0,5,10)	0	0.1	Basic Model Plus Windshield	Zero shifts on INCR and THYL during parts 100 through 102. Analog Tape Data
101	0.40	115	Variable (-5,0,5,10)	5	0.1		
102	0.40	145	Variable (-5,0,5,10) (-5 missing)	5	6.0		

TABLE 4 (b).

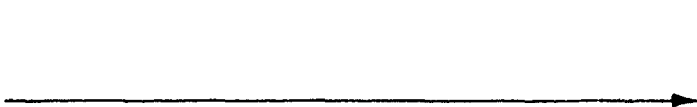| PART NO., PN	MACH NO., M	DYNAMIC PRESSURE Q (PSF)	FOREBODY ANGLE OF ATTACK, AFF16 (DEG.)	MODEL ANGLE OF SIDESLIP, BETAM (DEG.)	MAN/SEAT FOREBODY SEPARATION EJPOS (IN.)	MODEL CONFIGURATION	REMARKS
112	0.60	207	Variable (-5,0,5,10)	0	0.1	Basic Model Plus Flow Diverter	Analog Tape Data. Large zero shifts on limb strain gauges during parts 112 through 115.
113	0.60	207	Variable (-5,0,5,10)	5	0.1		Analog Tape Data.
114	0.60	207	Variable (-5,0,5,10)	5	18.0		
115	0.60	207	Variable (-5,0,5,10)	0	18.0		
118	0.80	258	Variable (-5,0,5,10)	5	0.1		Zero shifts on FHZ and FHYL during parts 118 through 165.
119	0.80	258	Variable (-5,0,5,10)	5	0.1		
120	0.80	258	Variable (-5,0,5,10)	5	6.0		
121	0.80	258	Variable (-5,0,5,10)	0	6.0		
122	0.80	258	Variable (-5,0,5,10)	0	12.0		
123	0.80	258	Variable (-5,0,5,10)	5	12.0		
124	0.80	258	Variable (-5,0,5,10)	5	18.0		
125	0.80	258	Variable (-5,0,5,10)	0	18.0		
126	0.80	258	Variable (-5,0,5,10)	0	23.4		
127	0.80	258	Variable (0,5,10)	5	25.4		
128	1.00	186	Variable (-5,0,5,10)	0	0.1		
129	1.00	186	Variable (-5,0,5,10)	5	0.1		
130	1.00	186	Variable (-5,0,5,10)	5	6.0		
131	1.00	186	Variable (-5,0,5,10)	0	6.0		
132	1.00	186	Variable (-5,0,5,10)	0	12.0		
133	1.00	186	Variable (-5,0,5,10)	5	12.0		
134	1.00	186	Variable (-5,0,5,10)	5	18.0		
135	1.00	186	Variable (-5,0,5,10)	0	18.0		
136	1.00	186	Variable (-5,0,5,10)	0	23.4		
137	1.00	186	Variable (-5,0,5,10)	5	23.4		
138	1.20	204	Variable (-5,0,5,10)	5	0.1		
139	1.20	204	Variable (-5,0,5,10)	5	0.1		
140	1.20	204	Variable (-5,0,5,10)	5	6.0		
141	1.20	204	Variable (-5,0,5,10)	0	6.0		

TABLE 4 (c).

PART NO., PN	MACH NO., M	DYNAMIC PRESSURE Q (PSF)	FOREBODY ANGLE OF ATTACK, AFF16 (DEG.)	MODEL ANGLE OF SIDESLIP, BETAM (DEG.)	MAN/SEAT FOREBODY SEPARATION EJPOS (IN.)	MODEL CONFIGURATION	REMARKS
142	1.20	204	Variable (-5,0,5,10)	0	12.0	Basic Model Plus Flow Diverter	Analog Tape Data
143	1.20	204	Variable (-5,0,5,10)	5	12.0		
144	1.20	204	Variable (-5,0,5,10)	5	18.0		
145	1.20	204	Variable (-5,0,5,10)	0	18.0		
146	1.20	204	Variable (-5,0,5,10)	0	23.5		
147	1.20	204	Variable (-5,0,5,10)	5	23.5		
148	0.60	207	Variable (-5,0,5,10)	0	0.1		
149	0.60	207	Variable (-5,0,5,10)	5	0.1		
150	0.60	207	Variable (-5,0,5,10)	5	6.0		
151	0.60	207	Variable (-5,0,5,10)	0	6.0		
152	0.60	207	Variable (-5,0,5,10)	0	12.0		
153	0.60	20	Variable (-5,0,5,10)	5	12.0		
154	0.60	207	Variable (-5,0,5,10)	0	23.5		
155	0.60	207	Variable (-5,0,5,10)	5	23.5		
156	0.40	145	Variable (-5,0,5,10)	0	0.1		
157	0.40	145	Variable (-5,0,5,10)	5	0.1		
158	0.40	145	Variable (-5,0,5,10)	5	6.0		
159	0.40	145	Variable (-5,0,5,10)	0	6.0		
160	0.40	145	Variable (-5,0,5,10)	0	12.0		
161	0.40	145	Variable (-5,0,5,10)	5	12.0		
162	0.40	145	Variable (-5,0,5,10)	5	18.0		
163	0.40	145	Variable (-5,0,5,10)	0	18.0		
164	0.40	145	Variable (-5,0,5,10)	0	23.4		
165	0.40	145	Variable (-5,0,5,10)	5	23.1		
168	0.10	115	Variable (-5,0,5,10)	5	6.0	Basic Model Plus Wind-Shield	Zero shifts on FHE, FHEL and FHER during parts 168 through 218. Analog Tape Data
169	0.40	145	Variable (-5,0,5,10)	0	6.0		
170	0.40	145	Variable (-5,0,5,10)	5	12.0		

TABLE 4 (a).

PART NO., PN	MACH NO., M	DYNAMIC PRESSURE Q (PSF)	FOREBODY ANGLE OF ATTACK, AFF16 (DEG.)	MODEL ANGLE OF SIDESLIP, BETAM (DEG.)	MAN/SEAT FOREBODY SEPARATION EJPOS (IN.)	MODEL CONFIGURATION	REMARKS
171	0.40	145	Variable (-5,0,5,10)	5	12.0	Basic Model Plus Windshield	Analog Tape Data
172	0.40	145	Variable (-5,0,5,10)	5	18.0		
173	0.40	145	Variable (-5,0,5,10)	0	18.0		
174	0.40	145	Variable (-5,0,5,10)	0	23.5		
175	0.40	145	Variable (-5,0,5,10)	5	23.6		
176	0.60	207	Variable (-5,0,5,10)	0	0.0		
177	0.60	207	Variable (-5,0,5,10)	5	0.0		
178	0.60	207	Variable (-5,0,5,10)	5	6.0		
179	0.60	207	Variable (-5,0,5,10)	0	6.0		
180	0.60	207	Variable (-5,0,5,10)	0	12.0		
181	0.60	207	Variable (-5,0,5,10)	5	12.0		
182	0.60	207	Variable (-5,0,5,10)	5	18.0		
183	0.60	207	Variable (-5,0,5,10)	5	18.0		
184	0.60	207	Variable (-5,0,5,10)	0	18.0		
185	0.60	207	Variable (-5,0,5,10)	0	23.5		
186	0.60	207	Variable (-5,0,5,10)	5	23.5		
187	0.80	258	Variable (-5,0,5,10)	0	0.1		
188	0.80	258	Variable (-5,0,5,10)	5	0.1		
189	0.80	258	Variable (-5,0,5,10)	5	6.0		
190	0.80	258	Variable (-5,0,5,10)	0	6.0		
191	0.80	258	Variable (-5,0,5,10)	0	12.0		
192	0.80	258	Variable (-5,0,5,10)	5	12.0		
193	0.80	258	Variable (-5,0,5,10)	5	18.0		
194	0.80	258	Variable (-5,0,5,10)	0	18.0		
195	0.80	258	Variable (-5,0,5,10)	0	23.4		
196	0.80	258	Variable (-5,0,5,10)	5	23.4		
197	1.00	186	Variable (-5,0,5,10)	0	0.1		
198	1.00	186	Variable (-5,0,5,10)	5	0.1		

TABLE 4 (e).

PART NO., PN	MACH NO., M	DYNAMIC PRESSURE Q (PSF)	FOREBODY ANGLE OF ATTACK, AFF16 (DEG.)	MODEL ANGLE OF SIDESLIP, BETAM (DEG.)	MAN/SEAT FOREBODY SEPARATION EJPOS (IN.)	MODEL CONFIGUR—ATION	REMARKS
199	1.00	186	Variable (-5,0,5,10)	5	6.0	Basic Model Plus Wind-shield	Analog Tape Data
200	1.00	186	Variable (-5,0,5,10)	0	6.0		
201	1.00	186	Variable (-5,0,5,10)	5	12.0		
202	1.00	186	Variable (-5,0,5,10)	5	12.0		
203	1.00	186	Variable (-5,0,5,10)	5	18.0		
204	1.00	186	Variable (-5,0,5,10)	0	18.0		
205	1.00	186	Variable (-5,0,5,10)	0	23.3		
206	1.00	186	Variable (-5,0,5,10)	5	23.3		
207	1.20	204	Variable (-5,0,5,10)	0	0.1		
208	1.20	204	Variable (-5,0,5,10)	5	0.1		
209	1.20	204	Variable (-5,0,5,10)	5	6.0		
210	1.20	204	Variable (-5,0,5,10)	0	6.0		
211	1.20	204	Variable (-5,0,5,10)	0	12.0		
212	1.20	204	Variable (-5,0,5,10)	5	12.0		
213	1.20	204	Variable (-5,0,5,10)	5	18.0		
214	1.20	204	Variable (-5,0,5,10)	0	18.0		
215	1.20	204	Variable (-5,0,5,10)	0	23.4		
216	1.20	204	Variable (-5,0,5,10)	5	23.4		
217	0.40	145	Variable (-5,0,5,10)	0	0.1		
218	0.40	145	Variable (-5,0,5,10)	5	0.1		
229	0.60	207	Variable (-5,0,5,10)	0	18.0	Basic Model Plus Flail-ing Arm	Large zero shifts on limb strain gauges during parts 229 and 230. Analog Tape Data. Zero shifts on FHZ, FHYL and FHYR during parts 235 through 242. Analog Tape Data.
230	0.60	207	Variable (-5,0,5,10)	0	23.5		
233	0.60	207	Variable (-5,0,5,10)	0	18.0		
234	0.60	207	Variable (-5,0,5,10)	0	23.4		
235	0.80	258	Variable (-5,0,5,10)	0	25.4		
236	0.80	258	Variable (-5,0,5,10)	0	18.0		

TABLE 4 (f)

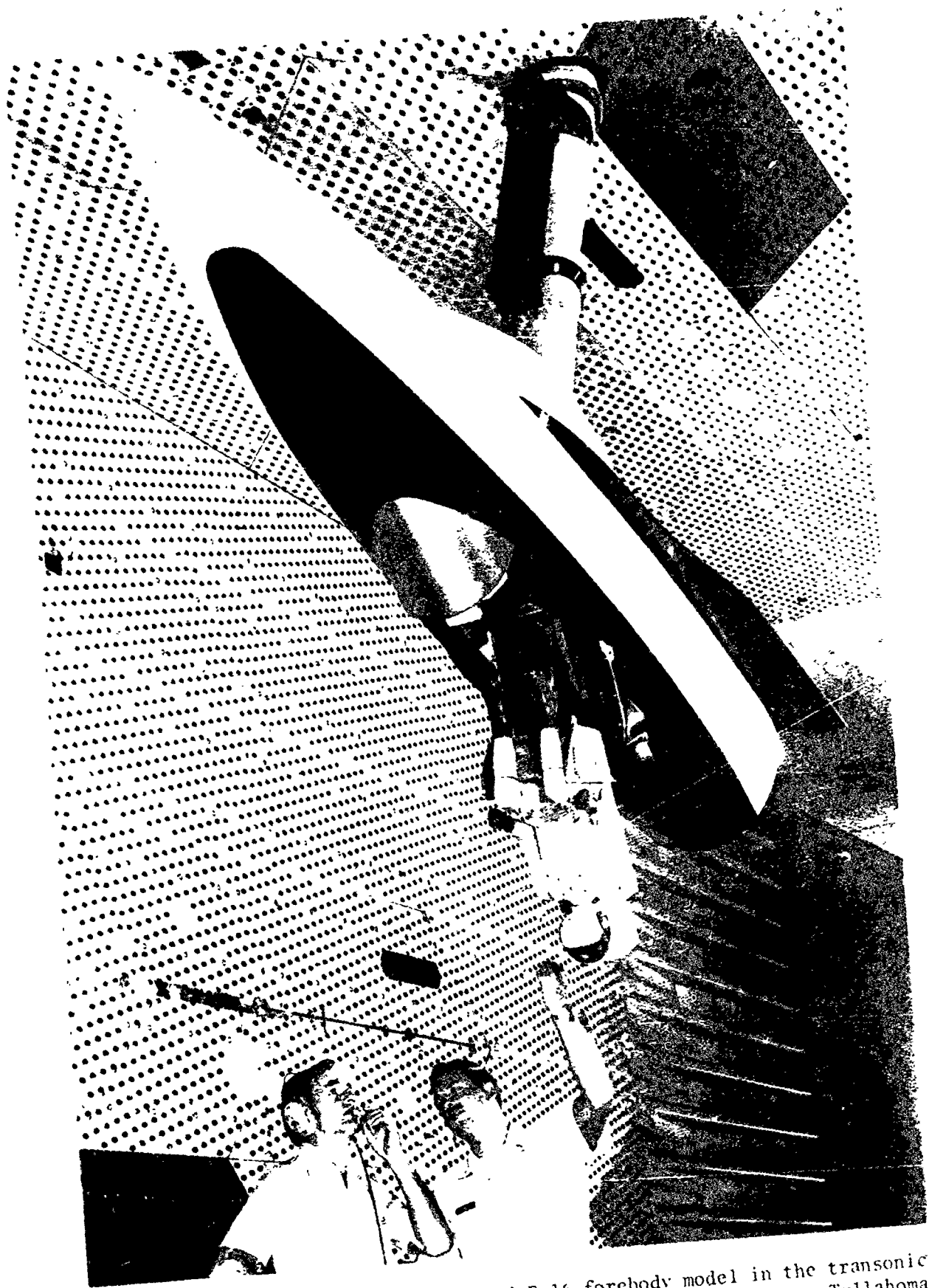| PART NO., PN	MACH NO., M	DYNAMIC PRESSURE Q (PSF)	FOREBODY ANGLE OF ATTACK, AFF16 (DEG.)	MODEL ANGLE OF SIDESLIP, BETAM (DEG.)	MAN/SEAT FOREBODY SEPARATION EJPOS (IN.)	MODEL CONFIGURATION	REMARKS
237	1.00	186	Variable (-5,0,5,10)	0	18.0	Basic Model Plus Flailing Arm	Analog Tape Data.
238	1.00	186	Variable (-5,0,5,10)	0	23.4		
239	1.20	204	Variable (-5,0,5,10)	0	23.4		
240	1.20	204	Variable (-5,0,5,10)	0	23.4		
241	0.40	145	Variable (-5,0,5,10)	0	18.0		
242	0.40	145	Variable (-5,0,5,10)	0	23.4		
247	0.40	145	Variable (-5,0,5,10)	0	18.0	Basic Model Plus Flailing Arm and Leg	Zero shifts on FHZ, FHYL and FHYR during parts 247 through 256.
248	0.40	145	Variable (-5,0,5,10)	0	23.4		
249	0.60	207	Variable (-5,0,5,10)	0	18.0		Analog Tape Data.
250	0.60	207	Variable (-5,0,5,10)	0	23.4		
251	0.80	258	Variable (-5,0,5,10)	0	18.0		
252	0.80	258	Variable (-5,0,5,10)	0	23.4		
253	1.00	186	Variable (-5,0,5,10)	0	18.0		
254	1.00	186	Variable (-5,0,5,10)	0	23.4		
255	1.20	204	Variable (-5,0,5,10)	0	18.0		
256	1.20	204	Variable (-5,0,5,10)	0	23.4		
260	0.40	145	Variable (-5,0,5,10)	0	18.0	Basic Model Plus Flailing Leg	Zero shifts on FHZ and FHYL during parts 260 through 269.
261	0.40	145	Variable (-5,0,5,10)	0	23.4		
262	0.60	207	Variable (-5,0,5,10)	0	18.0		Analog Tape Data.
263	0.60	207	Variable (-5,0,5,10)	0	23.4		
264	0.80	258	Variable (-5,0,5,10)	0	18.0		
265	0.80	258	Variable (-5,0,5,10)	0	23.4		
266	1.00	186	Variable (-5,0,5,10)	0	18.0		
267	1.00	186	Variable (-5,0,5,10)	0	23.4		
268	1.20	204	Variable (-5,0,5,10)	0	18.0		
269	1.20	204	Variable (-5,0,5,10)	0	23.4		

Figure 23. One half-scale crewman and F-16 forebody model in the transonic wind tunnel at Arnold Engineering Development Center, Tullahoma, Tennessee.
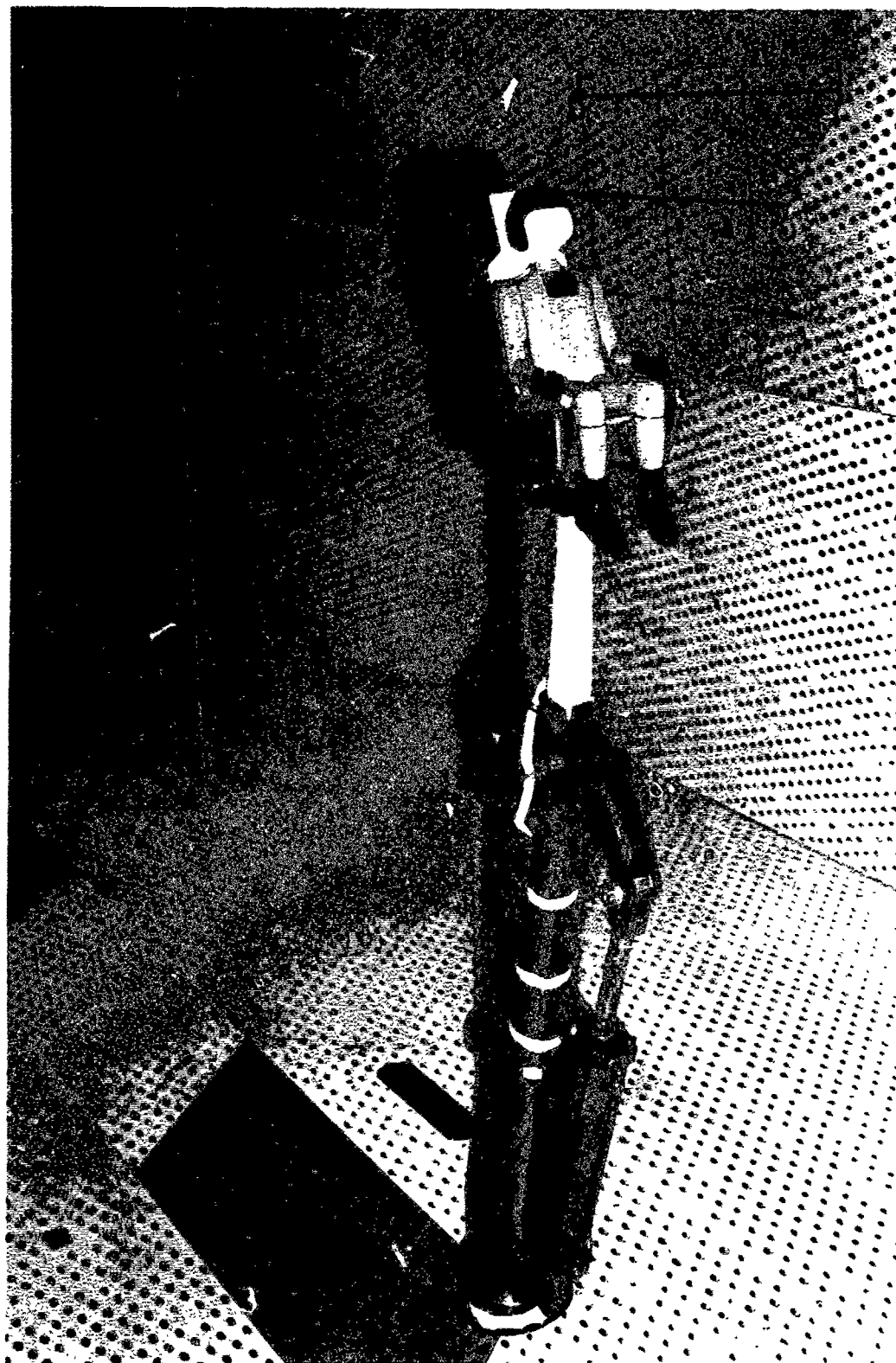
Figure 24. One half-scale crewman and ACES II seat in the transonic wind tunnel at Arnold Engineering Development Center.
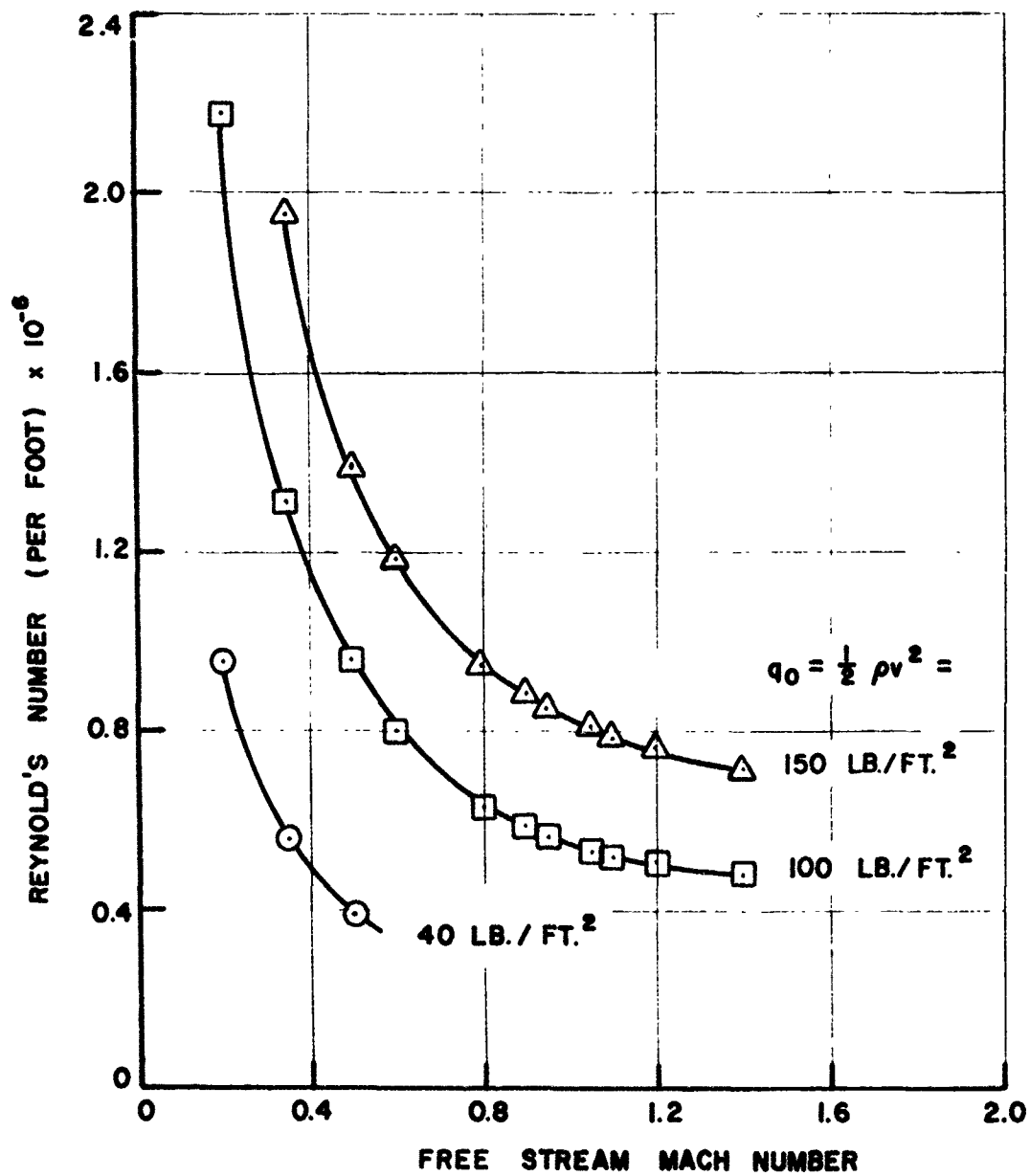
Figure 25. Free stream Reynolds number (per foot) as a function of Mach number.
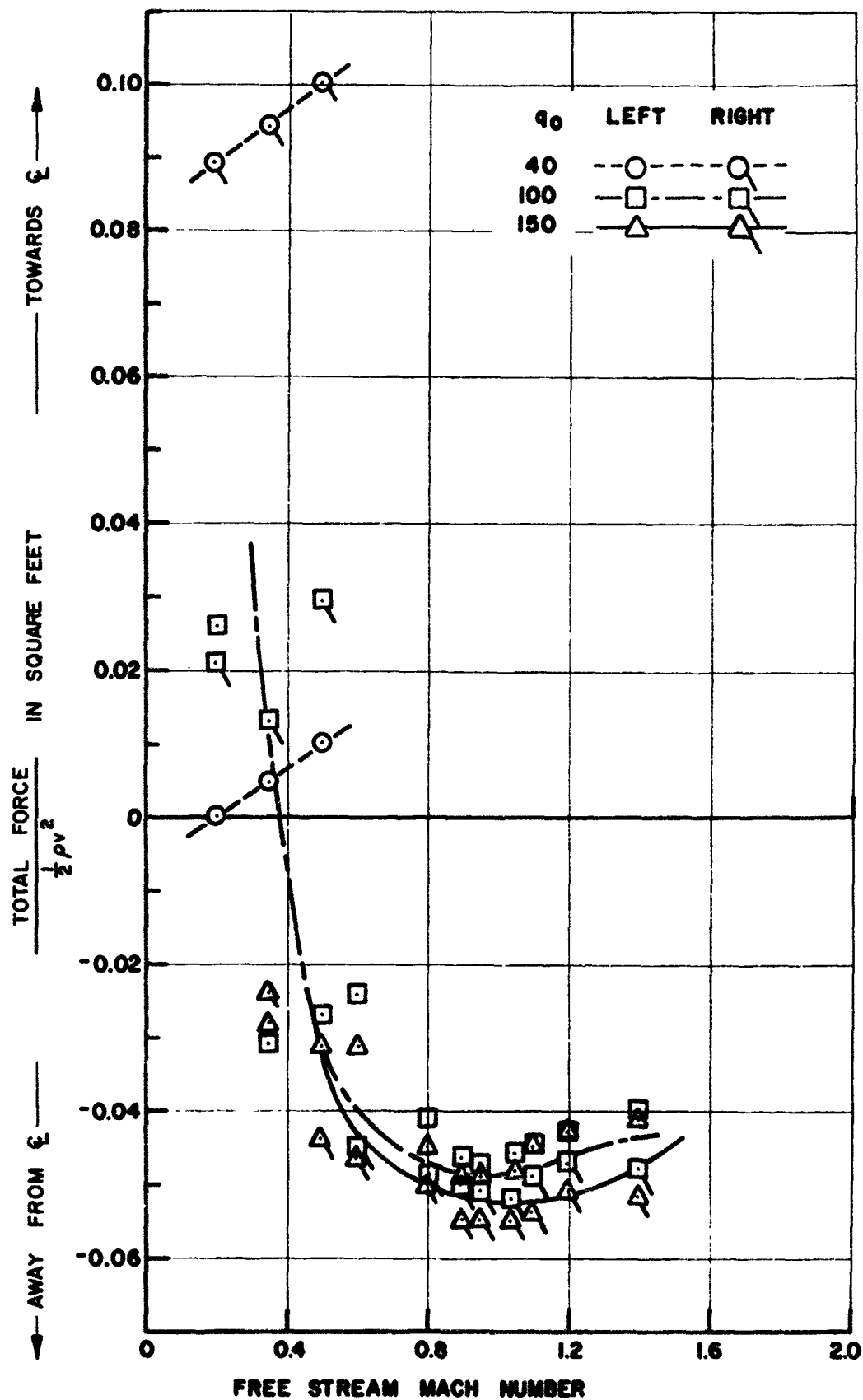
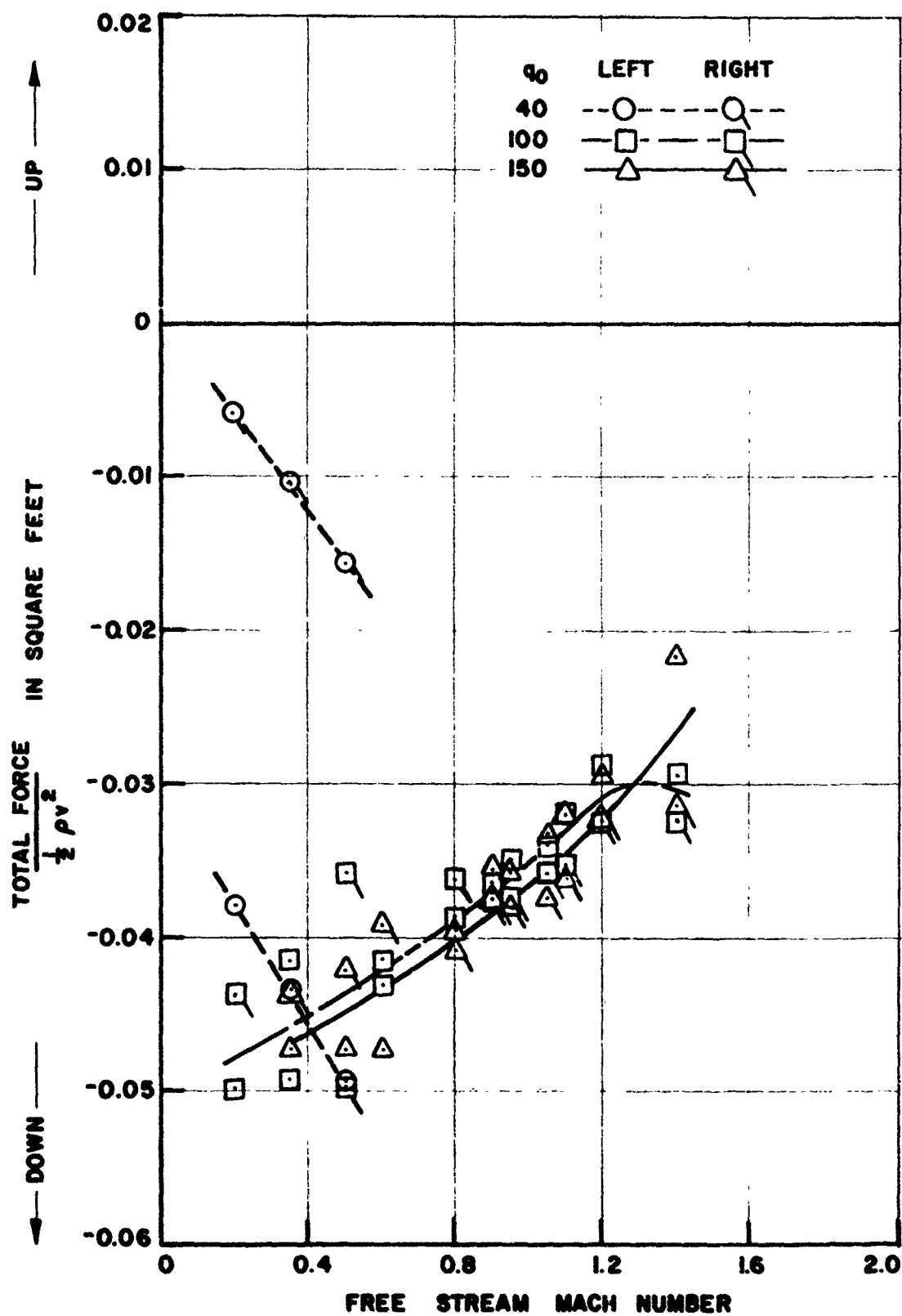Figure 26. Total lower arm side force at zero pitch and yaw for three different dynamic pressures (q_o).

Figure 27. Total lower arm lift force at zero pitch and yaw for three different dynamic pressures (q_o).
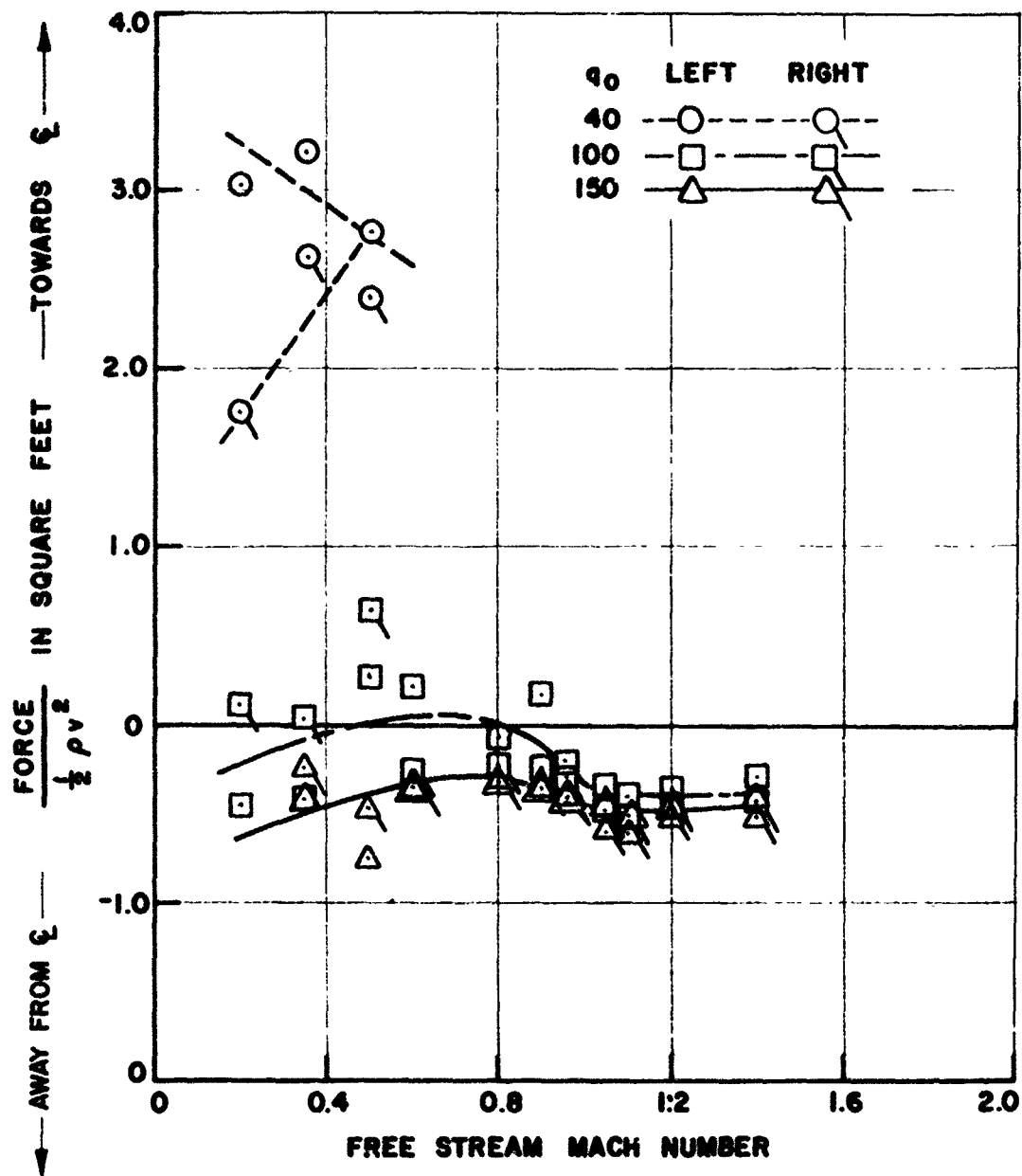
Figure 28. Total upper arm side force for zero pitch and yaw for three different dynamic pressures (q_o).
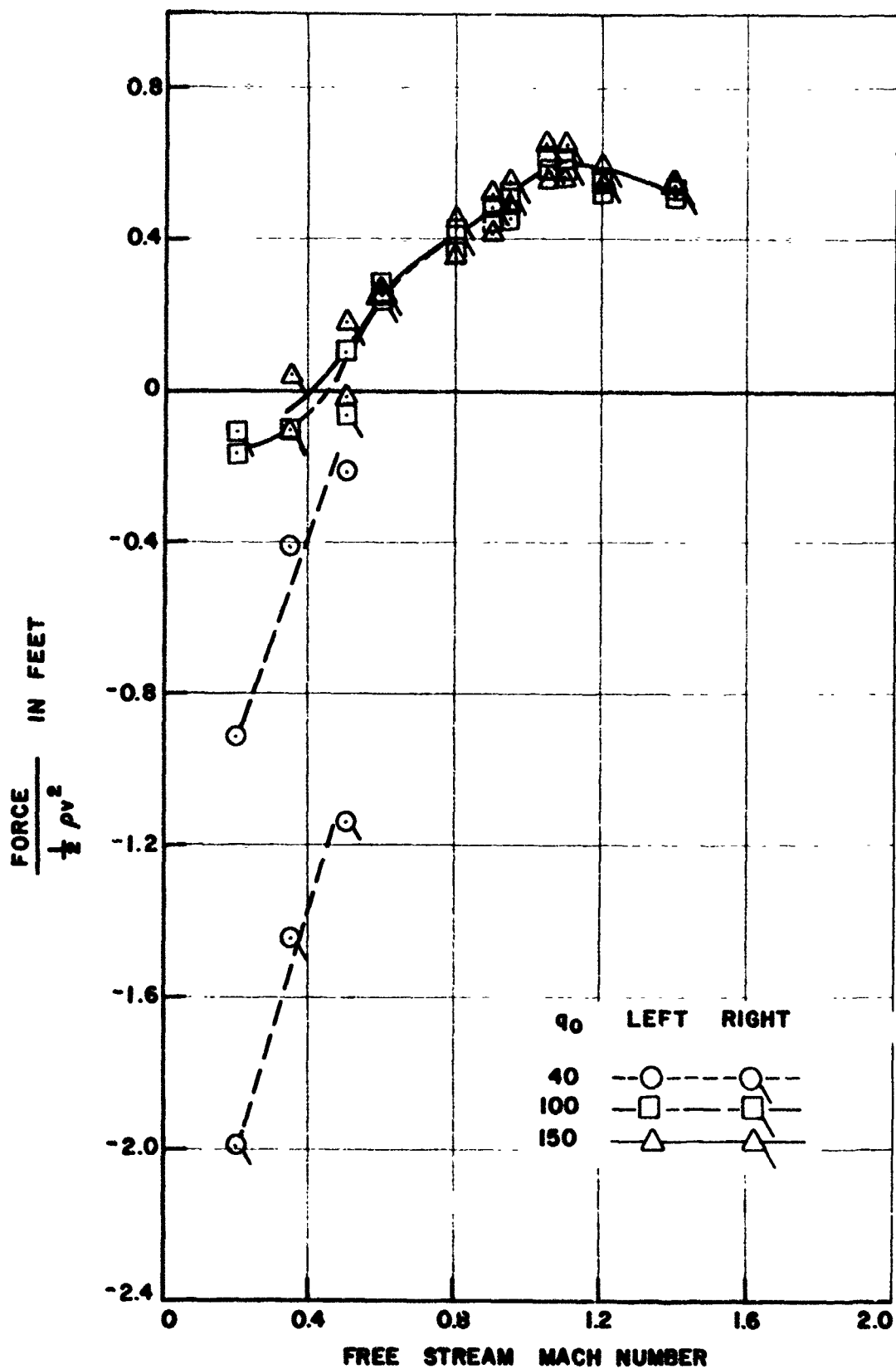
Figure 29. Total upper arm drag at zero pitch and yaw for three different dynamic pressures (q_o).
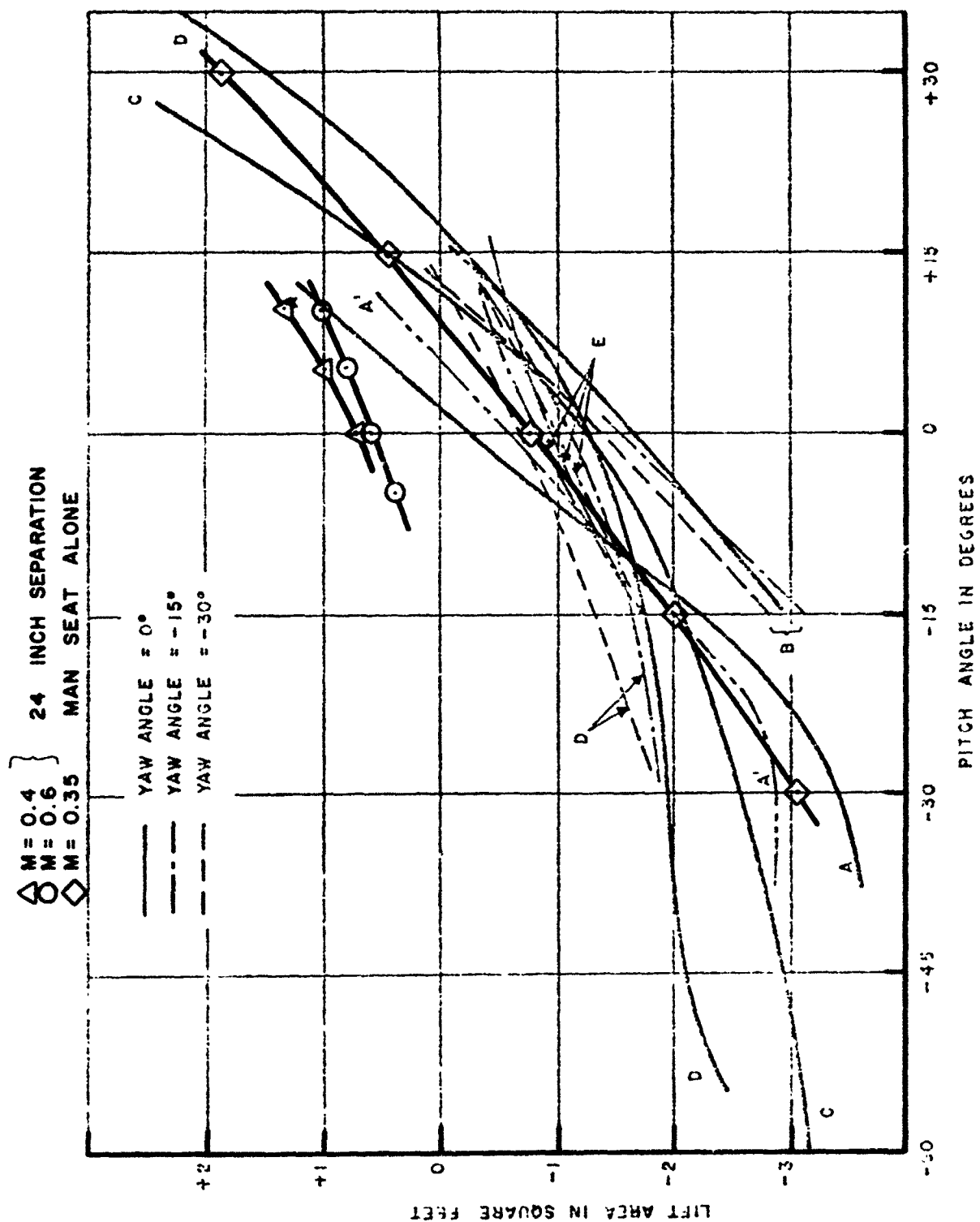
Figure 50. Lift area versus pitch angle comparison with other ejection seat models.
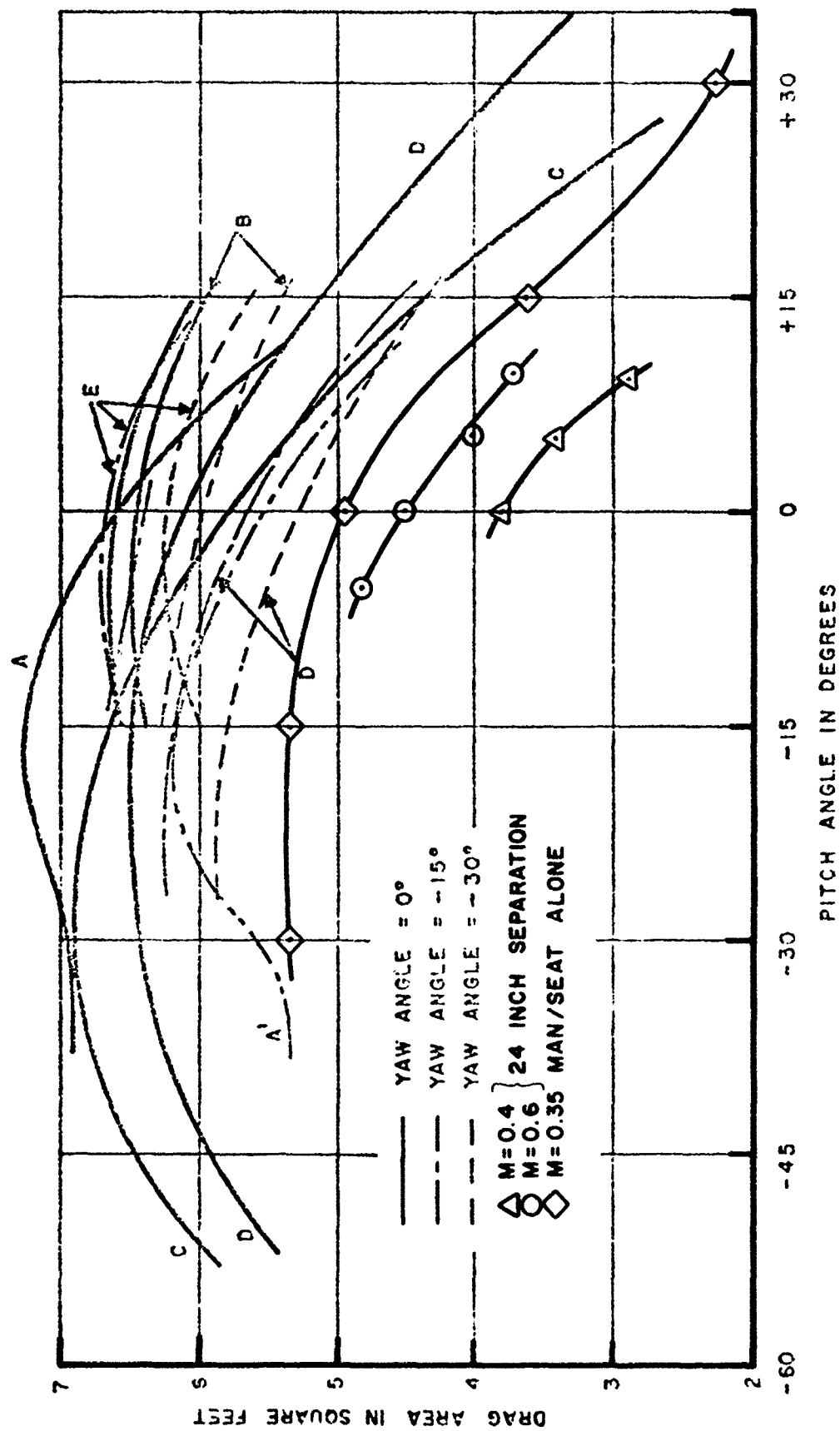
Figure 31. Drag area versus pitch angle comparison with other ejection seat models.
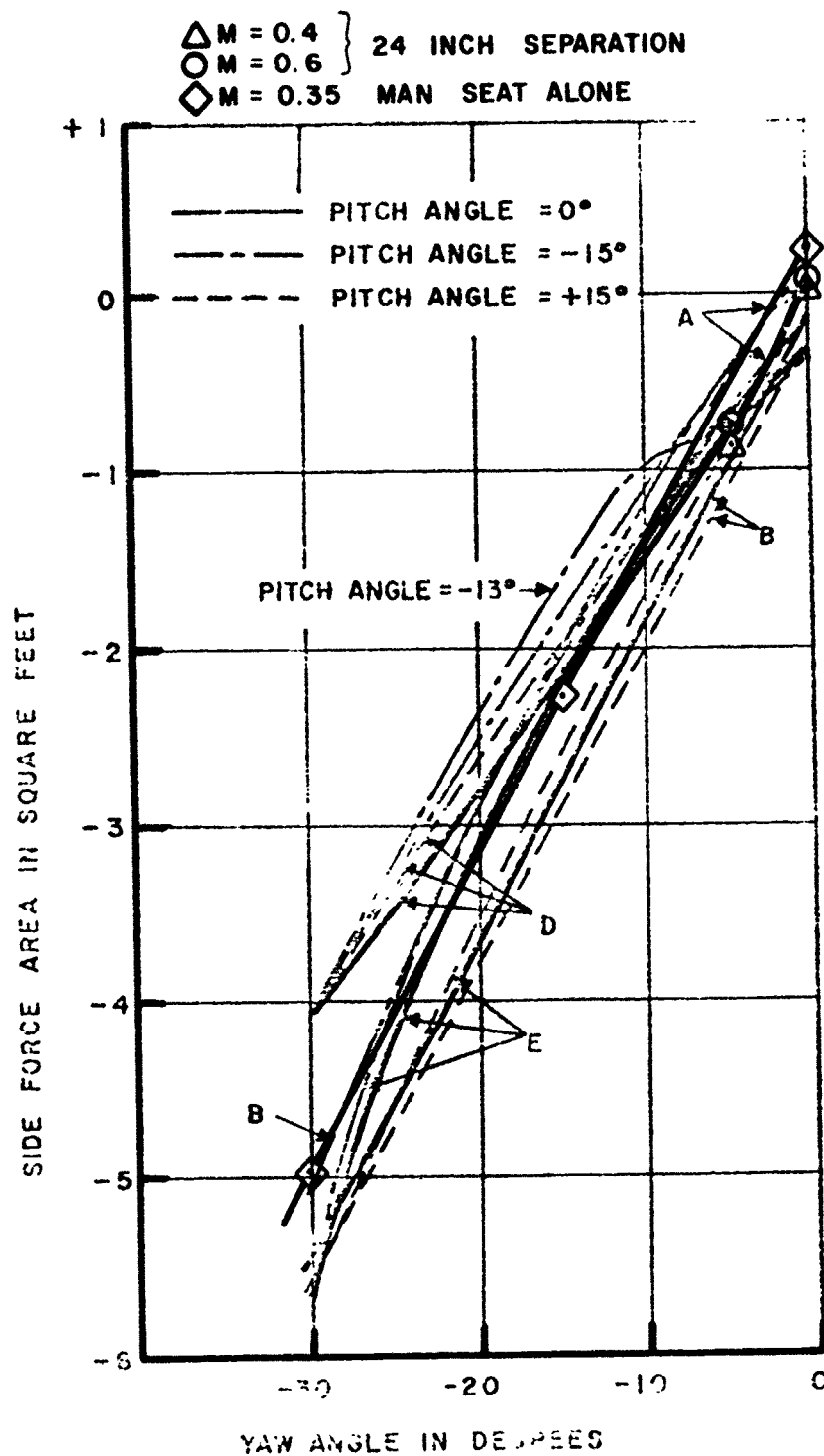
Figure 32.   Side force versus yaw angle comparison
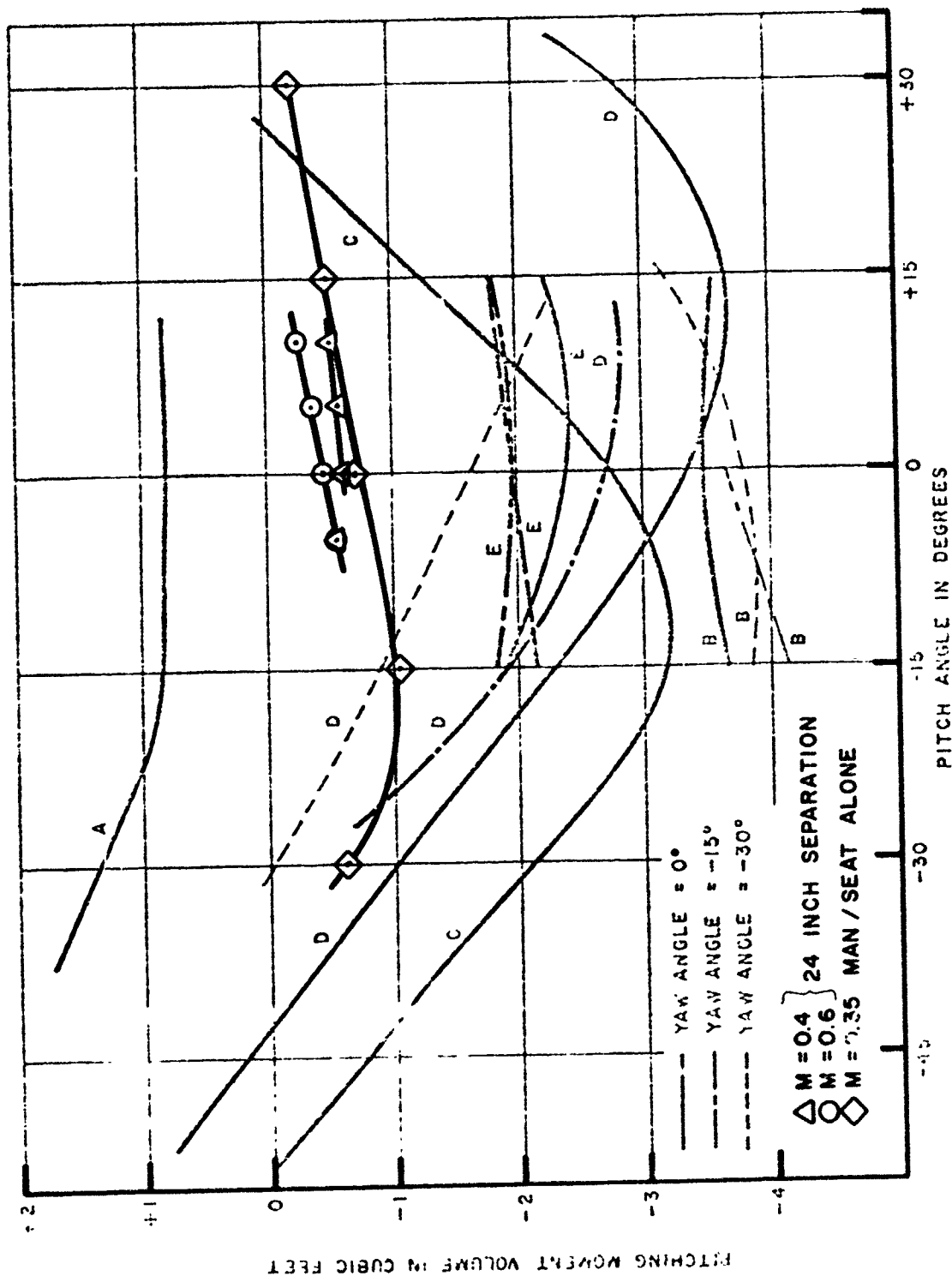with other ejection seat models.

Figure 53. Pitching moment volume versus pitch angle comparison with other ejection seat models.
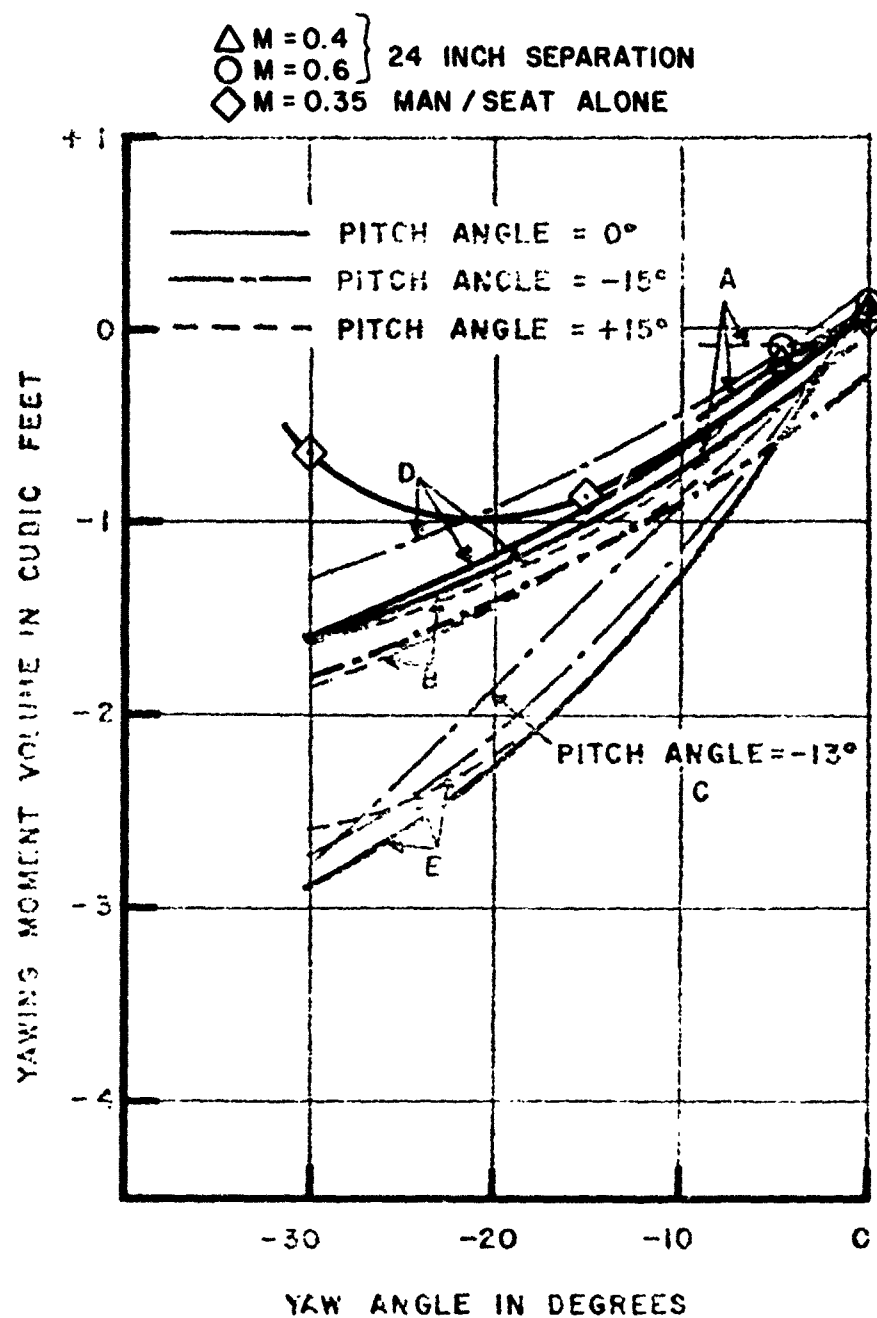
-54-

Figure 34. Yawing moment volume versus yaw angle comparison with other ejection seat models.
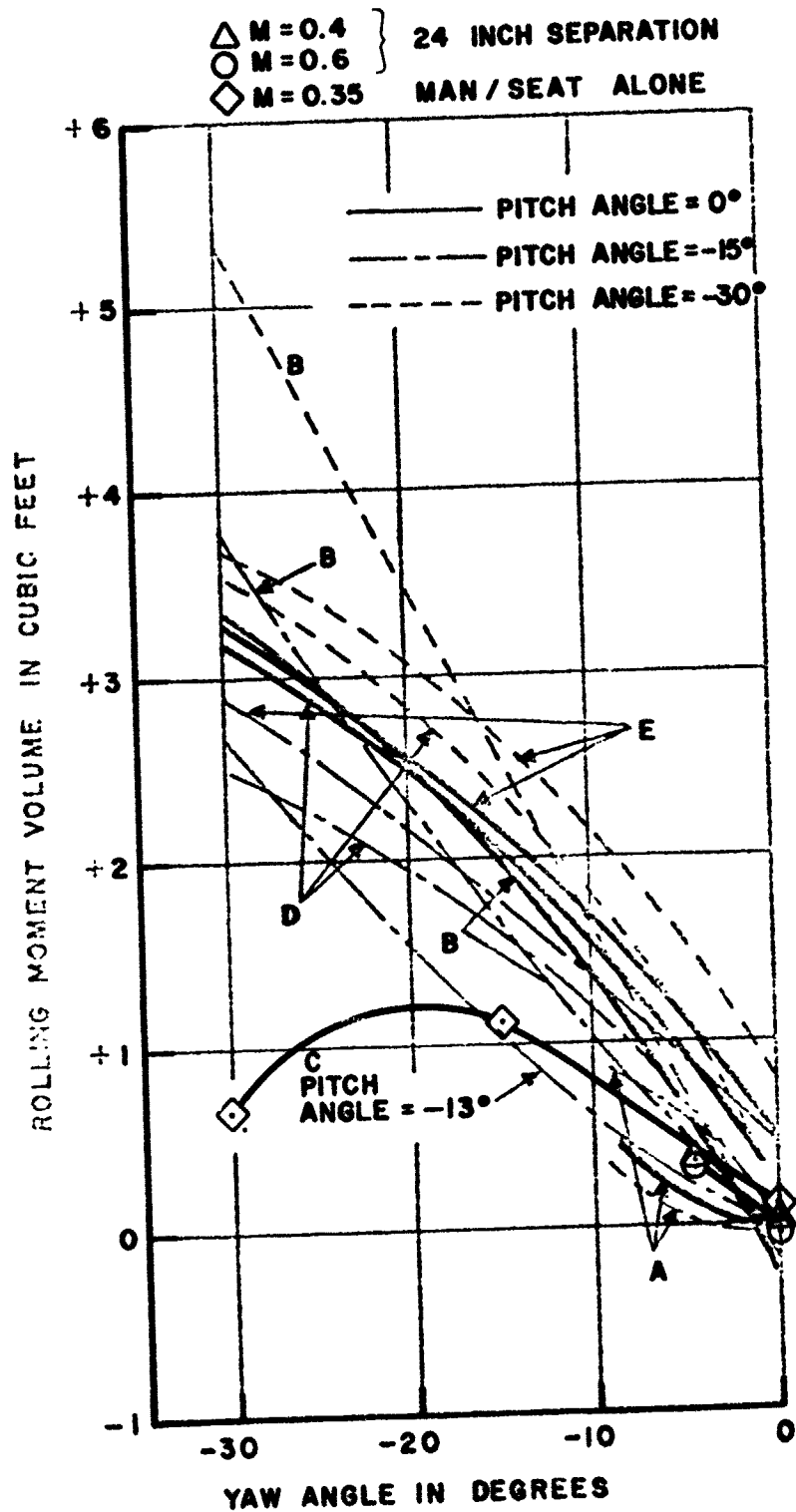
Figure 35. Rolling moment volume versus yaw
angle comparison with other
ejection seat models.

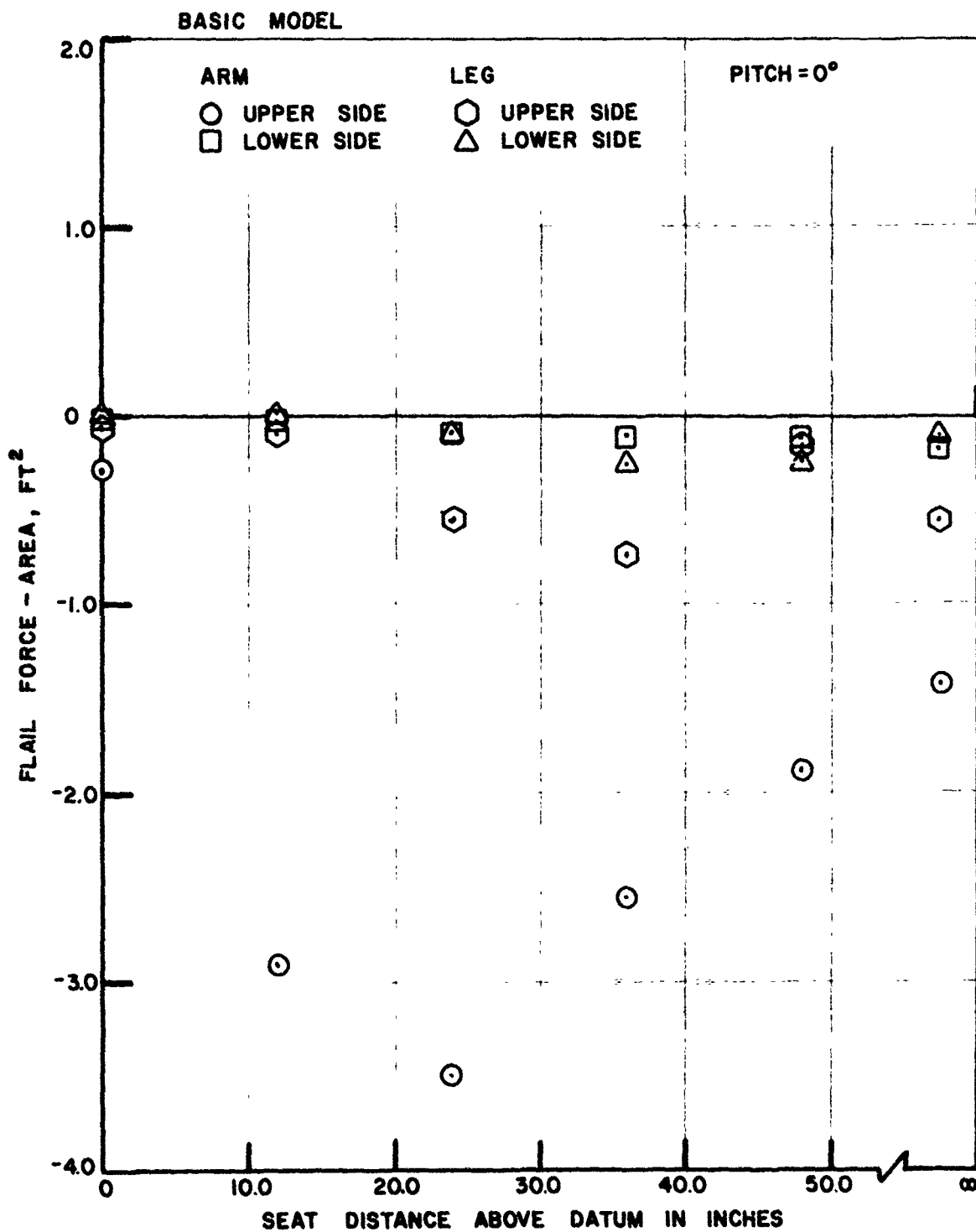Figure 36. Half-scale crew member with "flailing" right arm and displaced right leg.

Figure 37. Outward acting flail forces on arms and legs for the open cockpit as a function of separation distance. (M = 0.6, q_o = 207 lb/ft^2, zero yaw)
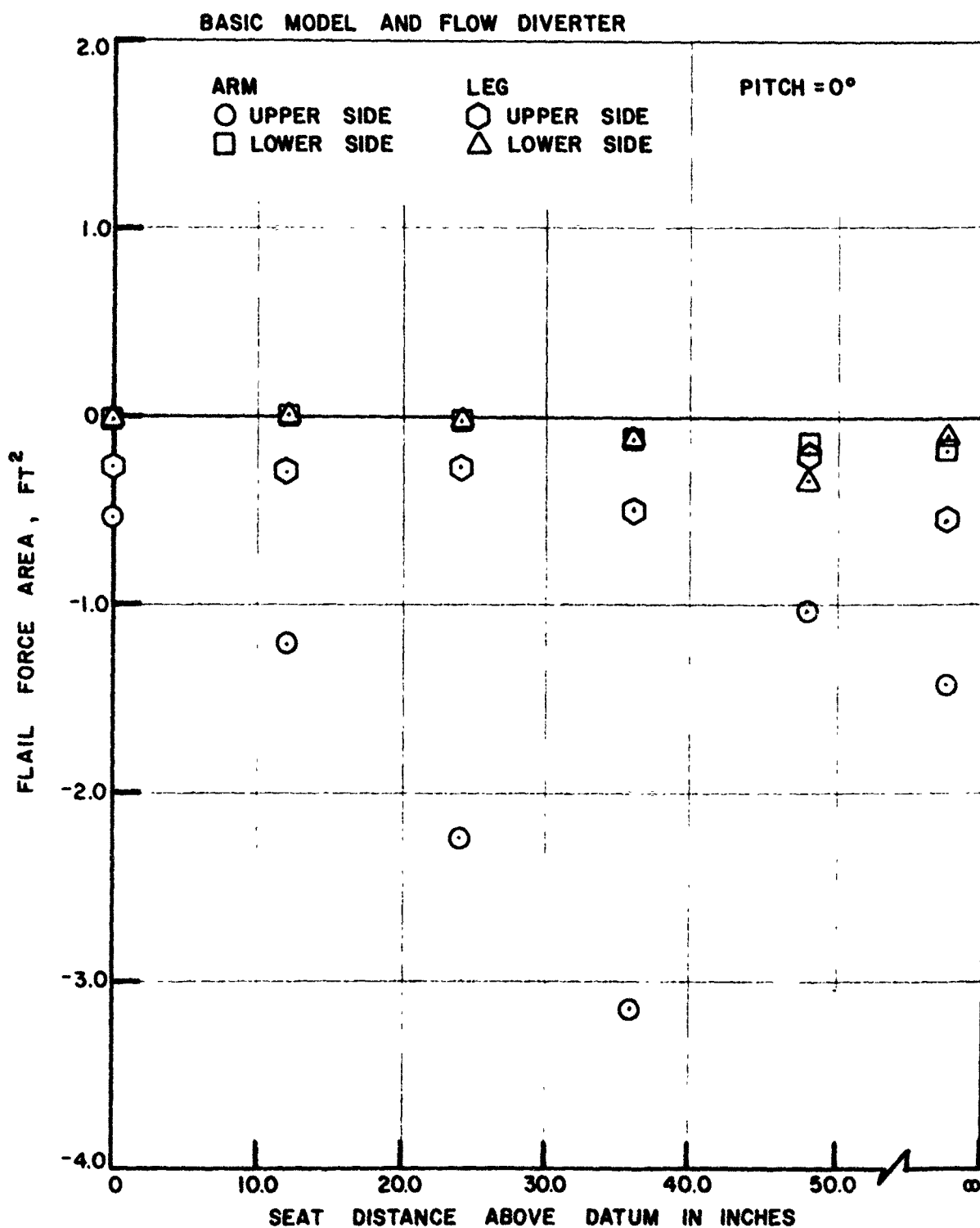
Figure 38. Outward acting flail forces on arms and legs for the open cockpit with flow diverter, as a function of separation distance. (M = 0.6, q_c - 207 lb/ft^2, zero yaw)
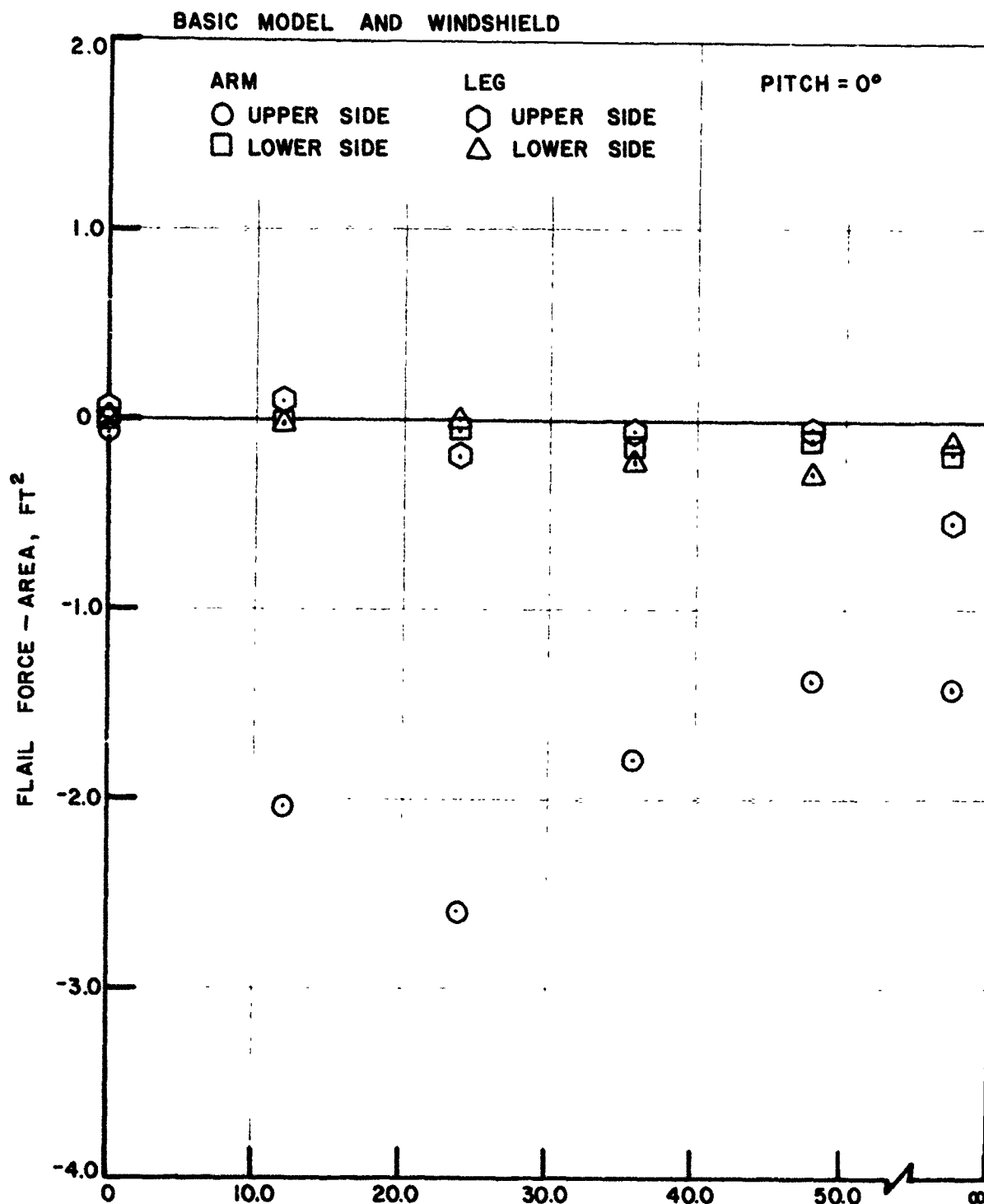
Figure 39. Outward acting flail forces on arms and legs for the open cockpit with windshield, as a function of separation distance. ($M = 0.6$, $q_o = 207$ lb/ft^2, zero yaw)
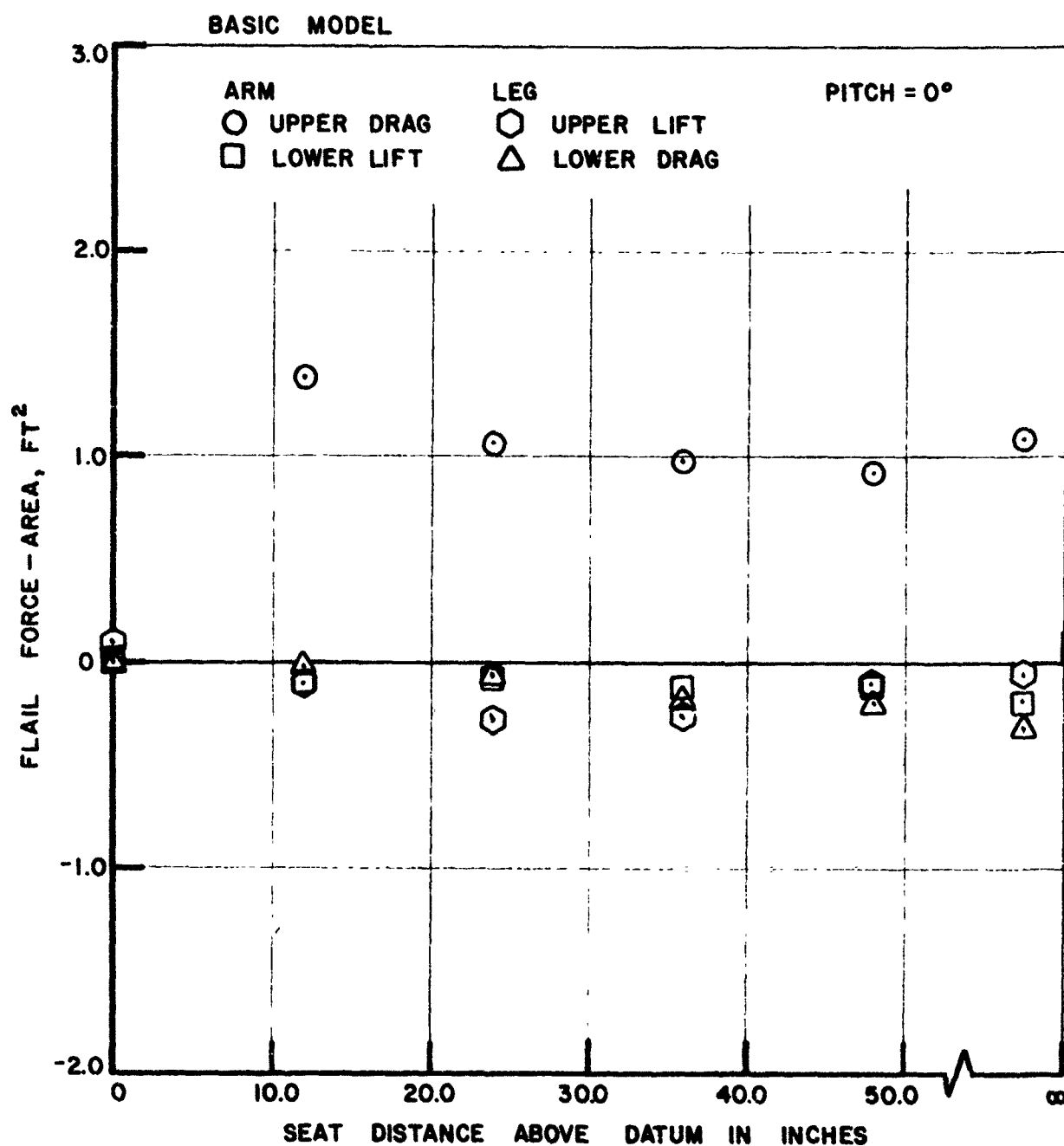
Figure 40. In-plane flail forces on arms and legs for the open cockpit as a function of separation distance. ($M = 0.6$, $q_o = 207$ lb/ft^2, zero yaw)

Figure 41.   In-plane flail forces on arms and legs for the open cockpit
with flow diverter, as a function of separation distance.
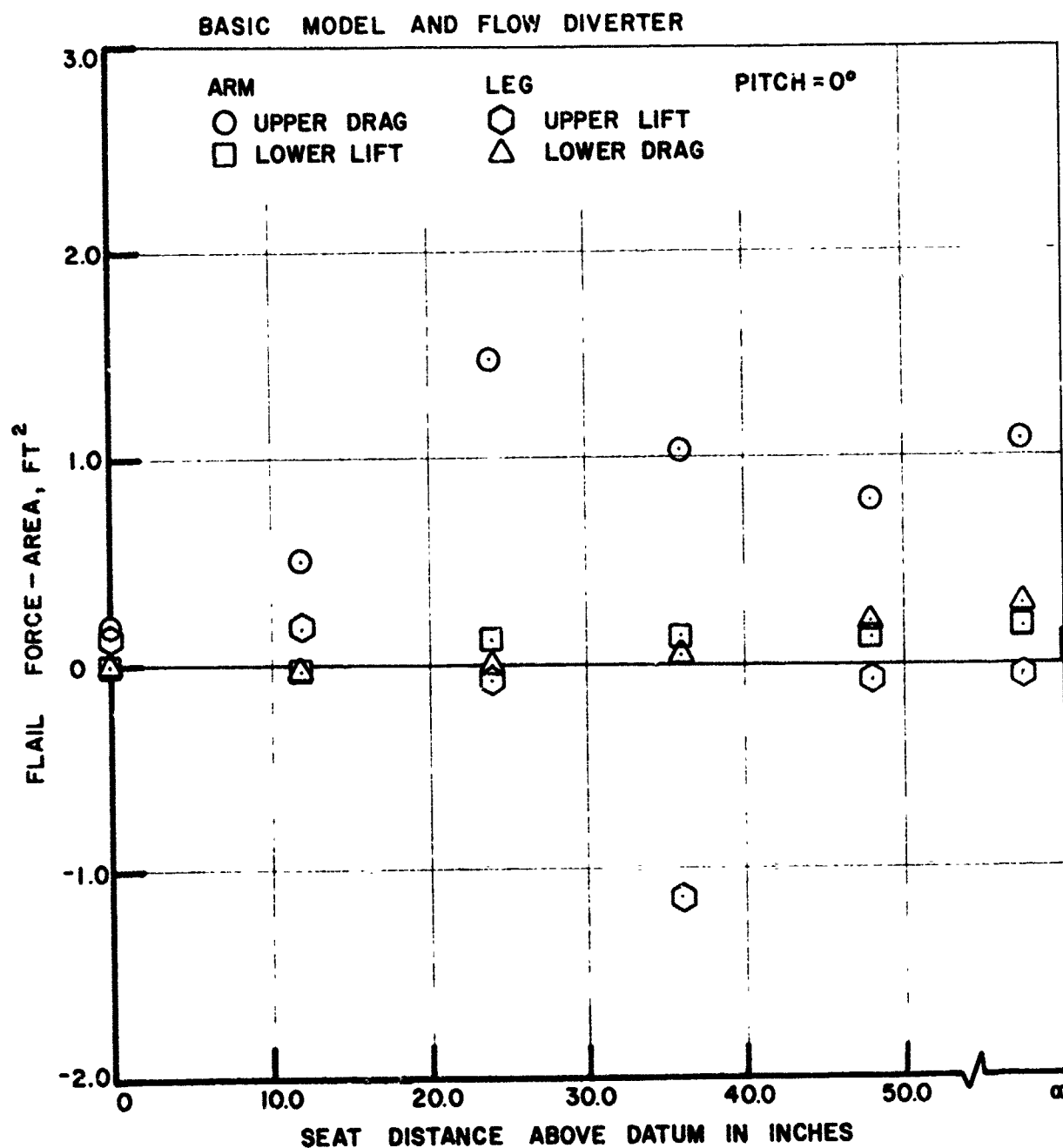(M = 0.6, q_o = 207 lb/ft^2, zero yaw)

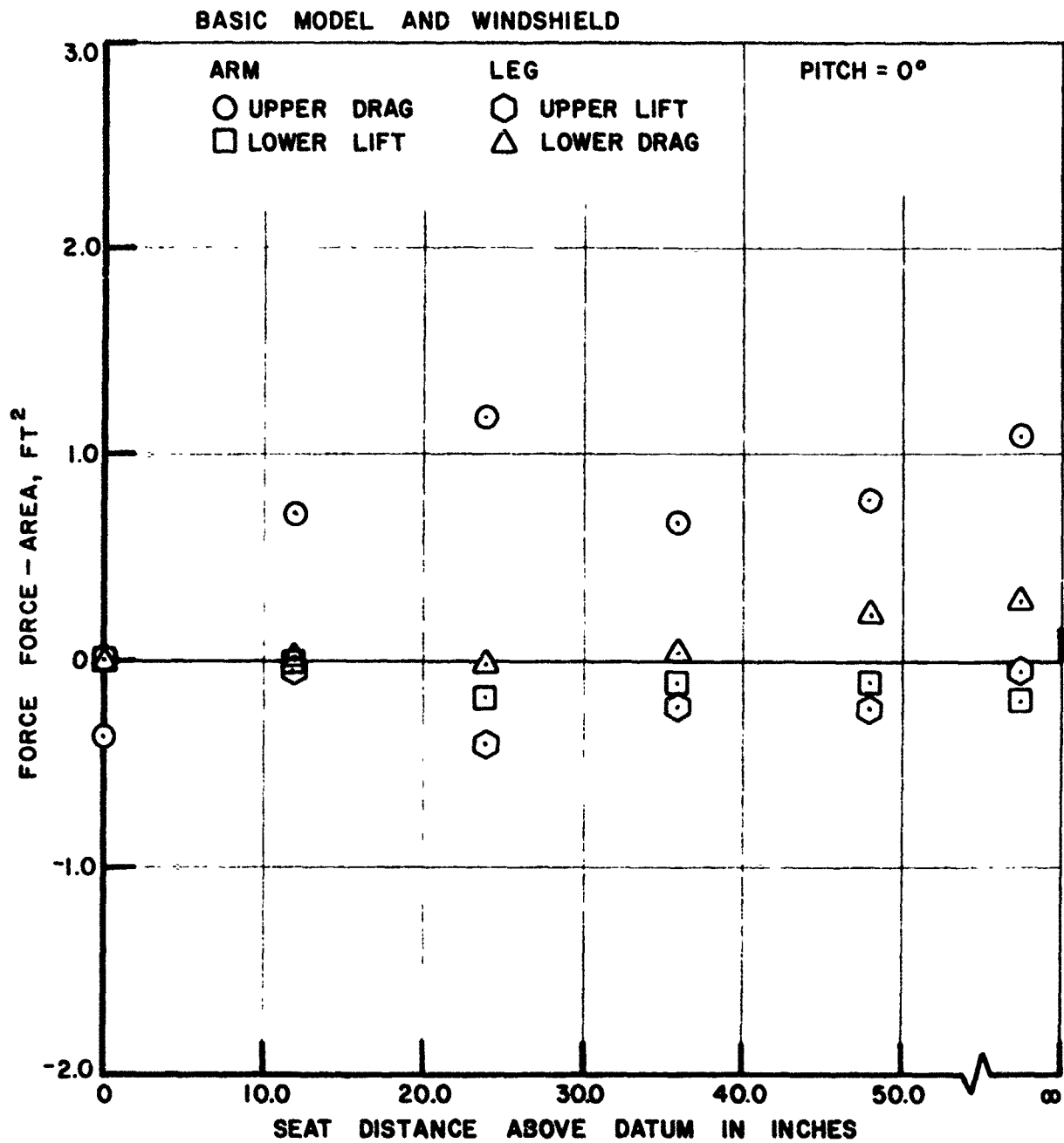Figure 42.   In-plane flail forces on arms and legs for the open cockpit
with windshield, as a function of separation distance.
$(M = 0.6, q_0 = 207 \text{ lb/ft}^2, \text{ zero yaw})$
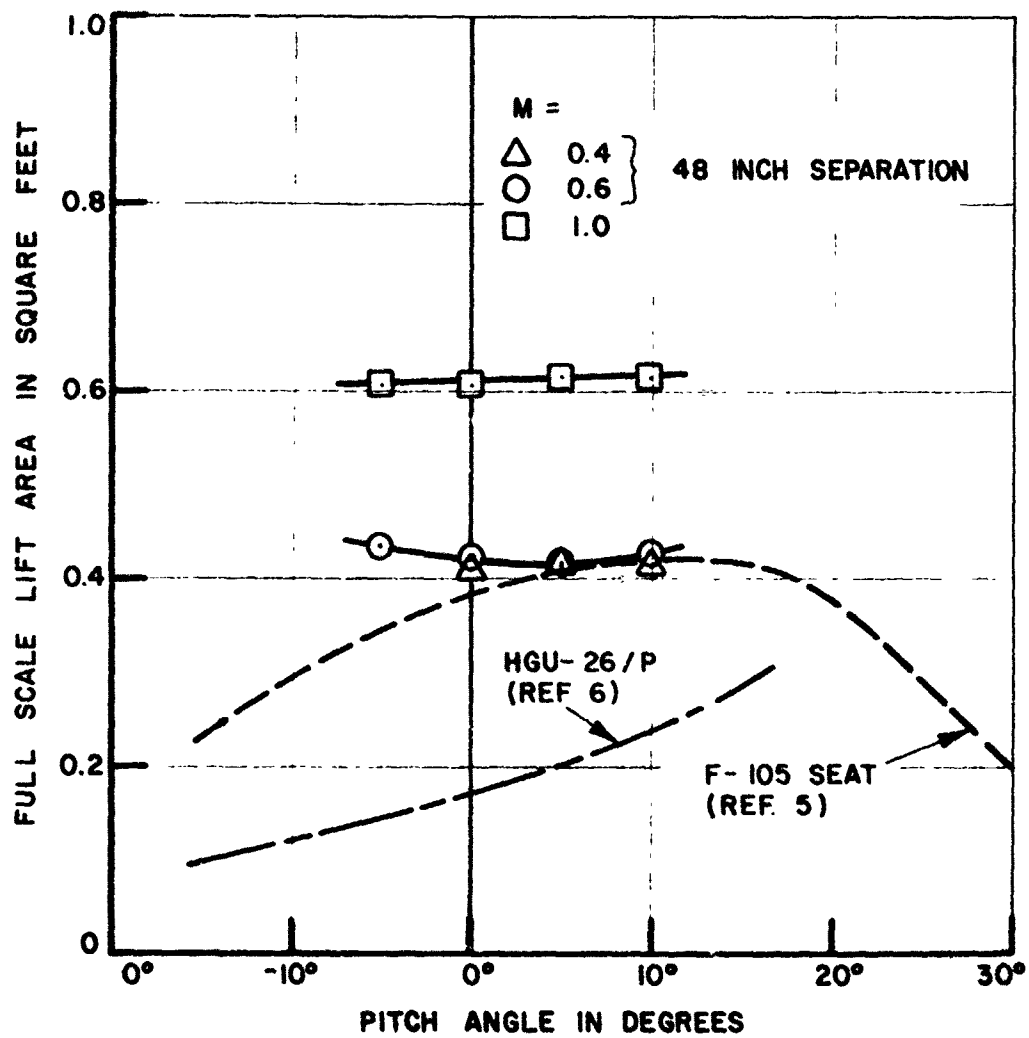
Figure 43. Helmet lift force at zero yaw.
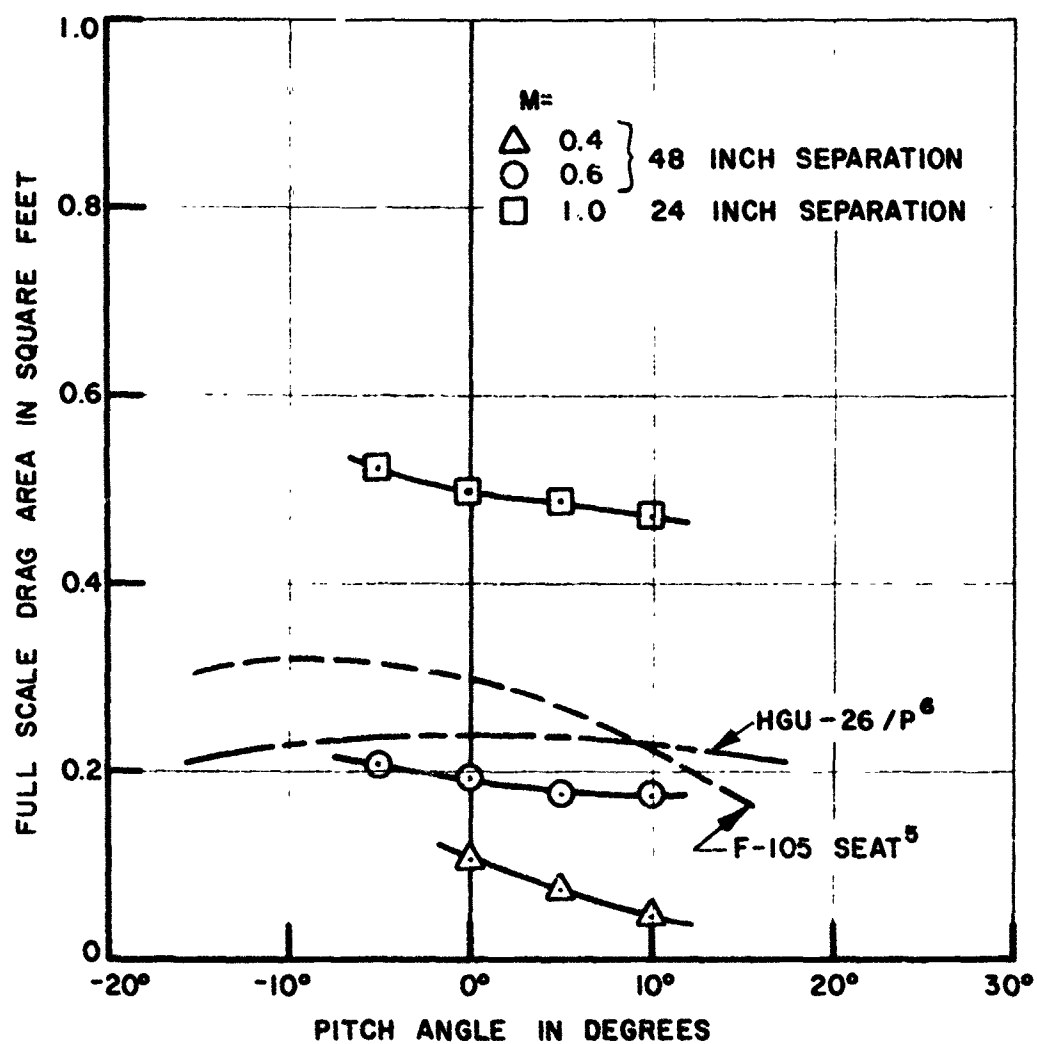
Figure 44. Helmet drag force at zero yaw.

Figure 45. The effect of separation distance on helmet lift, for the basic model without windshield or flow diverter. Yaw = 0.0°. Pitch = 0.0°.

Figure 46. The effect of separation distance on helmet drag, for the basic model without windshield or flow diverter. Yaw = 0.0°. Pitch = 0.0°.

Figure 47. The effect of separation distance on helmet lift,
for the basic model without windshield or flow
diverter. Yaw = 0.0°. Pitch = 5.0°.

Figure 48. The effect of separation distance on helmet drag, for the basic model without windshield or flow diverter. Yaw = 0.0°, Pitch = 5.0°.
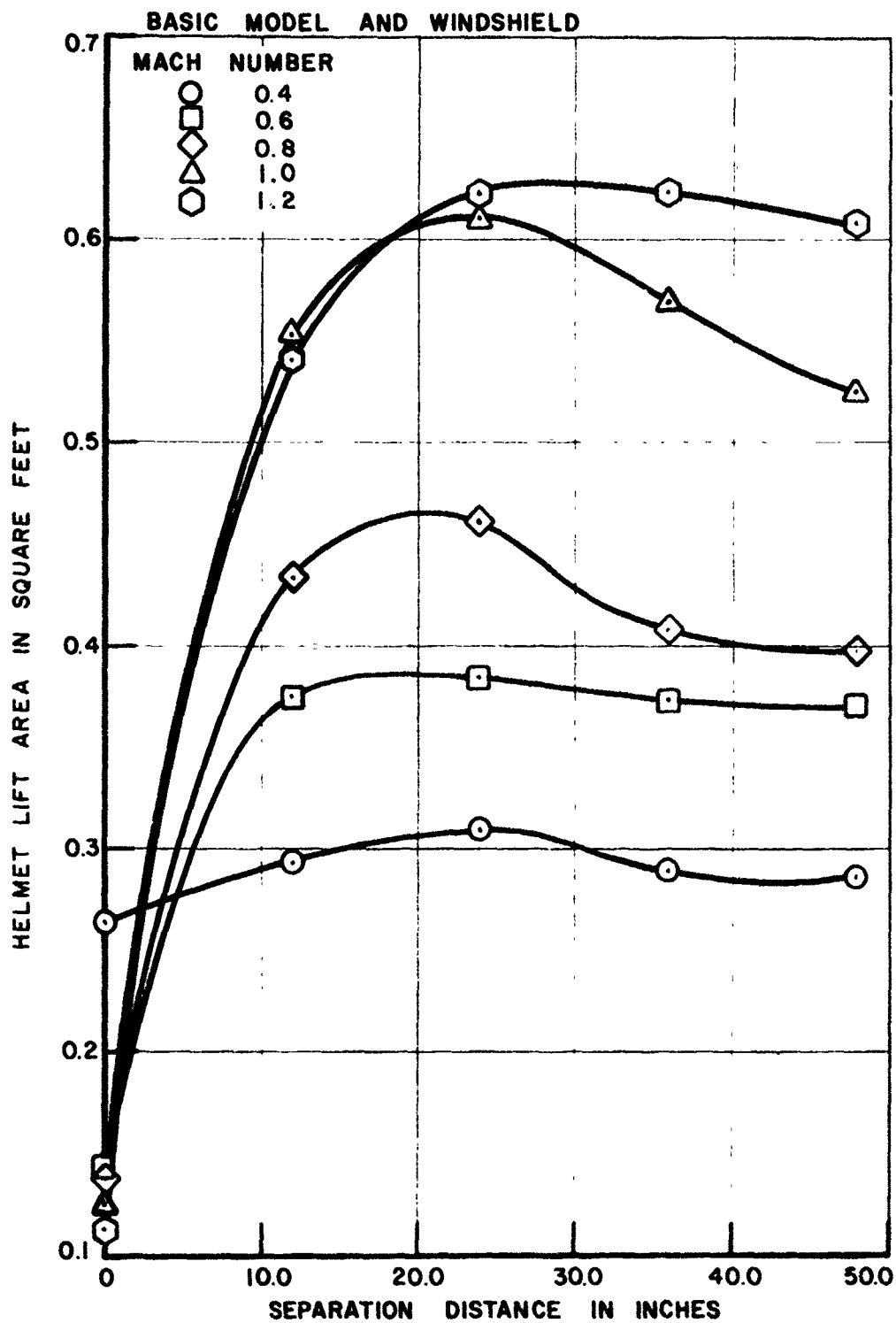
Figure 49. The effect of separation distance on helmet lift for the basic model and windshield, without flow diverter. Yaw = 0.0°, Pitch = 0.0°.
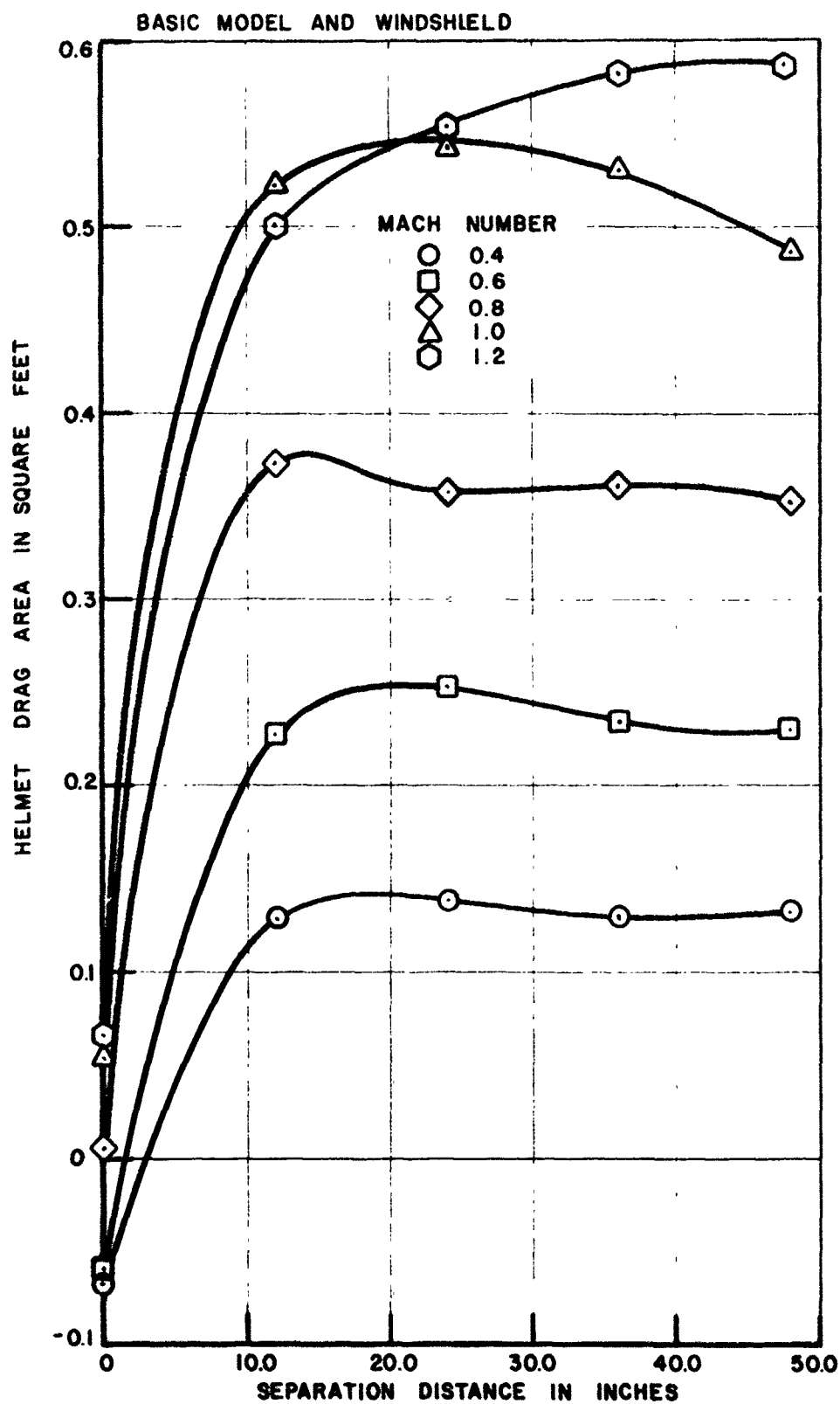
Figure 50. The effect of separation distance on helmet drag, for the basic model and windshield, without flow diverter. Yaw = 0.0°. Pitch = 0.0°.
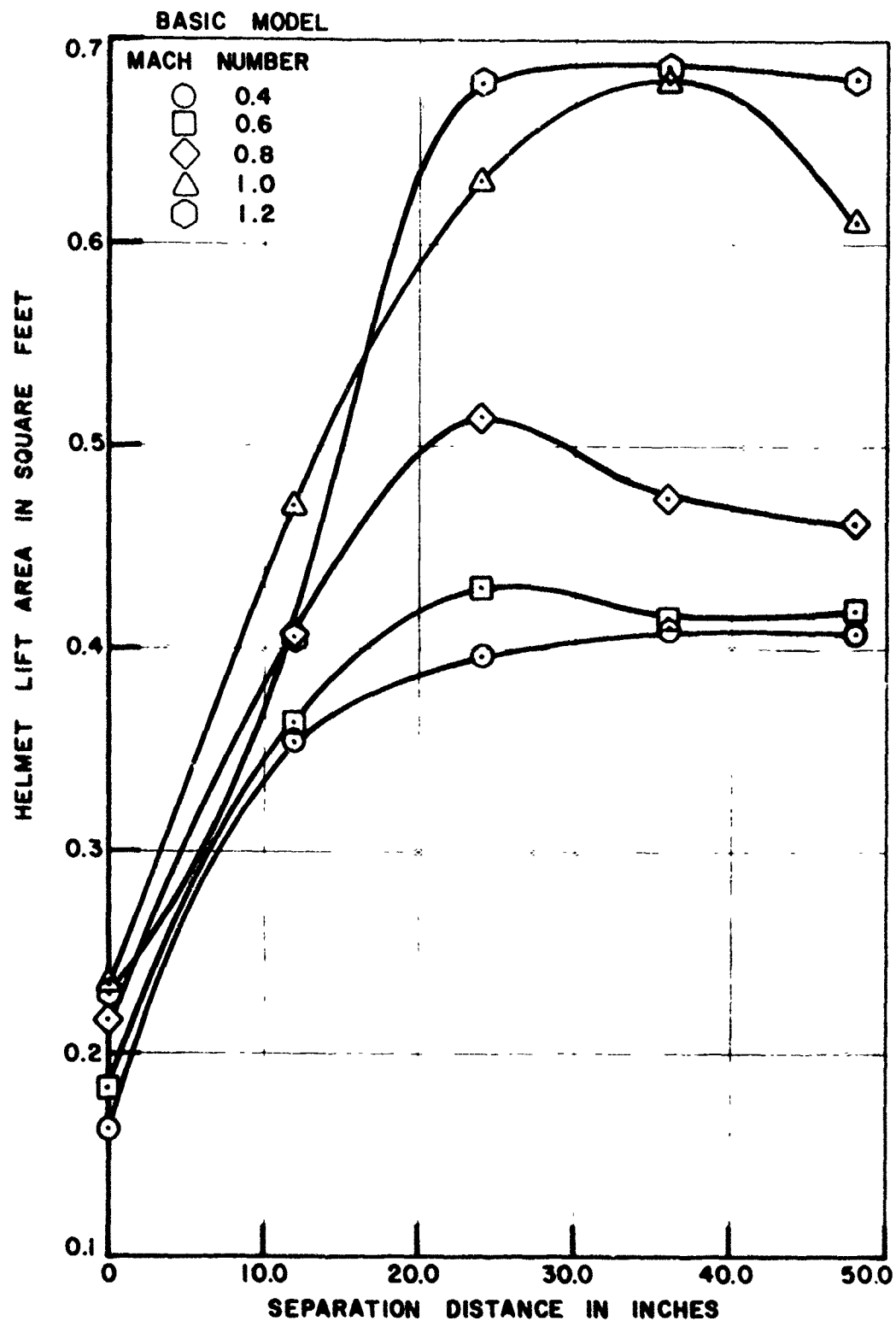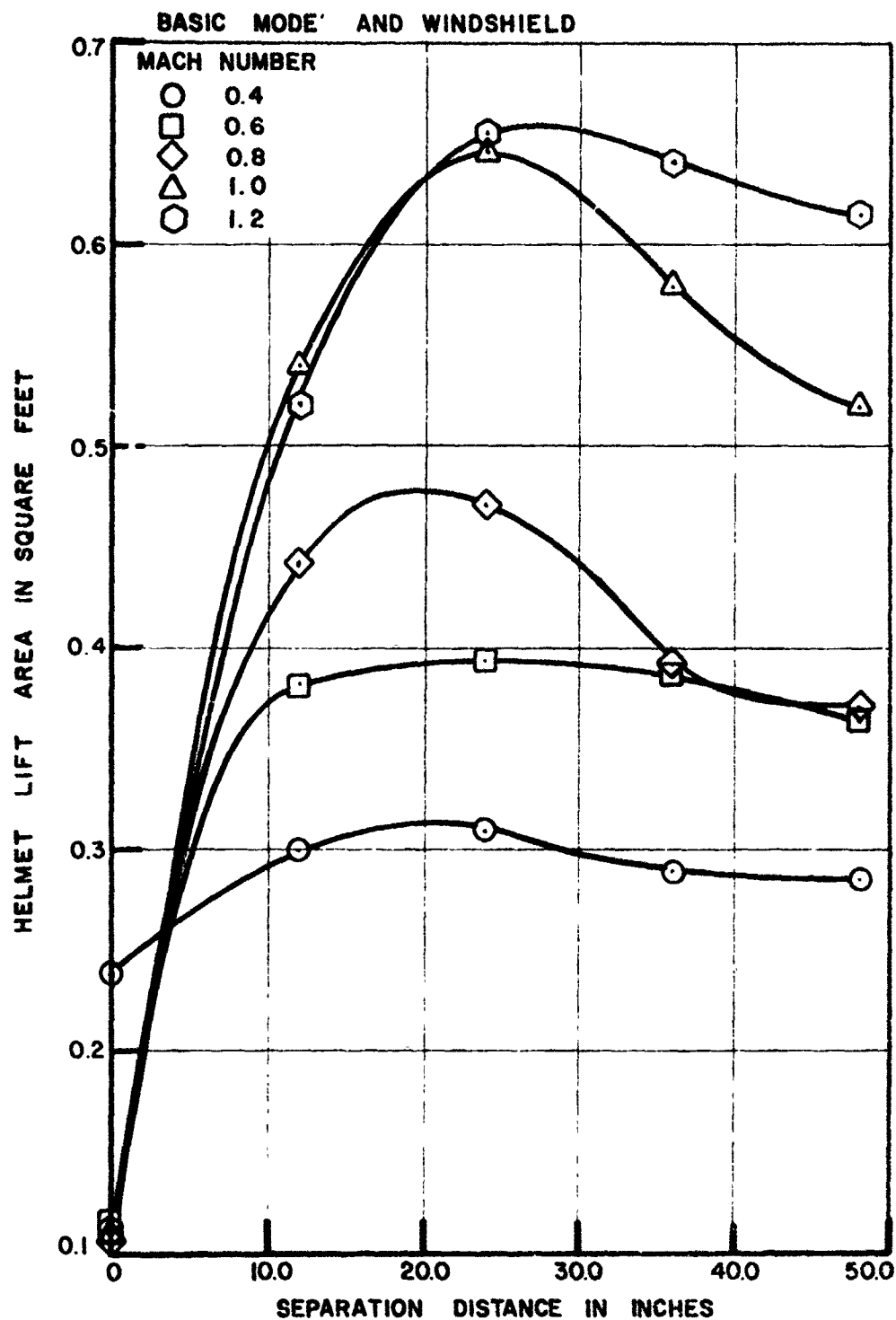
Figure 51. The effect of separation distance on helmet lift for the basic model and windshield, without flow diverter. Yaw = 0.0°. Pitch = 5.0°.
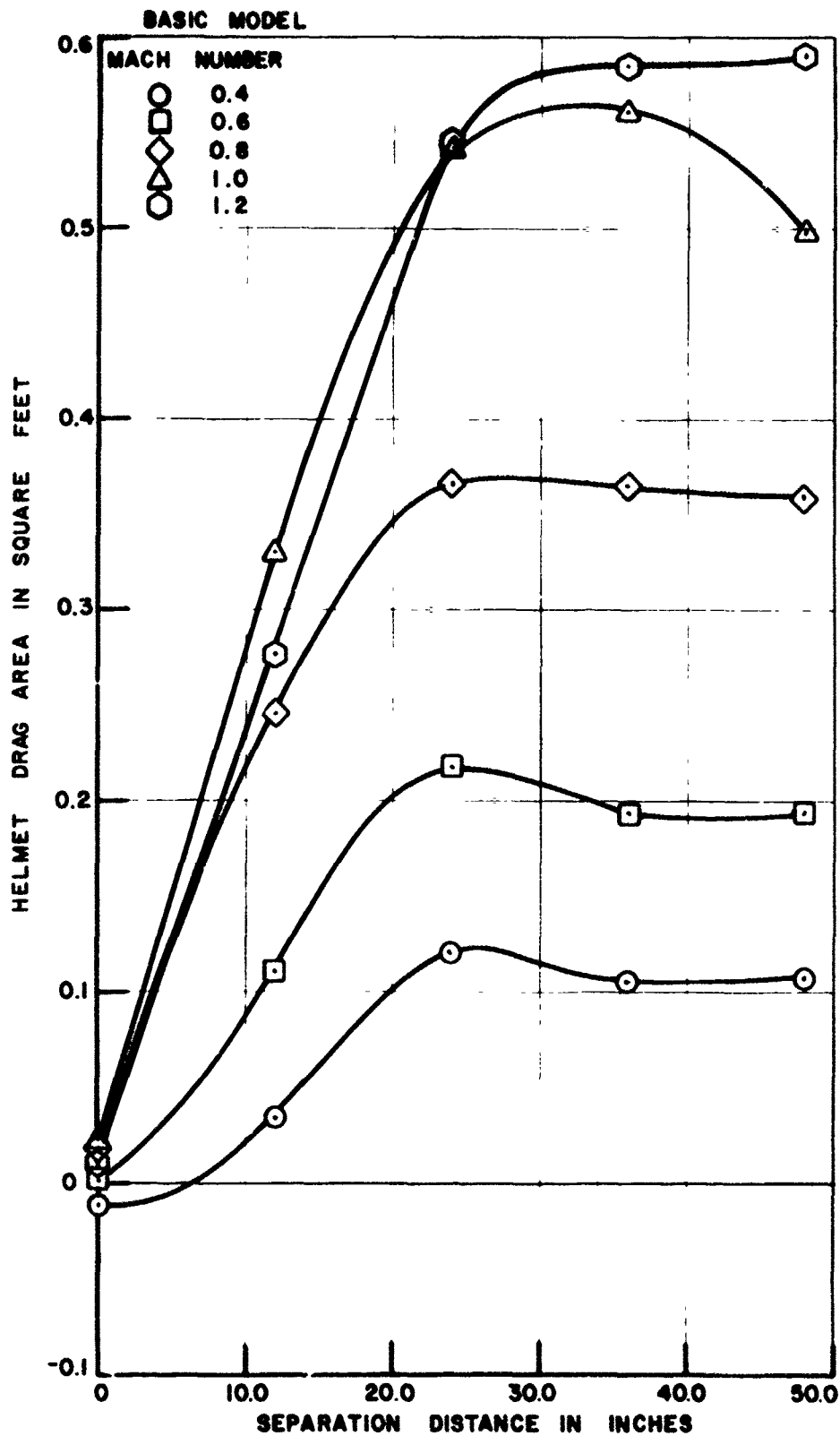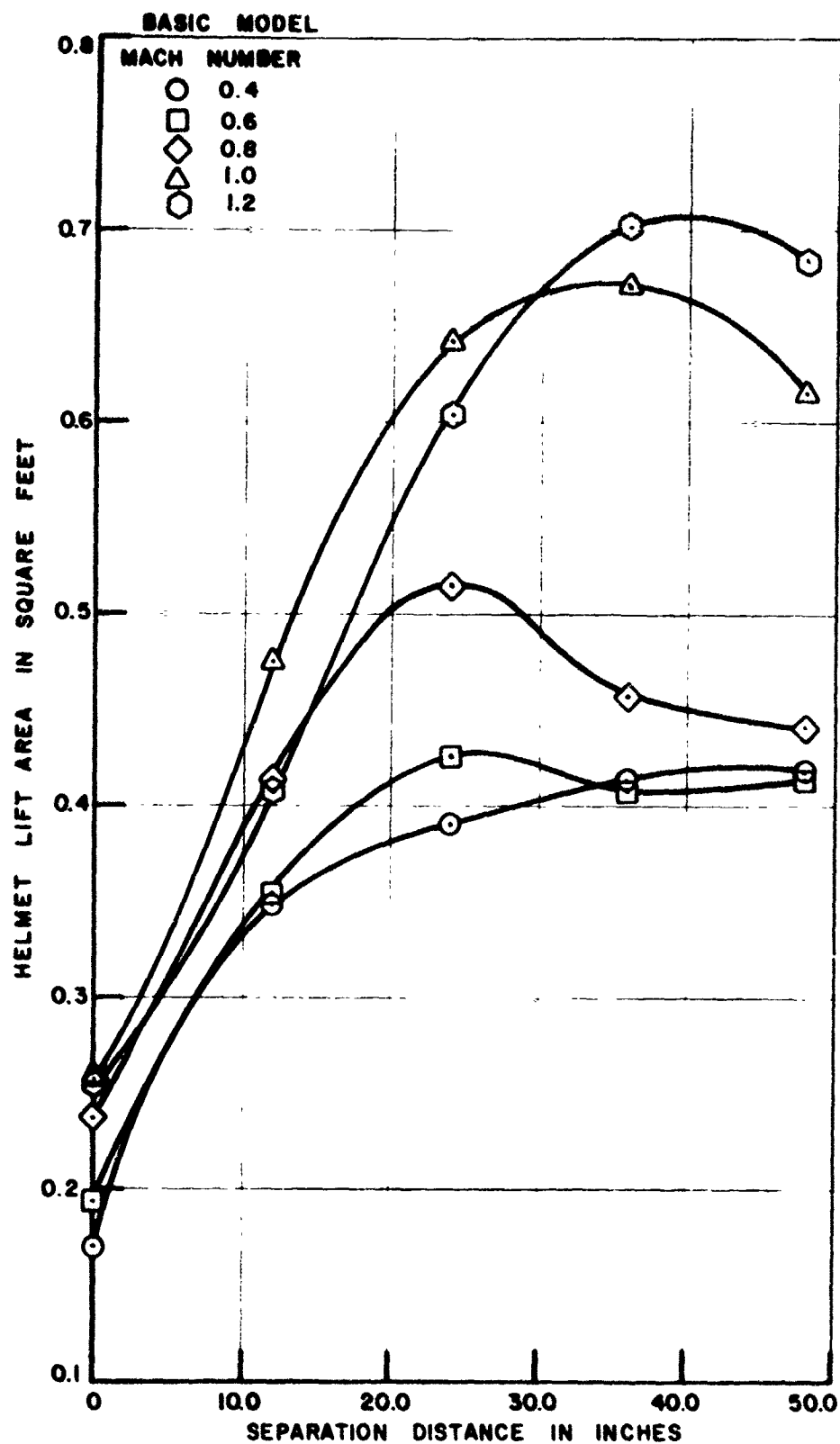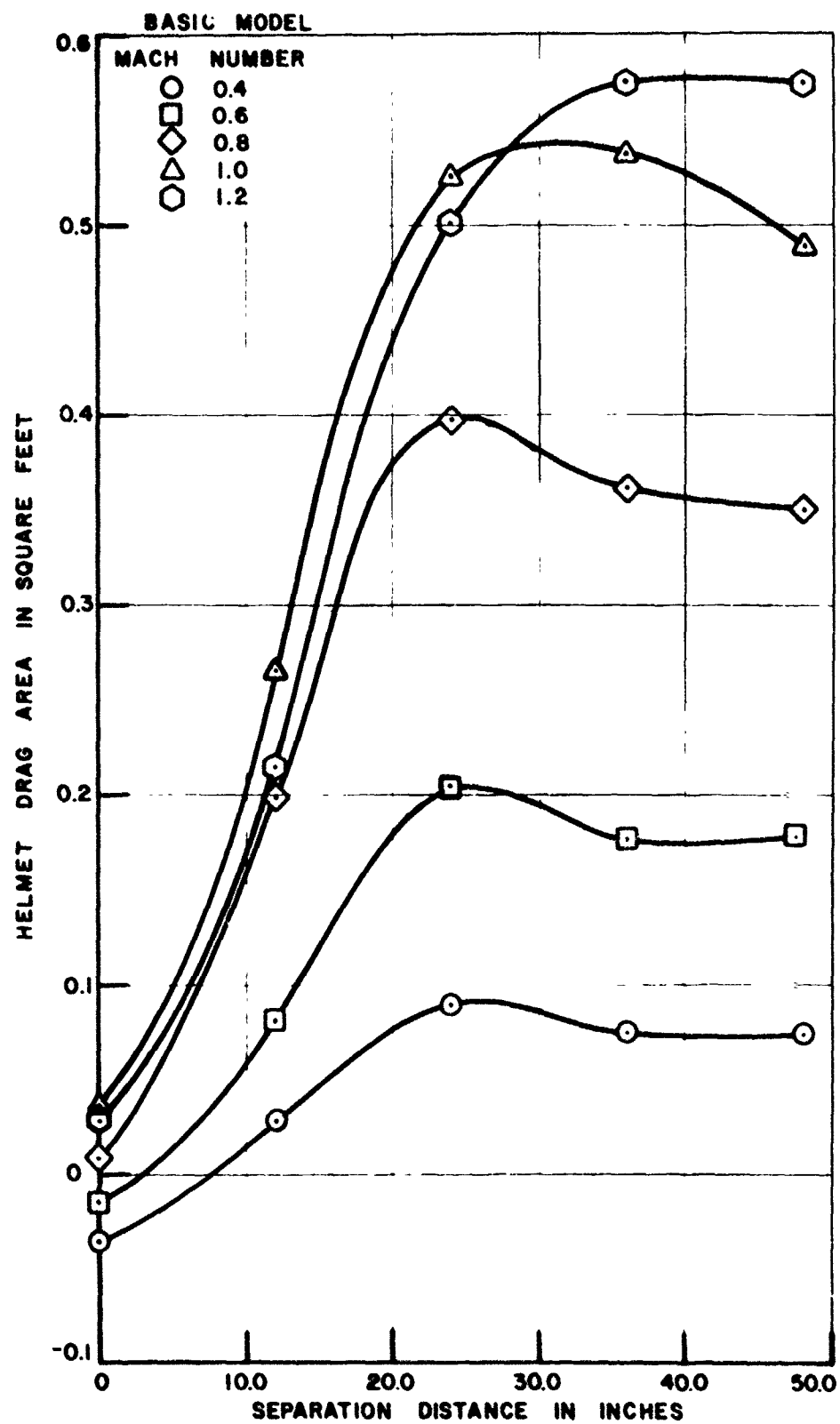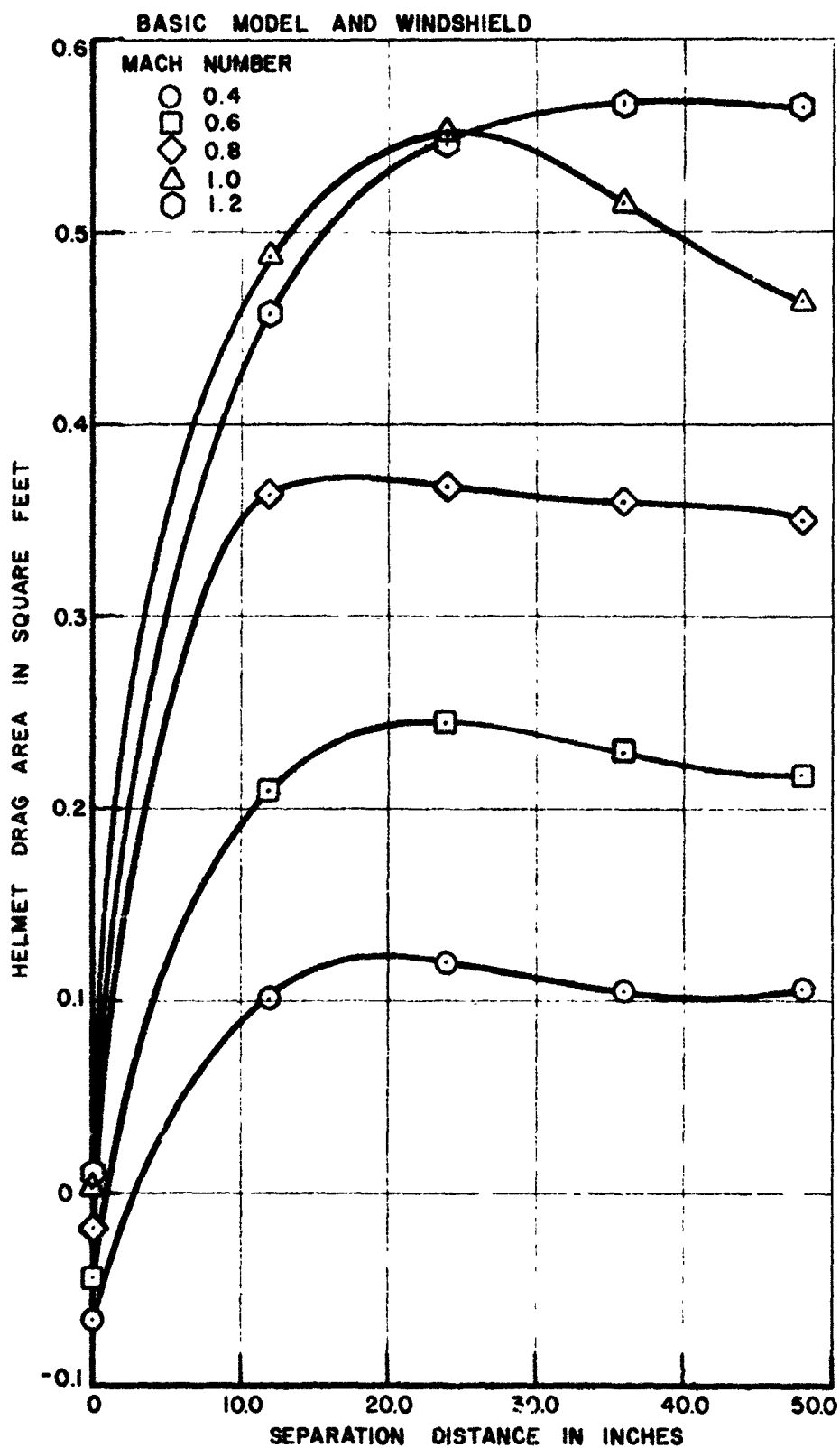
Figure 52. The effect of separation distance on helmet drag, for the basic model and windshield, without flow diverter. Yaw = 0.0°. Pitch = 5.0°.
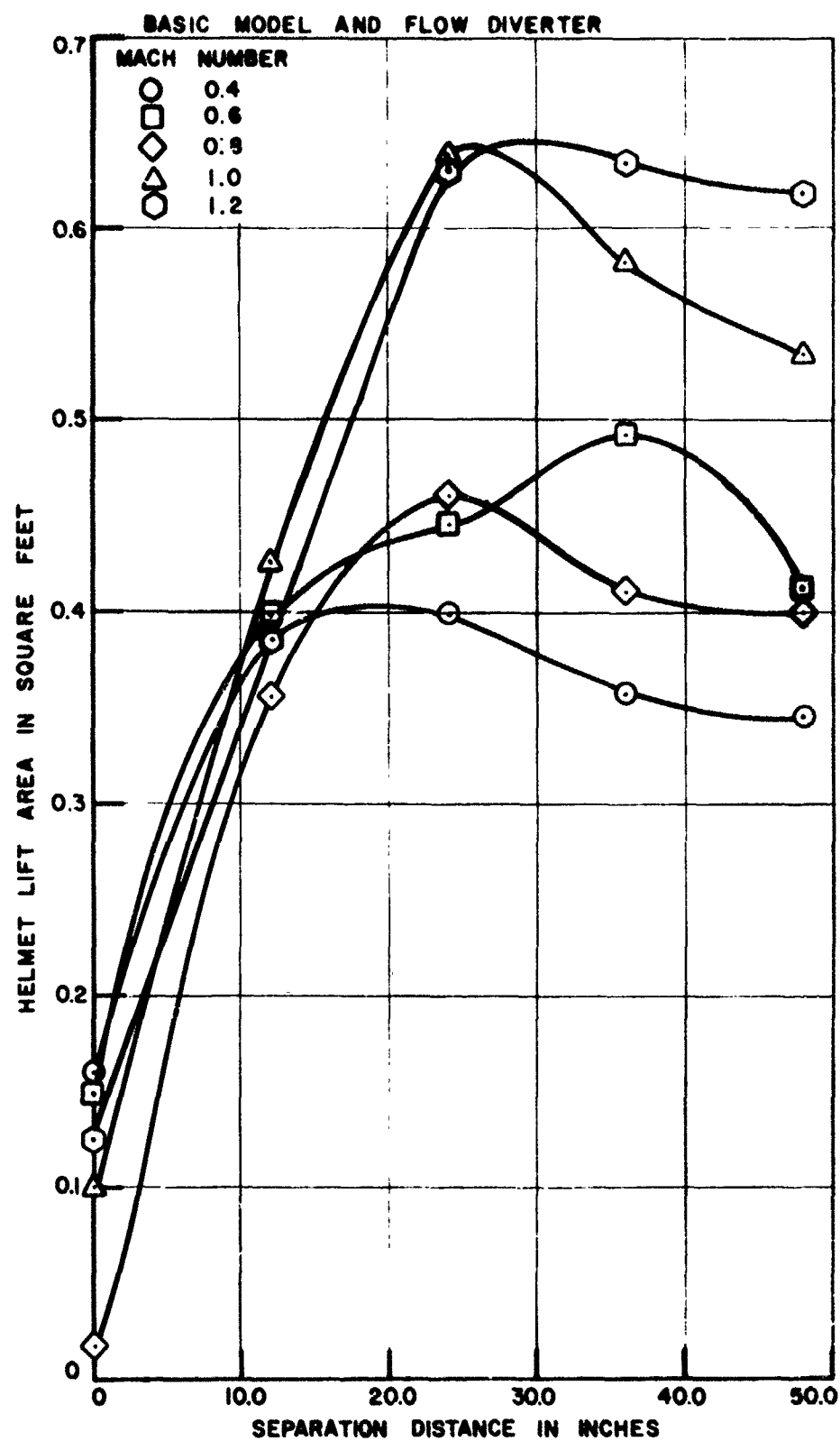
Figure 53. The effect of separation distance on helmet lift, for the basic model when flow diverter is present. Yaw = 0.0°. Pitch = 0.0°.
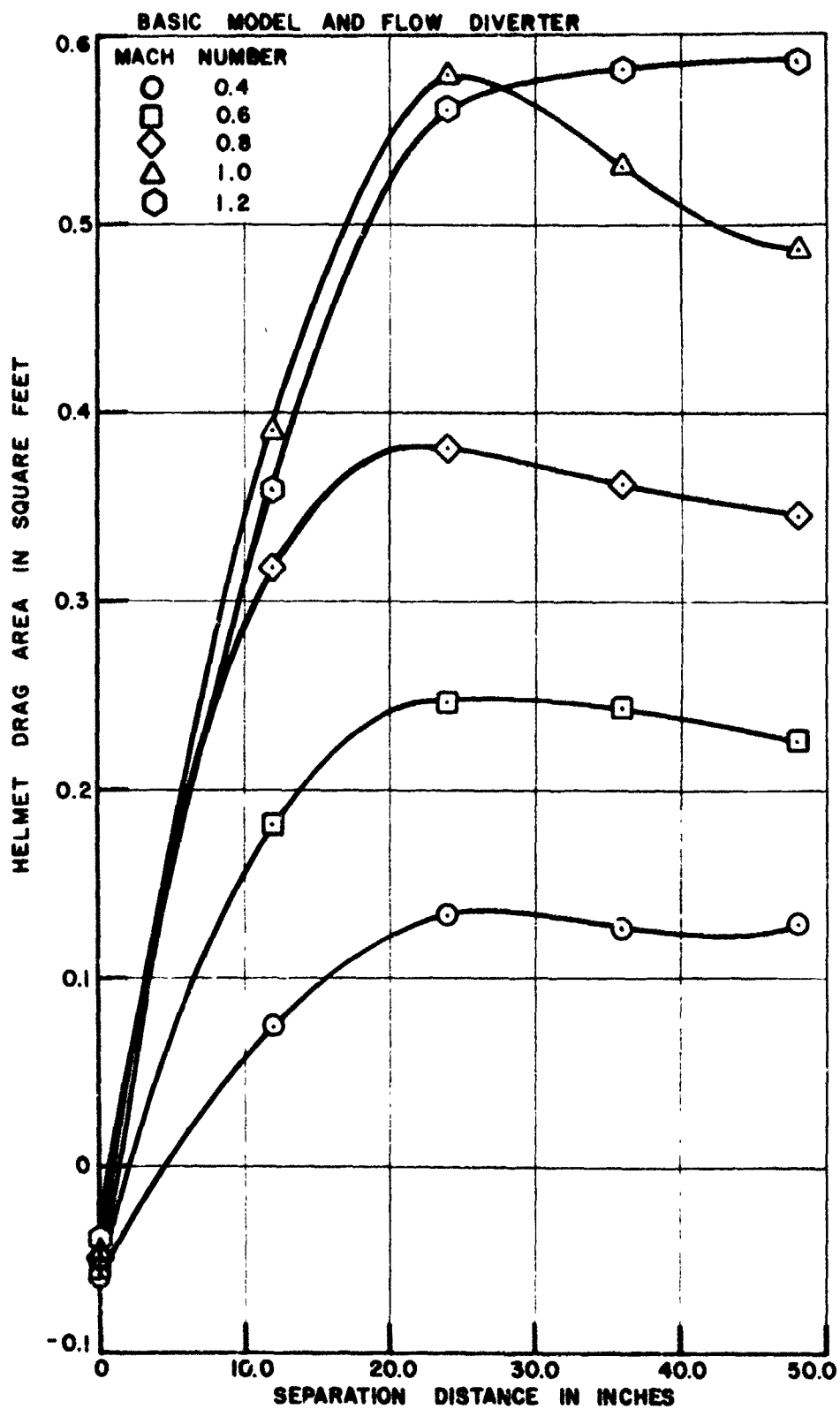
Figure 54   The effect of separation distance on helmet drag,
for the basic model when flow diverter is present.
Yaw = 0.0°.   Pitch = 0.0°.
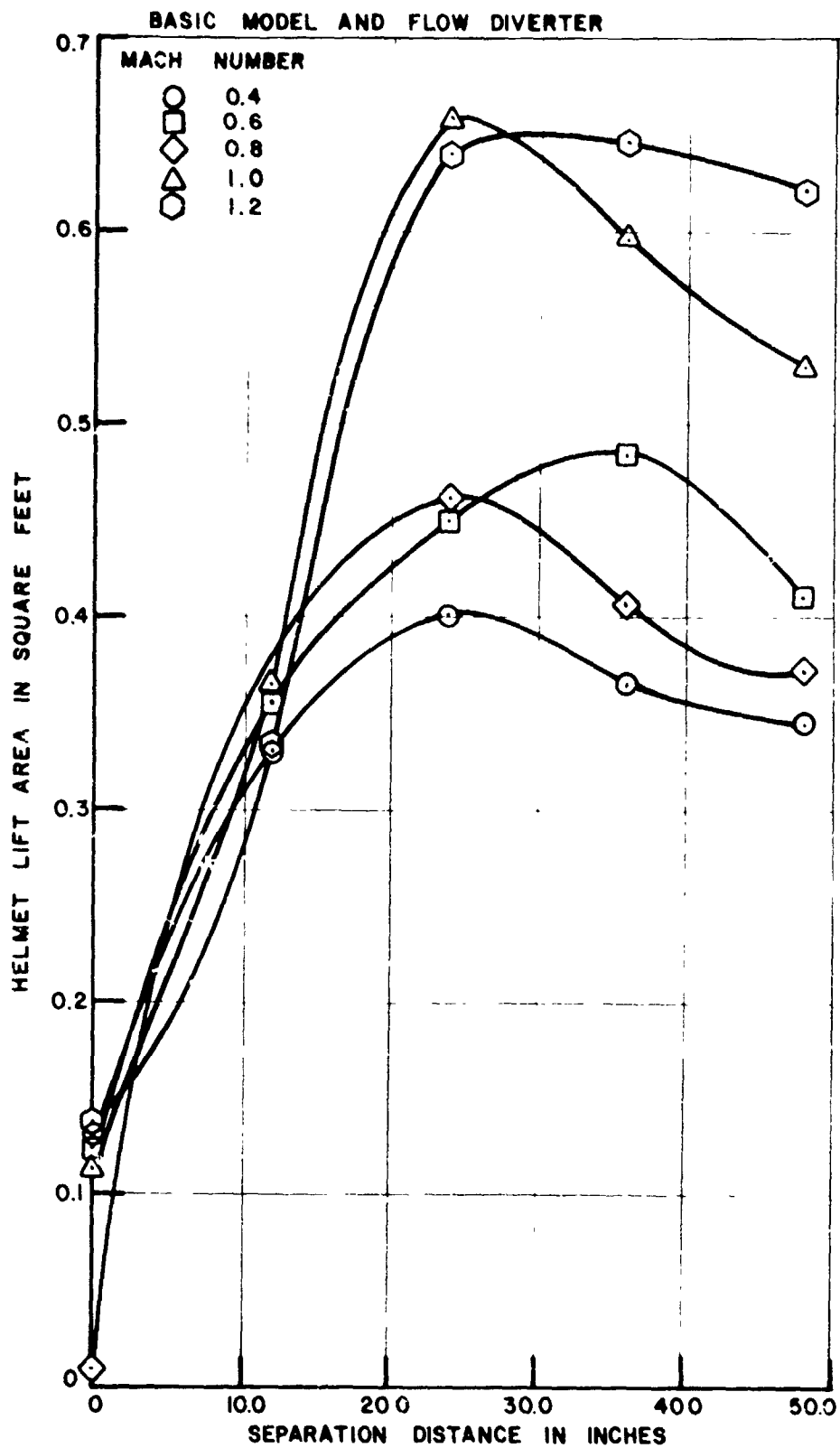
Figure 55. The effect of separation distance on helmet lift, for the basic model when flow diverter is present. Yaw = 0.0°. Pitch = 5.0°.
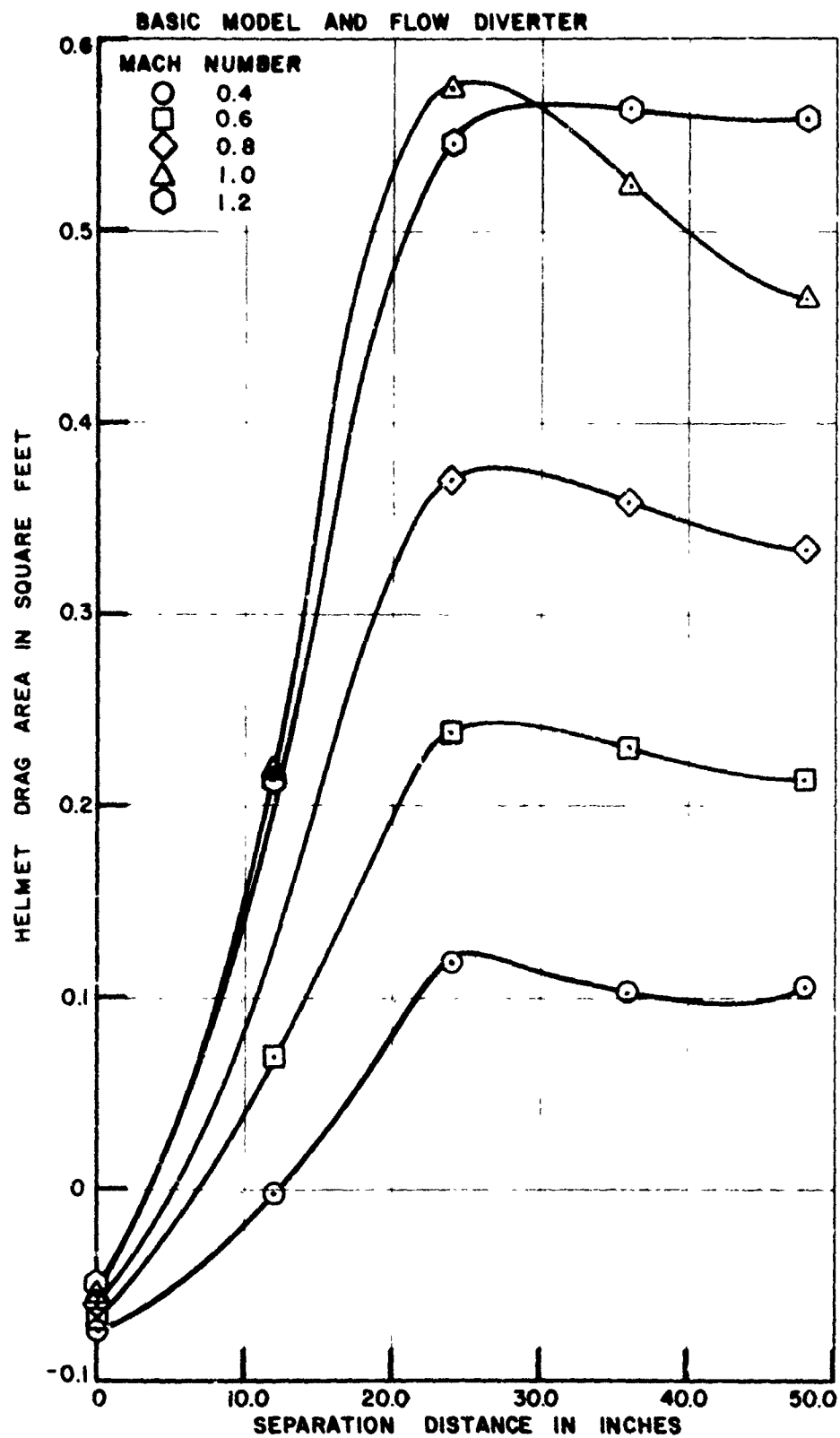
Figure 56. The effect of separation distance on helmet drag,
for the basic model when flow diverter is present.
Yaw = 0.0°. Pitch = 5.0°.

Figure 57. Lift force area on the helmet for zero separation, zero yaw and pitch.

Figure 58. Lift force on the helmet for zero separation, zero yaw and pitch.

Figure 59. Drag force areas on the helmet for zero separation, zero yaw and pitch.

Figure 60. Drag force on the helmet for zero separation, zero pitch and yaw.

CONCLUSIONS

1. The data obtained are supercritical. Gross moment and force data agree
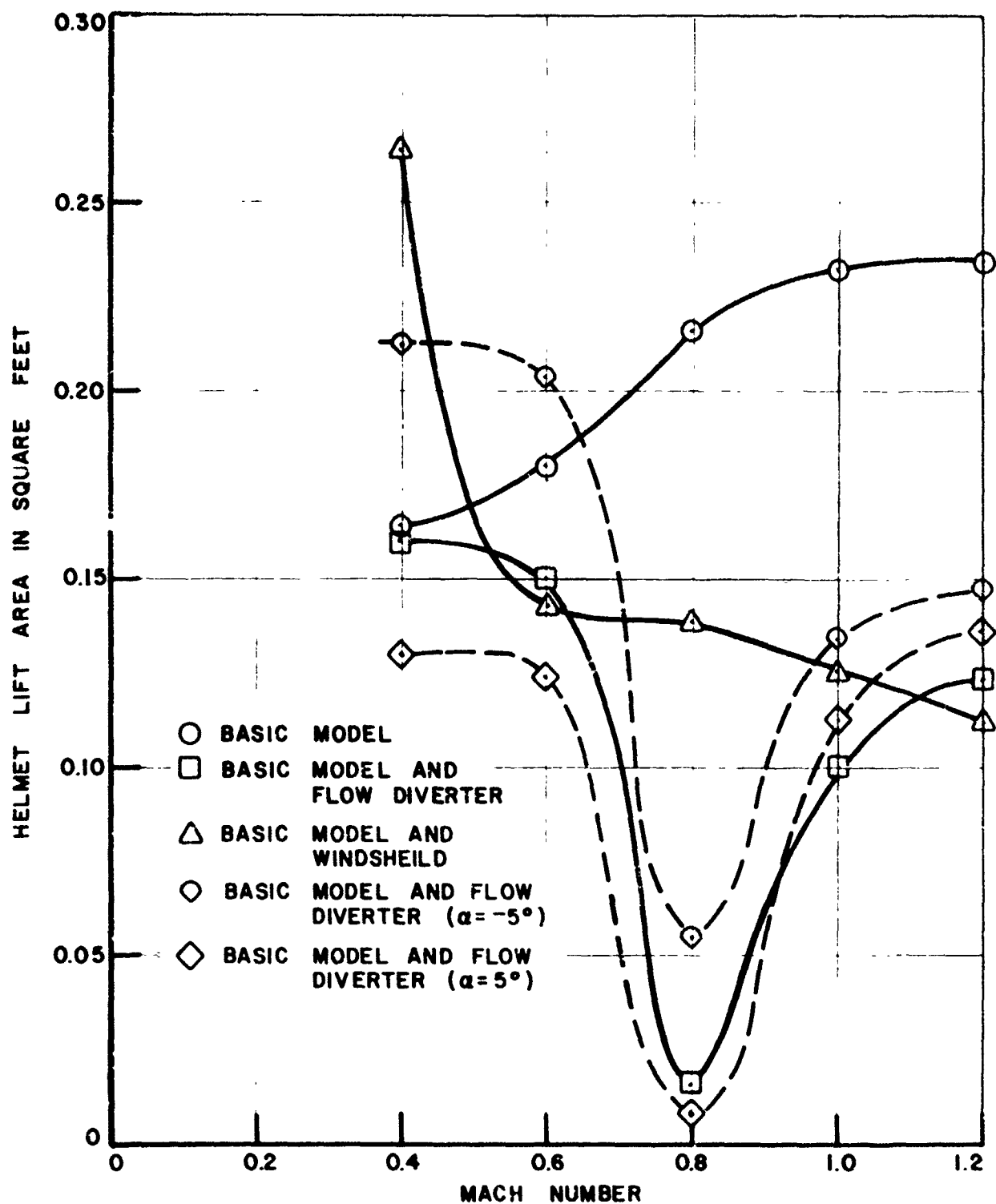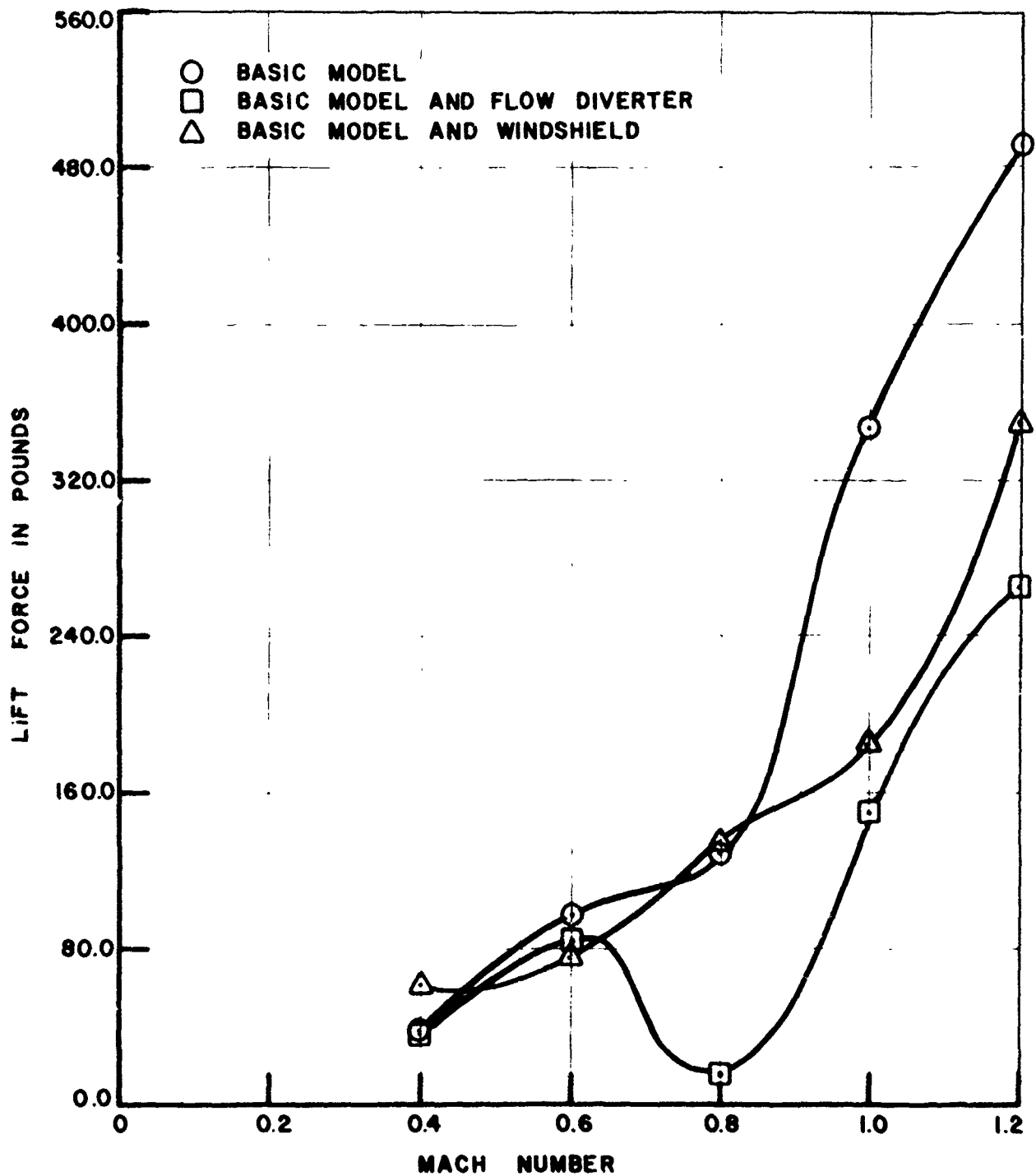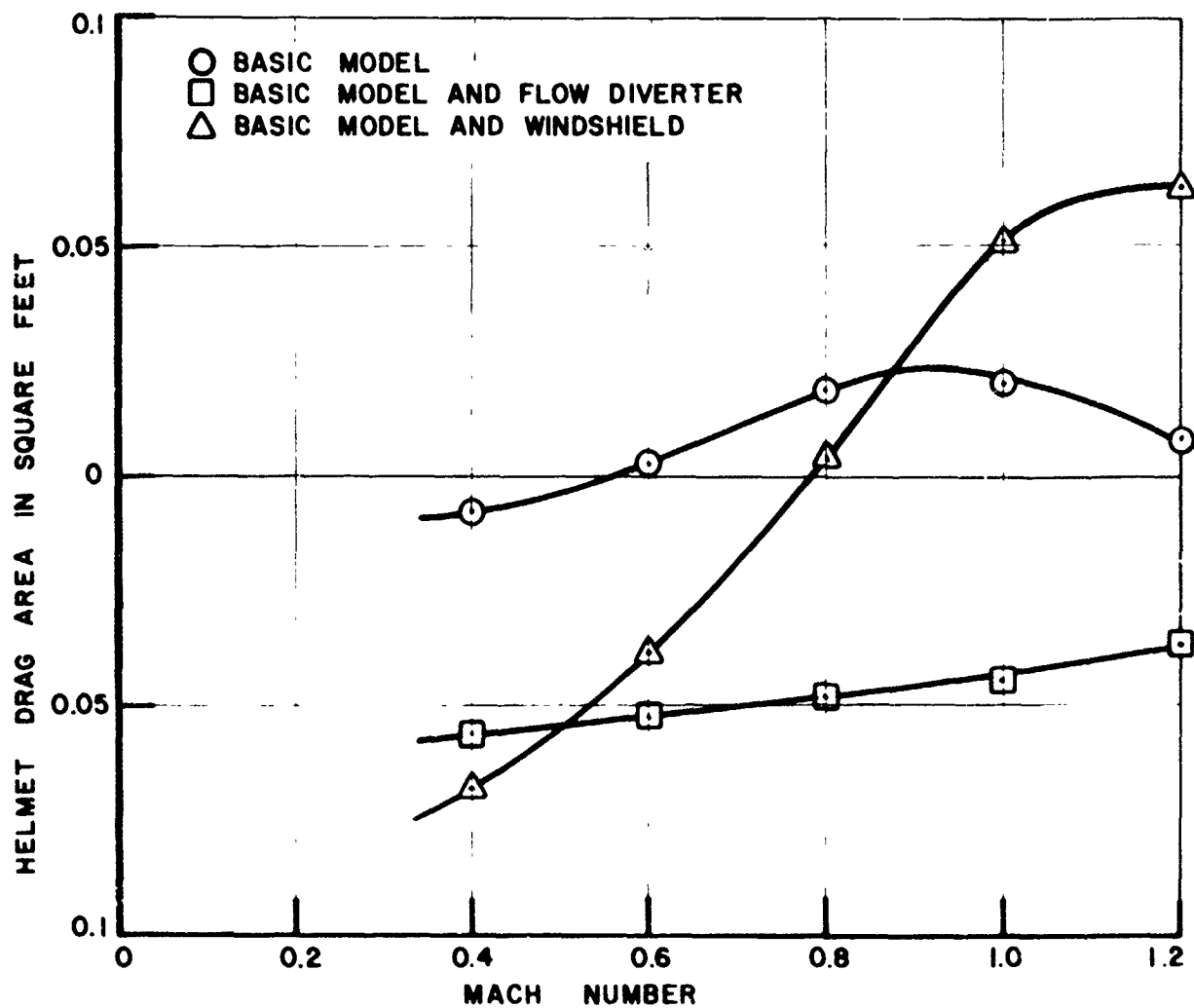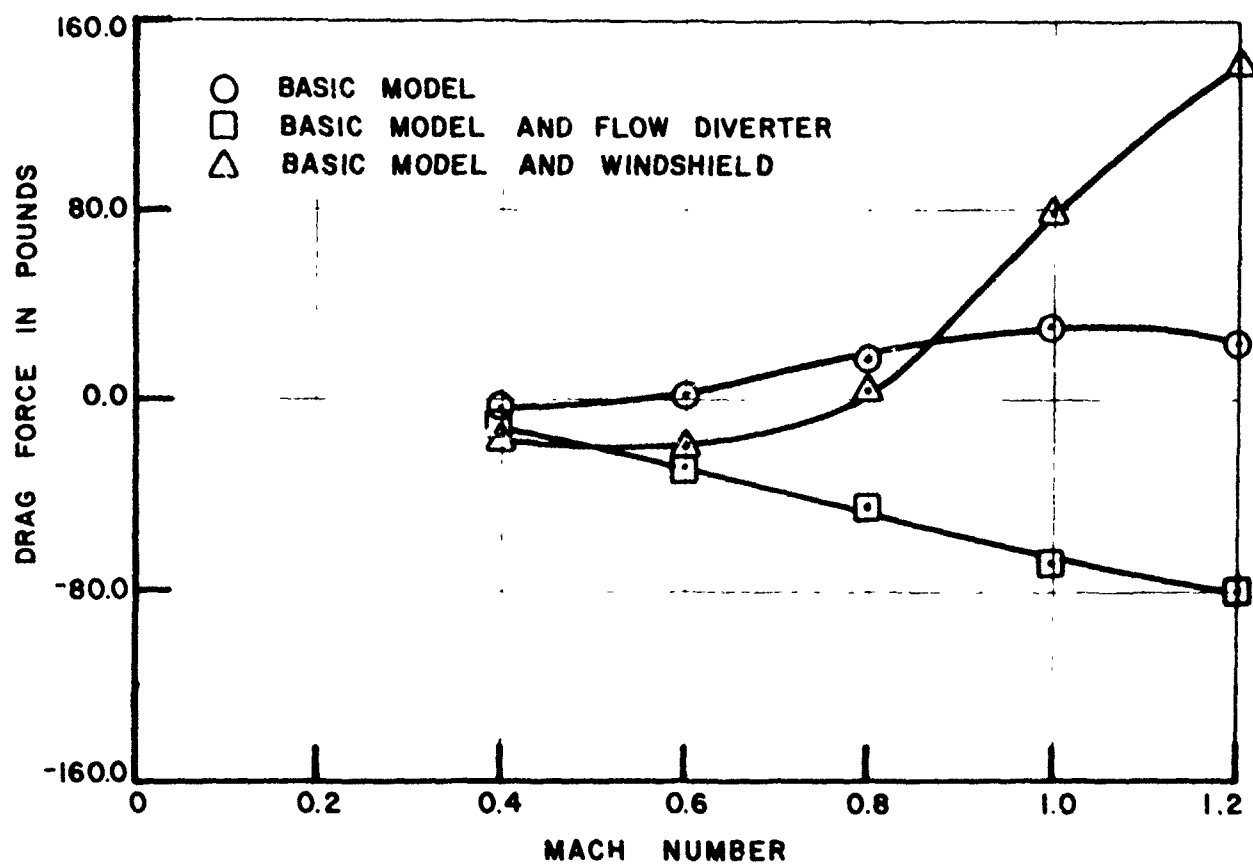   (except for drag) with measurements made with other models and full
   scale seats. Drag is thought to be low because the model is rigid.
   (e.g. , no flapping clothing) and smoother than a full scale escape system.

2. Proximity to the fuselage reduces seat drag and increases its lift
   significantly. The changes are equivalent to a $10°-15°$ change in seat
   angle of attack. Pitching moment is also changed markedly, but yawing and
   rolling moments are not much affected. There is a small increase in side
   force.

3. A flailing leg or arm, or both, causes a major increase in yawing moment,
   even though the change in limb position (from the symmetrical case) is
   quite small. This effect is very destabilizing.

4. Upper arm flail potential forces are roughly doubled by the presence
   of the fuselage. This effect is sensitive to changes in
   cockpit configuration and is most severe with the flow diverter in place.
   There is also a large magnification of upper leg flail force which is
   chiefly experienced in the lift direction, corresponding to a (full scale)
   lift area of 1.1 ft^2, or a lift force of about 600 lb/leg at $M = 0.6$.

5. Helmet forces broadly agree with other measurements in the literature,
   except that low speed drag is much lower; presumably due to the smoothness
   of the model head. There is some magnification of helmet forces by fuse-
   lage proximity.

6. Helmet lift forces are still large when the crew member is in his normal
   flight position in the cockpit, and for $M = 0.4-0.6$ are not much affected
   by either the windshield or the flow diverter. Above this speed both
   windshield and flow diverter give some relief (particularly the latter
   near $M = 0.8$). But both these deflectors also result in negative helmet
   drag readings, indicating the strong likelihood of severe buffeting.

7. Helmet loss is likely for all conditions tested.

REFERENCES

Anthony, Alistair, July 1978, <u>Preliminary Analysis of Wind Tunnel Test of</u>
<u>a 1/2 Scale Model of an Ejecting Crewman and Ejection Seat</u>, AMRL-TR-78-107.
Payne, Inc.,(AD A-069229)

Cowgill, Duane W., Van Haastert, J. A., Sears, William J.,Lt. Col., and
Stork, Roger L.,Capt., June 1978, <u>Evaluation of the Sierra Engineering</u>
<u>Company Lightweight Helmet</u>, SAM-TR-78-13,(AD A-061799)

Ervin, W. D., June 1978, <u>Aerodynamic Characteristics of a Half-Scale Aces II</u>
<u>Ejection Seat with an Anthropomorphic Dummy Crewman at Freestream Mach Numbers</u>
<u>from 0.2 to 1.4</u>, AEDC-TSR-78-P1, Arnold Air Force Station, Tennessee

Glaigher, L. L., March 1972, <u>Aerodynamic Characteristics of a Full-Scale</u>
<u>F-101 Ejection Seat with an Anthropomorphic Dummy at Mach Numbers from 0.2</u>
<u>to 0.8</u>, AEDC-TR-72-38, Arnold Air Force Station, Tennessee

Hawker, Fred W., and Euler, Anthony J., January 1975, <u>Extended Measurements</u>
<u>of Aerodynamic Stability and Limb Dislodgement Forces with the Aces II</u>
<u>Ejection Seat,</u> AMRL-TR-75-15, Payne, Inc.,(AD A-014432)

Hoerner, S. F. and Borst, H. V., August 1975, <u>Fluid-Dynamic Lift</u>, Hoerner
Fluid Dynamics, P. O. Box 342, Brick Town, N. J. 08723

Payne, Peter R., Hawker, Fred W., and Euler, Anthony J., January 1975,
<u>Stability and Limb Dislodgement Force Measurements with the F-105 and Aces-II</u>
<u>Ejection Seats</u>, AMRL-TR-75-8, Payne, Inc.,(AD A-015726)

Payne, Peter R., July 1975, <u>Low Speed Aerodynamic Forces and Moments Acting</u>
<u>on the Human Body</u>, AMRL-TR-75-6   (AD A015 801)

Reichenau, David E. A., October 1969, <u>Aerodynamic Characteristics of an</u>
<u>Ejection Seat Escape System with Cold Flow Rocket Plume Simulation at Mach</u>
<u>Numbers from 0.6 through 1.5</u>, AEDC-TR-69-218, Arnold Air Force Station,
Tennessee

Reichenau, David E. A., October 1978, <u>Aerodynamic Characteristics of a</u>
<u>0.5-Scale Crewman/Ejection Seat Model During a Simulated Ejection from an</u>
<u>F-16 Fighter at Free-Stream Mach Numbers from 0.4 to 1.2</u>, AEDC-TSR-78-P42,
Arnold Air Force Station, Tennessee

Riegels, F. W., September 1961, <u>Aerofoil Sections</u>, Butterworths, London

Visconti, Floravente, and Nuber, Robert J., December 1951, <u>A Wind Tunnel</u>
<u>Investigation of the Static Stability Characteristics of a 1/8-Scale</u>
<u>Ejectable Pilot-Seat Combination at a Mach Number of 0.8</u>, NACA-TM L51-08